IN-1481

225
9-9

DR-1912

UC-80

SEMISCALE BLOWDOWN AND EMERGENCY CORE COOLING (ECC) PROJECT TEST REPORT -- TESTS 824 AND 825

D. J. Olson
C. M. Moser
H. W. Heiselmann

IDAHO NUCLEAR CORPORATION
NATIONAL REACTOR TESTING STATION
IDAHO FALLS, IDAHO 83401

Date Published—June 1971

PREPARED FOR
U.S. ATOMIC ENERGY COMMISSION
IDAHO OPERATIONS OFFICE
UNDER CONTRACT NO. AT(10-1)-1230

Printed in the United States of America
Available from
National Technical Information Service
U. S. Department of Commerce
5285 Port Royal Road
Springfield, Virginia 22151
Price: Printed Copy $3.00; Microfiche $0.95

IN-1481

Reactor Technology
TID-4500

SEMISCALE BLOWDOWN AND EMERGENCY CORE COOLING (ECC) PROJECT TEST REPORT -- TESTS 824 AND 825

BY

D. J. Olson
C. M. Moser
H. W. Heiselmann

IDAHO NUCLEAR CORPORATION

A Jointly Owned Subsidiary of

AEROJET GENERAL CORPORATION
ALLIED CHEMICAL CORPORATION
PHILLIPS PETROLEUM COMPANY

Date Published — June 1971

PREPARED FOR THE U. S. ATOMIC ENERGY COMMISSION
IDAHO OPERATIONS OFFICE
UNDER CONTRACT NO. AT(10-1)-1230

ABSTRACT

This document presents the results of two decompression experiments (Tests 824 and 825) performed in the Semiscale Blowdown and Emergency Core Cooling (ECC) Project as part of the Water Reactor Safety Program of the U. S. Atomic Energy Commission. Semiscale Tests 824 and 825 were initiated by hot-leg breaks of a system that includes both an operating loop and a vessel with simulated core, and were the first semiscale tests in which electrical power was applied to the core. The objective of these tests was to obtain experimental data relative to the effects of an initial temperature difference across the core, core heat addition, and steam generator heat removal on decompression phenomena. This objective was accomplished.

The purpose of this report is to present the data from Semiscale Tests 824 and 825 in sufficient detail to be directly usable by those groups engaged in loss-of-coolant accident (LOCA) analysis development for pressurized water reactors. The decompression test results presented include pressure, fluid and material temperatures, density, thrust, and loop strain, and derived flow rates and core heat transfer coefficients as functions of time.

SUMMARY

The objective of the Semiscale Blowdown and Emergency Core Cooling (ECC) Project is to provide the experimental data base required to access the capability and adequacy of analytical models which are used to quantify thermal-hydraulic phenomena in large pressurized water reactors during a LOCA. The project is part of the Water Reactor Safety Program of the U. S. Atomic Energy Commission.

Semiscale Tests 824 and 825 were initiated by hot-leg breaks of a system that includes a vessel with internals and one complete operating loop, and were the first semiscale tests employing an electrically heated core. The objective of these two tests was to obtain experimental data relative to the effects of an initial temperature difference across the core, core heat addition, and steam generator heat removal on decompression phenomena. An evaluation of the experimental data for both tests has shown that the data are consistent and that measurements of fluid properties as functions of time and location in the system are adequate to provide the experimental data needed to evaluate the capability of analytical models to predict LOCA behavior.

The purpose of this report is to present the data from these two tests in sufficient detail to be directly usable by those groups engaged in model development for the analysis of the LOCA in a pressurized water reactor (PWR). The individual variables measured at each system location are presented for the two tests. The results are compared for the two tests to show effects of the different test conditions. Where possible, data have been given in engineering units and plotted for convenience of interpretation. Local heat transfer coefficients have been derived from heater rod surface temperatures and fluid temperatures, mass flow rates have been derived from density and drag disc measurements, and local qualities and void fractions have been estimated from fluid state measurements. Corrections have been applied to the data. The techniques for these corrections are described and raw data are provided as appendices.

A summary of observations noted in analyzing the data for consistency and accuracy is presented. These observations qualitatively identify the influence on the decompression process of the primary variables being investigated. The more significant observations noted include the following:

(1) Subcooled expansion of the liquid was complete about 70 to 80 msec after system rupture. The fluid at the lower initial temperature (cold leg) remained subcooled, however, until the system decompressed to a pressure corresponding to the saturation pressure for a localized temperature.

(2) Severe pressure oscillations occurred across the semiscale steam generator during the subcooled portion of blowdown for Tests 824 and 825. A maximum pressure difference of ± 400 psi occurred immediately after rupture. The pressure difference diminished to ± 100 psi within 30 to 40 msec.

(3) The calculated fluid flow rates indicated that the core flow during the transient was affected by the duration of core power. The density of the fluid in the loop was not greatly affected by continuation of core power after rupture.

(4) Departure from nucleate boiling (DNB) occurred at the top elevation of the center heater rod 12.5 sec after rupture for the test in which core power was maintained after rupture (Test 825). The temperature of the heater subsequently increased at a rate of about 150°F/sec. Wetting of the cladding surface was quickly reestablished after core power was terminated.

(5) The heat transfer coefficient for the pin surfaces increased immediately after rupture to a value 2 to 7-1/2 times the steady state value.

(6) At DNB the heat transfer coefficients for the heater pin surfaces dropped to essentially zero. After core power was terminated the heat transfer coefficient for the heater pin surfaces rapidly increased as wetting was reestablished.

(7) The amount of water remaining in the system after each test was 2 to 3% of the initial water inventory. The operation of the steam generator during blowdown (Test 825) resulted in some water remaining in that section of the system.

CONTENTS

FIGURES

TABLES

SEMISCALE BLOWDOWN AND EMERGENCY CORE COOLING (ECC) PROJECT TEST REPORT -- TESTS 824 AND 825

I. INTRODUCTION

The Semiscale Blowdown and Emergency Core Cooling (ECC) Project[1] consists of experiments to investigate the hydraulic, thermodynamic, and mechanical behavior characteristic of pressurized water reactors (PWR's) during a loss-of-coolant accident (LOCA). The project is part of the Water Reactor Safety Program of the U. S. Atomic Energy Commission.

The primary objective of the semiscale project is to provide the experimental data base required to access the capability and adequacy of analytical models which are used for quantifying thermal-hydraulic phenomena in large PWR's during a LOCA. The following information is needed:

(1) System decompression characteristics and fluid mass flow from the system.

(2) The availability of primary coolant to the core during blowdown.

(3) The heat transfer mechanisms controlling core thermal response during system decompression.

(4) The demand requirements for ECC delivery to the core and the importance of various system and break parameters affecting that demand.

(5) The effect of ECC injection on primary system decompression.

(6) The forces generated during blowdown and the mechanical response to those forces by system components.

The experimental approach is to first quantify individual phenomena in simple geometries with break size and location as independent variables. Once each phenomenon is quantified, the coupling between the various phenomena controlling hydraulic behavior during decompression is investigated by systematically increasing the system complexity until essentially all aspects of a large PWR are simulated.

The semiscale tests discussed in this report employed a vessel with internals (simulated core) and one complete operating loop. Tests 824 and 825 were the first semiscale tests in which electrical power was applied to the simulated core. The objective of these two tests was to obtain data relative to the effects of an initial temperature difference across the core, core heat addition, and steam generator heat removal on decompression phenomena. Data obtained in these tests remain to be compared with the results of previous semiscale tests with an identical system configuration but without core heat (Tests 821, 822, and 823)[2,3]. Semiscale test results have been reported for

tests involving vessels with and without unheated internals[4] and for tests with the present single-loop system configuration but without vessel internals[5].

The purpose of this report is to present the results of Tests 824 and 825 for the benefit of those groups engaged in model development and evaluation. Included in this report are a description of the hardware configuration and test conditions, an account of procedures and the sequence of events for these first tests involving applied core heat, a presentation of the measured test data, and a discussion of the test results with a summary of observations. Also included, as appendices, are a summary of the data recorded, the methods used to normalize the data, and examples of the digitized test data for Tests 824 and 825.

II. HARDWARE CONFIGURATION AND TEST CONDITIONS

Specific information on the single-loop semiscale system hardware configuration, operating procedures, data recording equipment, and data processing techniques has been presented previously[6]. Figure 1 shows the general arrangement of components for the single-loop tests. Tests 824 and 825 were conducted with the rupture disc assembly attached to the vessel outlet tee and with the blowdown nozzle orificed to 10% (0.009 ft^2) of the pipe cross-sectional area.

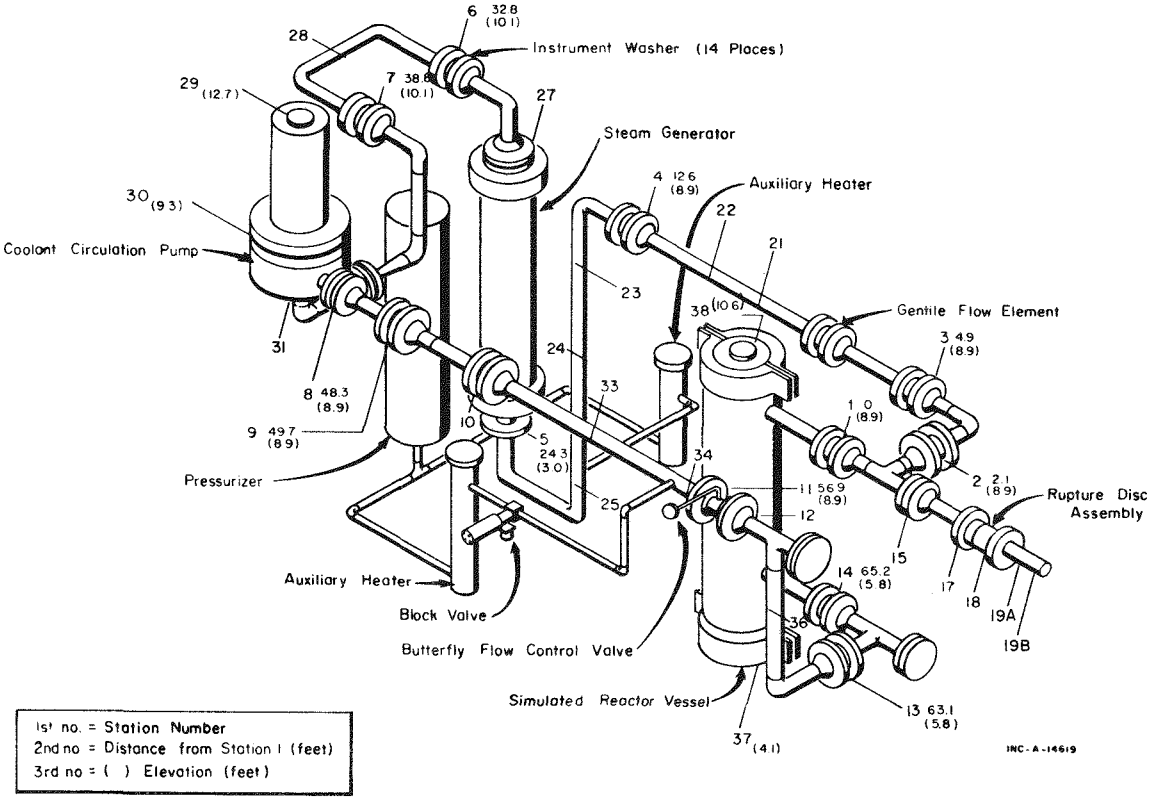

Fig. 1 Single-loop semiscale system.

Tests 824 and 825 were the first semiscale tests performed with applied core power. The electrically-heated core utilized in these tests consists of 120 heater pins located in the vessel in a triangular pattern on a 31/32 in. pitch. The vessel internals, heater rod positions, and thermocouple locations are shown in Figure 2. The cartridge-type heater rods are clad with 65-mil, 0.44-in.-OD Nickel-200 and have 9-in. Nichrome heating elements. The heated length is insulated with boron nitride; the remainder is insulated with magnesium oxide. The heater rods are capable of operating at a heat flux of 1000 $W/in.^2$ giving a total core power capability of about 1.5 MW.

The test conditions for Test 824 were selected to permit investigation of the effect of an initial temperature difference across the core on fluid behavior during decompression. An initial core temperature difference of 50°F was established through application of core heat prior to rupture. The

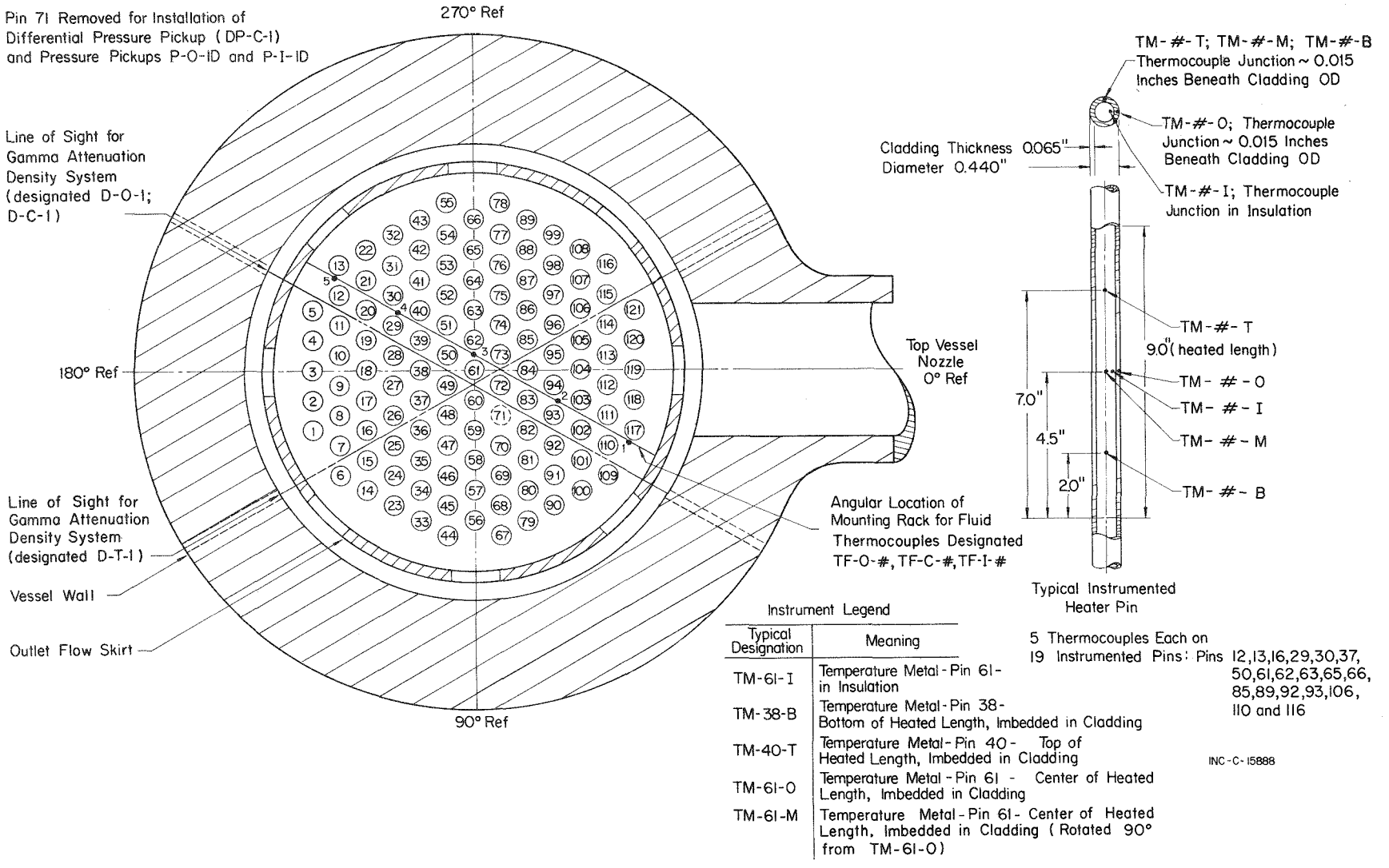

Instrument Legend

Typical Designation	Meaning
TM-61-I	Temperature Metal-Pin 61-in Insulation
TM-38-B	Temperature Metal-Pin 38-Bottom of Heated Length, Imbedded in Cladding
TM-40-T	Temperature Metal-Pin 40- Top of Heated Length, Imbedded in Cladding
TM-61-O	Temperature Metal-Pin 61 - Center of Heated Length, Imbedded in Cladding
TM-61-M	Temperature Metal-Pin 61- Center of Heated Length, Imbedded in Cladding (Rotated 90° from TM-61-O)

5 Thermocouples Each on 19 Instrumented Pins: Pins 12,13,16,29,30,37, 50,61,62,63,65,66, 85,89,92,93,106, 110 and 116

INC-C-15888

Fig. 2 Vessel internals and heater pin and thermocouple locations.

core power was shut off essentially simultaneously with rupture. Steam generator operation continued throughout decompression for Test 824.

In order to evaluate the effects of heat addition during blowdown on fluid behavior, core power was continued after rupture for Test 825. The core heaters were shut off when the temperature of the heater rod cladding reached 900°F, about 14 sec after rupture. For Test 825, the secondary flow through the steam generator was terminated at the time of rupture.

Table I summarizes the initial and test conditions for Tests 824 and 825. A summary of the test procedures and sequence of events for both tests is included in the next section.

TABLE I

INITIAL AND TEST CONDITIONS FOR SEMISCALE TESTS 824 AND 825

	Test 824	Test 825
Vessel internals[a]	9-in. core	9-in. core
ECC system	None	None
Break location[b]	Outlet (hot-leg tee)	Outlet (hot-leg tee)
Break area (ft^2)	0.009	0.009
Rupture technique	Overpressure	Overpressure
System pressure (psia)	2262	2282
Temperature (°F)		
Vessel outlet	640	600
Vessel inlet	590	560
System total pressure drop (psi)	40.6	40.6
Core power (MW)	1.07 (Off at rupture)	1.10 (Off at 14 sec after rupture)
Steam generator operation	On throughout blowdown	Off at rupture
Water analysis		
Dissolved gases - cc(STP)/kg	120	60
Suspended solids (ppm)	95	142
pH	6.0	5.9
Electrical conductivity (μmhos)	15.6	11.0

[a] Vessel internals shown in Figure 2.

[b] Break location shown in Figure 1.

III. SEQUENCE OF EVENTS FOR SEMISCALE TESTS 824 AND 825

Tests 824 and 825 were the first semiscale tests performed with applied core heat to produce an initial temperature difference across the core. Previous tests on the same system were conducted from isothermal initial conditions. As mentioned in the previous section, the primary difference between the test conditions for Tests 824 and 825 were the durations of core heat application and steam generator operation. The major events and their sequence for both tests are displayed in Figure 3.

Pretest procedures were essentially identical for Tests 824 and 825. Warmup of the system to the desired system pressure and isothermal temperature was achieved by operation of the two auxiliary heaters (Figure 1) in the auxiliary circulation loop. This process required about 8 to 10 hr. During warmup, the excess fluid due to thermal expansion was drained from the system through a throttle valve near the pump inlet.

About 10 to 20 min prior to test initiation, the auxiliary heaters were turned off and the block valve in the auxiliary loop was closed. Steam generator operation was initiated and about 0.85 MW power was applied to the core to continue heatup. The power was gradually increased to the desired pretest level (about 1.1 MW). The initial core temperature difference and the temperature distribution throughout the loop were established by throttling the flow and concurrently controlling the steam generator secondary spray. Just prior to system rupture, the pressurizer makeup pump and auxiliary heaters were turned off.

System rupture was initiated by overpressurizing the outer rupture disc of the rupture assembly in the blowdown nozzle; system pressure immediately ruptured the inner disc within 1 to 2 msec. For both tests, the blowdown nozzle was attached to a tee at the vessel outlet and was orificed to a flow area of 0.009 ft^2, or 10%, of the pipe cross-sectional area.

For Test 824, core power was shut off at rupture. Steam generator operation continued throughout the test. For Test 825, the steam generator was shut off at test initiation. Core power was continued for about 14 sec subsequent to rupture.

Pump power for both tests was shut off at 16.5 sec. The decompression process for both tests was essentially completed within 40 sec of system rupture.

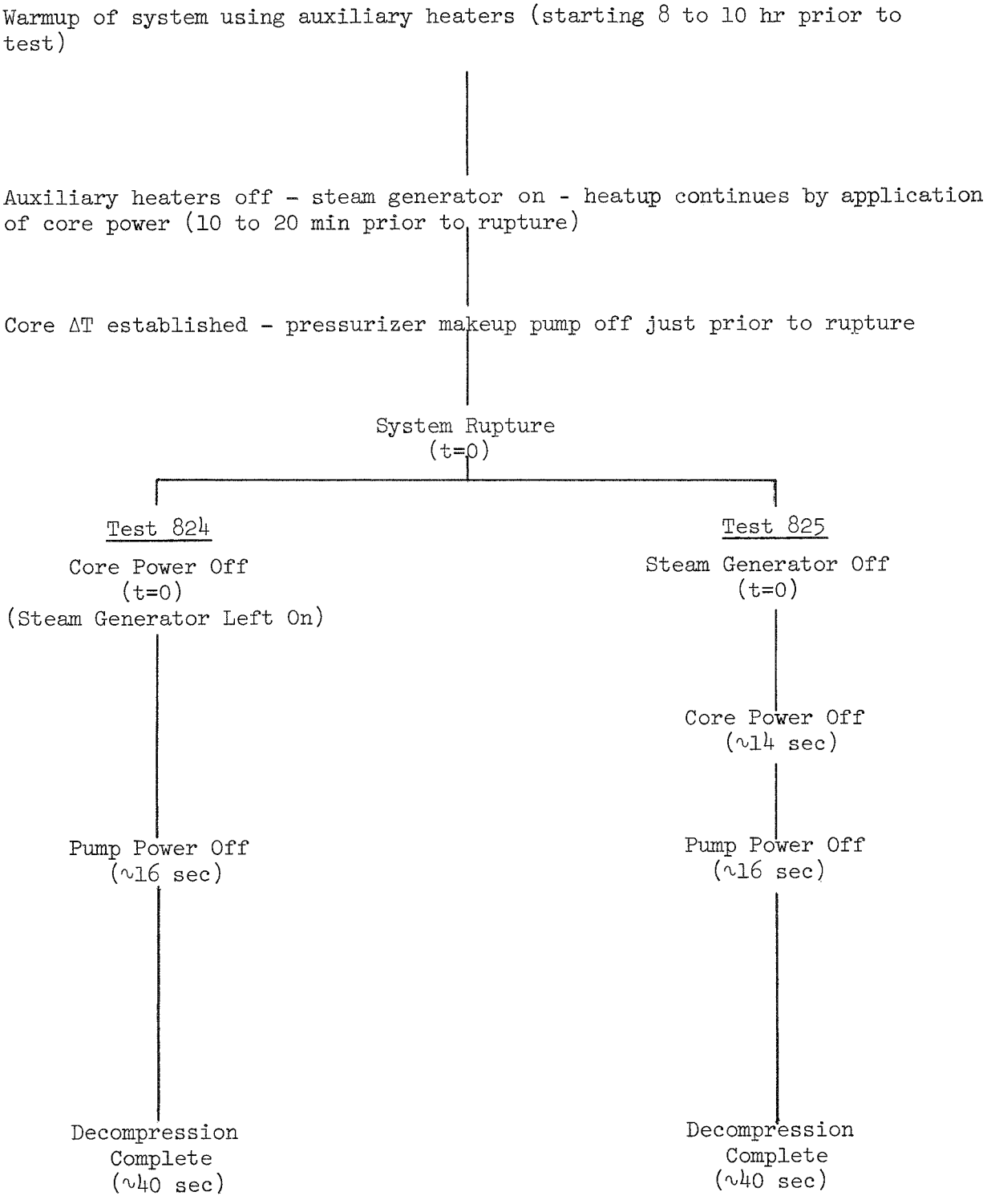

Fig. 3 Sequence of events for semiscale Tests 824 and 825.

IV. PRESENTATION OF TEST DATA

This section presents and discusses the measured test data for Semiscale Tests 824 and 825. A summary of the measurements made for these two tests is included in the appendices. This section includes discussion of fluid pressures, fluid and material temperatures, fluid density, system thrust, loop strain, and water remaining in the system following decompression.

Section V of the report further discusses the test results from the standpoint of certain variables (for example, flow rates and core heat transfer) calculated from measured test data. An additional measured quantity, momentum flux, is included in the discussion of the fluid flow in Section V. Momentum flux data are used in conjunction with density data to determine the flow rates.

1. PRESSURE

Because of the different phenomena controlling system behavior during the subcooled and saturated portions of decompression, presentation and discussion of the pressure measurements is divided into two sections. The first section, subcooled decompression, presents short-term data obtained for the first 70 to 80 msec of the blowdown transient. Subsequent (long term) pressure data are reviewed in the second section, saturated decompression.

1.1 Subcooled Decompression

The short-term pressure measurements recorded at the vessel inlet and outlet nozzles and the vessel outlet plenum for Tests 824 and 825 are shown in Figures 4 and 5, respectively. The first decompression wave recorded at the vessel outlet nozzle (break location) in both tests occurred 1 to 2 msec before system rupture and results from a volume change caused by yielding of the upstream rupture disc prior to rupture. The second, and largest, decompression wave results from the rupture itself; pressure fluctuations at the outlet nozzle are 250 to 350 psi. Comparisons of the vessel outlet nozzle pressure traces (P-1) with those for the vessel outlet plenum (P-0-1S) in Figures 4 and 5 show that the severe pressure fluctuations occurring near the break location are not transmitted into the vessel. The first pressure fluctuations at the inlet nozzle (P-14) for both tests occur some 25 msec after rupture which corresponds with the approximate sonic transport time around the loop (Stations 1 to 14, about 65 ft of pipe).

The short-term (subcooled) in-vessel pressure data from stations in the outlet (P-0-1S) and inlet (P-I-1S) plenums for Tests 824 and 825 are presented in Figures 6 and 7. Included in these figures is the difference between the inlet and outlet plenum pressures (that is, the pressure difference across the core). During subcooled decompression, a maximum core pressure difference for the two tests of 40 to 70 psi is indicated; in both cases, the maximum occurs within a few milliseconds after system rupture. Later in the subcooled decompression, the data for Test 824 (Figure 6) show a positive pressure difference (the pressure drop is in the direction of normal flow)

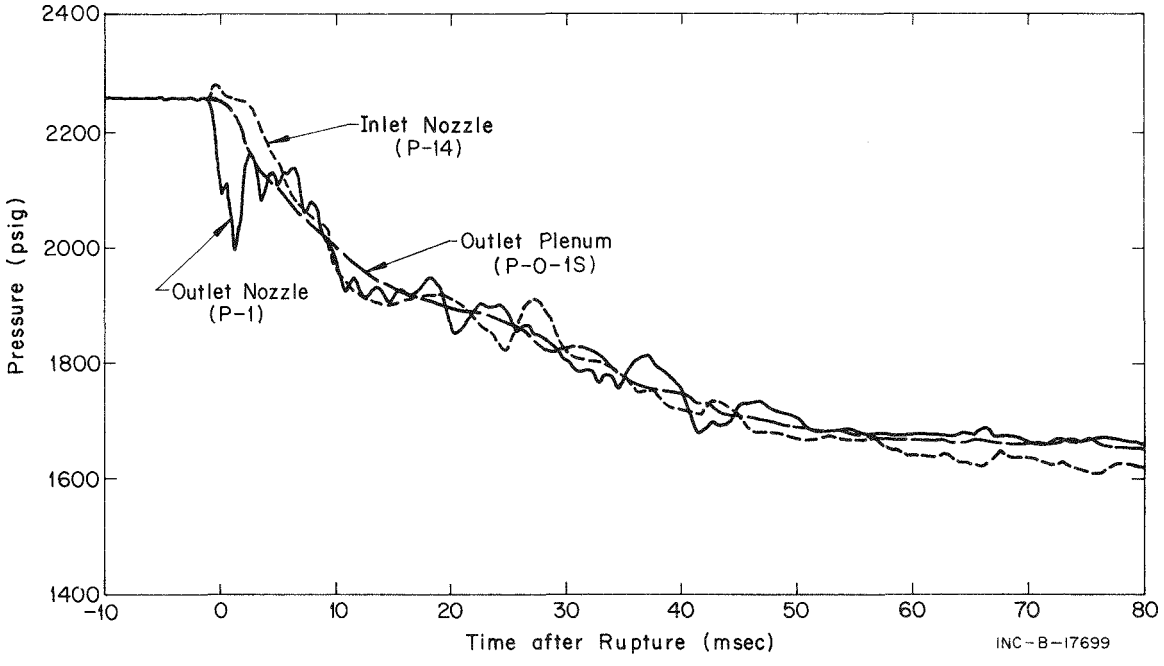

Fig. 4 Subcooled decompression during Test 824 - vessel nozzles and outlet plenum.

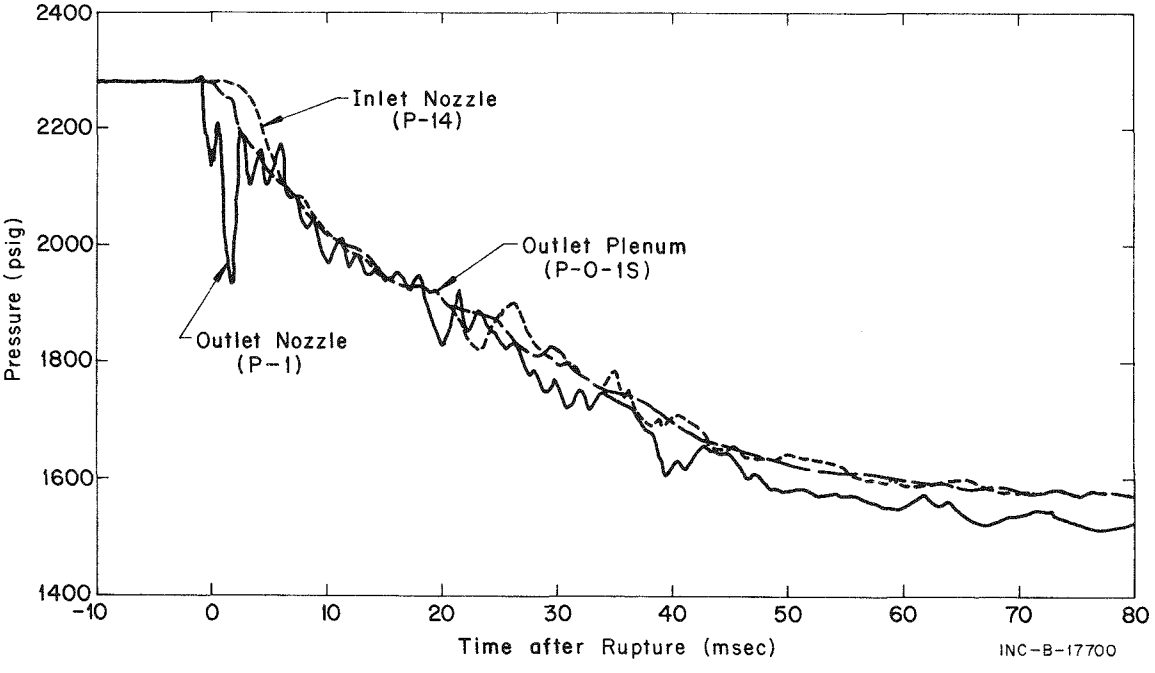

Fig. 5 Subcooled decompression during Test 825 - vessel nozzles and outlet plenum.

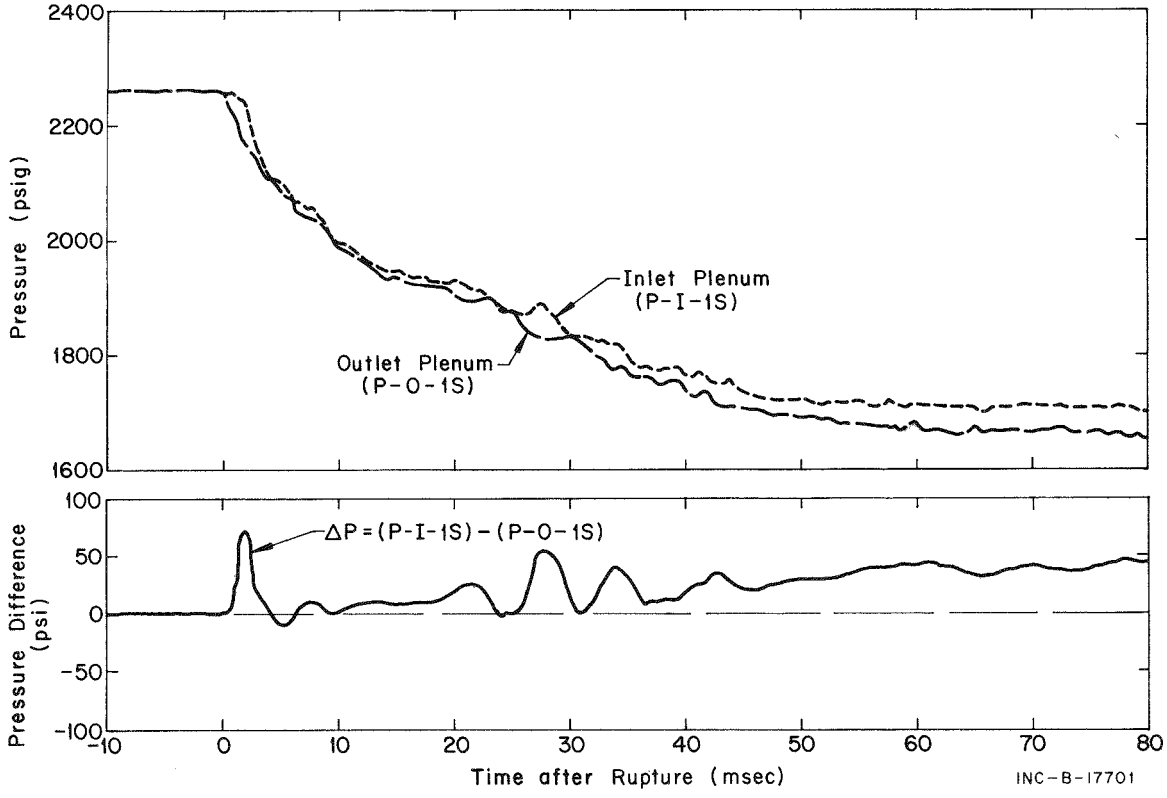

Fig. 6 Vessel pressures during subcooled decompression - Test 824.

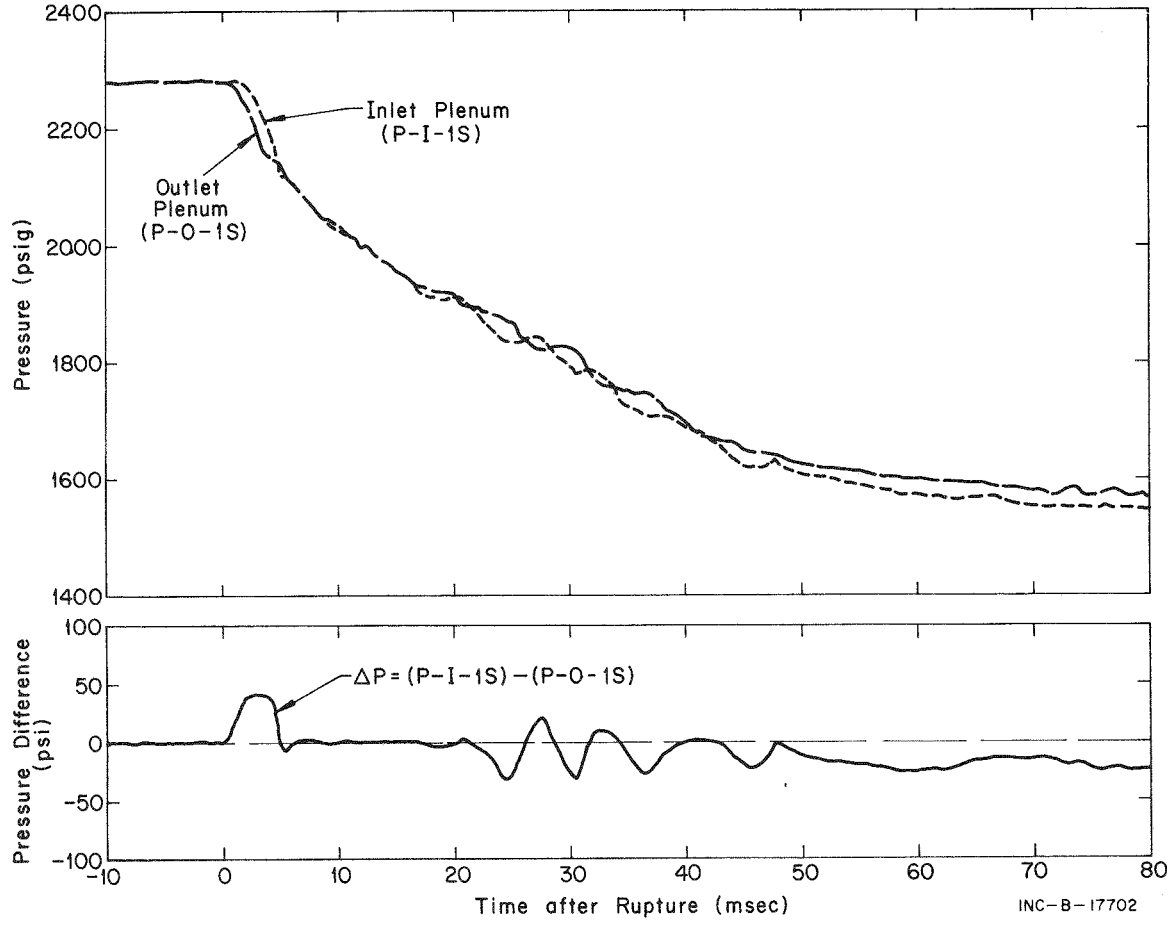

Fig. 7 Vessel pressures during subcooled decompression - Test 825.

whereas the data for Test 825 (Figure 7) indicate a negative pressure difference (the pressure drop is opposite the direction of normal flow).

The inlet and outlet pressures of the steam generator during subcooled decompression for Tests 824 and 825 are presented in Figures 8 and 9 along with the pressure difference across the steam generator. Differential pressure oscillations occur throughout subcooled blowdown and beyond, peaking (± 400 psi) immediately after rupture but diminishing to ± 100 psi within 30 to 40 msec.

1.2 Saturated Decompression

The subcooled phase of decompression is complete within 70 to 80 msec following rupture for Tests 824 and 825. Fluid pressures during the major portion of subsequent decompression generally follow saturation conditions. Exceptions exist in both tests, however, in the early stages of saturated decompression (that is, during transition from subcooled decompression) when the fluid conditions at various points in the system have not yet fully reached saturation. Of particular significance from the standpoint of core integrity are the pressures in the vessel inlet and outlet plenums, shown for the first few seconds of decompression in Figures 10 and 11 for Tests 824 and 825. The indicated difference in pressures is small (less than 70 psi) during this period for Test 825 and for at least the first two seconds for Test 824.

The initial temperature difference between the inlet and outlet plenums for both tests was of the order of 40 to 50°F. The corresponding pressure difference for saturation conditions would be about 400 to 500 psi, significantly greater than the difference in measured pressures. The conclusion is that saturation conditions consistent with the initial cold and hot leg temperatures did not exist in both the inlet and outlet plenun s of the semiscale vessel during the initial portion of saturated blowdown for Tests 824 and 825. This conclusion is supported by fluid temperature data presented in the next section. Briefly, the temperature data show that the fluid in the inlet plenum is subcooled for the first 2.3 sec of blowdown in Test 824 and the first 3.2 sec in Test 825. As shown in Figure 10, the inlet plenum pressure becomes greater than the outlet plenum pressure for Test 824 as soon as saturation conditions are reached. The abrupt recovery and subsequent magnitude of the inlet plenum pressure after 2.4 sec in Test 824 are not supported by other test data. The unaccountable difference between inlet and outlet plenum pressures, if real, indicates that flow through the core continued in the normal flow direction and that a strong fluid coupling existed across the core.

Complete vessel pressure histories for Tests 824 and 825 are presented in Figures 12 and 13. Saturation conditions throughout the vessel are reached only after the outlet plenum pressure has decreased to a value which corresponds to saturation at the inlet plenum temperature. Until saturation occurs, the cold leg fluid is a subcooled liquid. Due to the temperature sensitivity of the pressure transducers, the digitized data have been corrected for thermal drift in accordance with the method outlined in Appendix B. Nevertheless, caution should be used in relying on the absolute pressure values for the latter portion of blowdown.

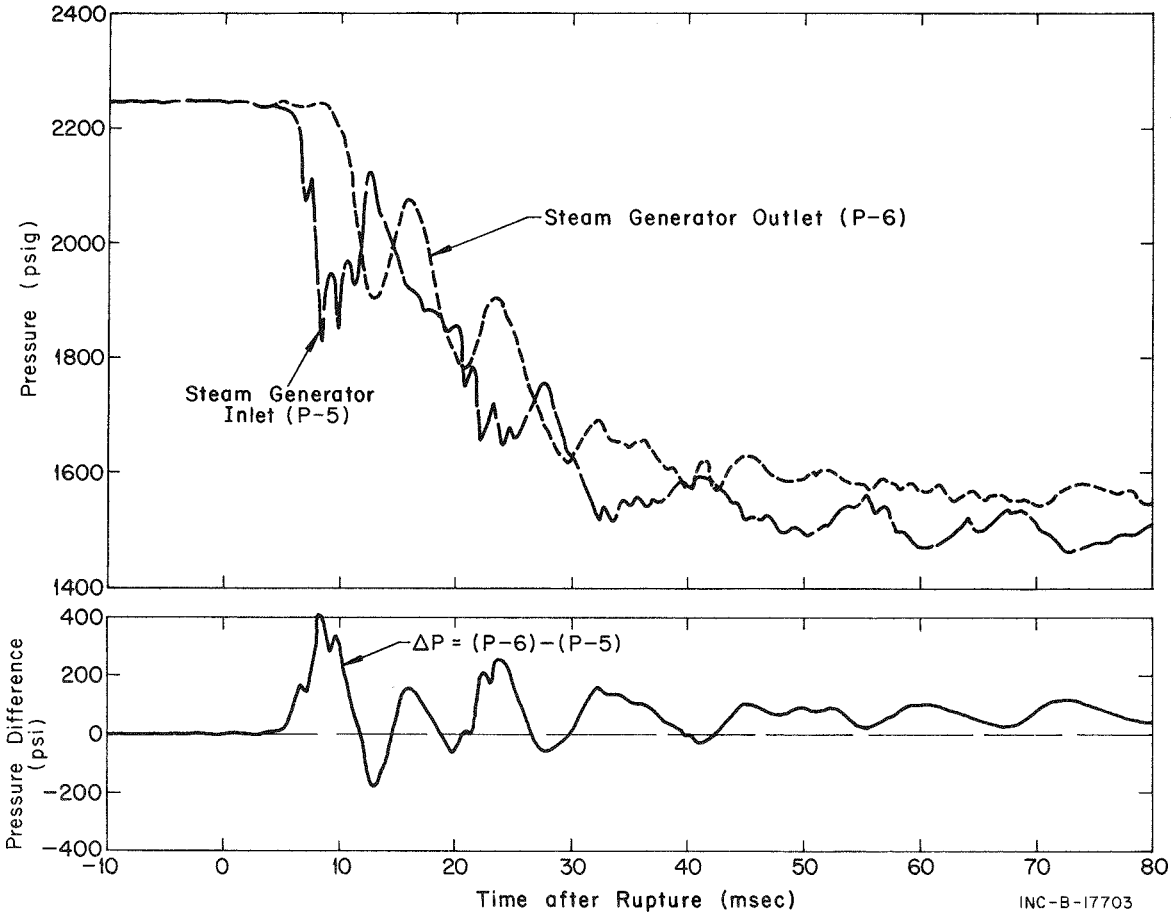

Fig. 8 Steam generator pressures during subcooled decompression - Test 824.

Examples of the digitized pressure histories at various locations in the system for Tests 824 and 825 are presented in Appendix C.

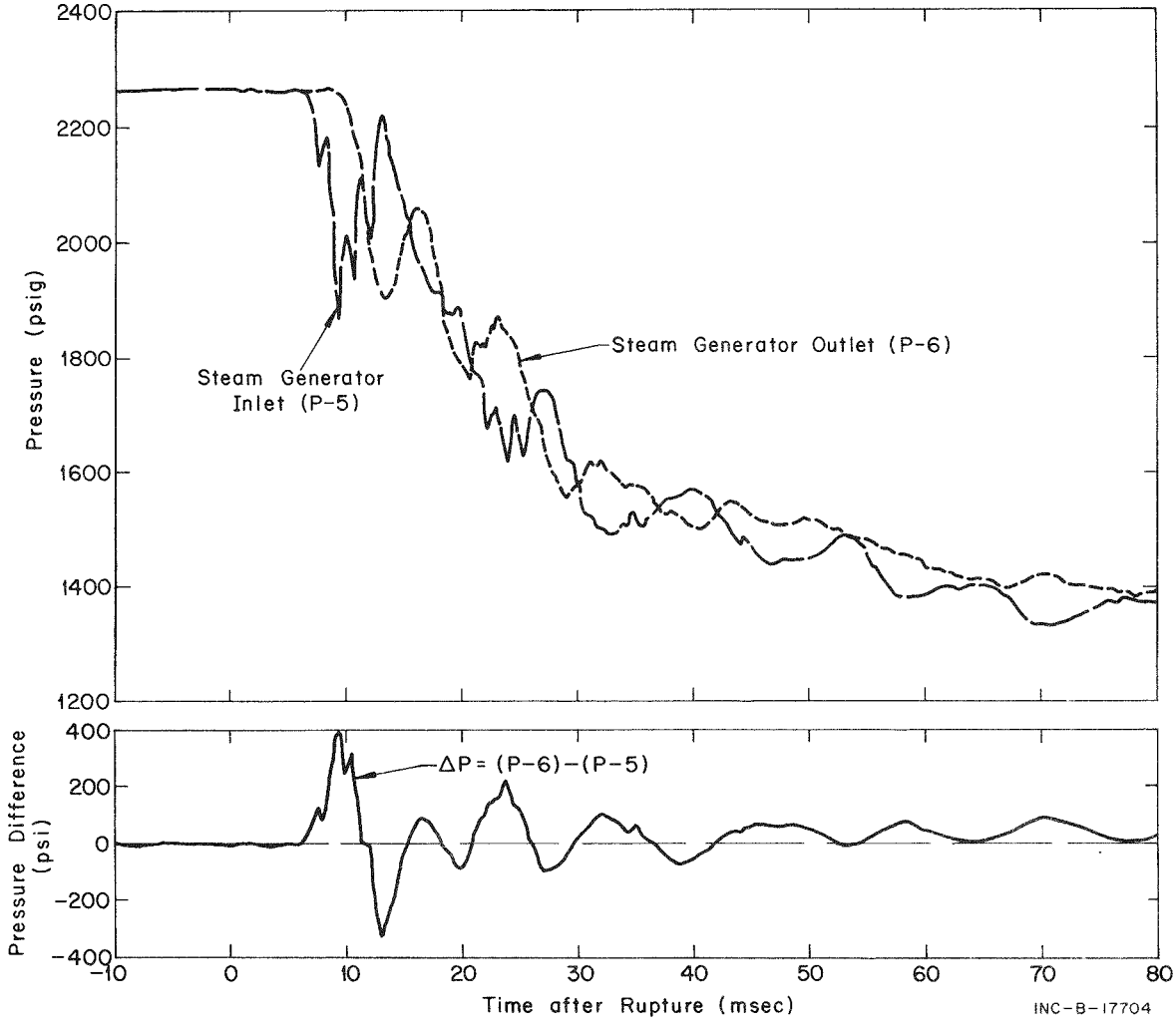

Fig. 9 Steam generator pressures during subcooled decompression - Test 825.

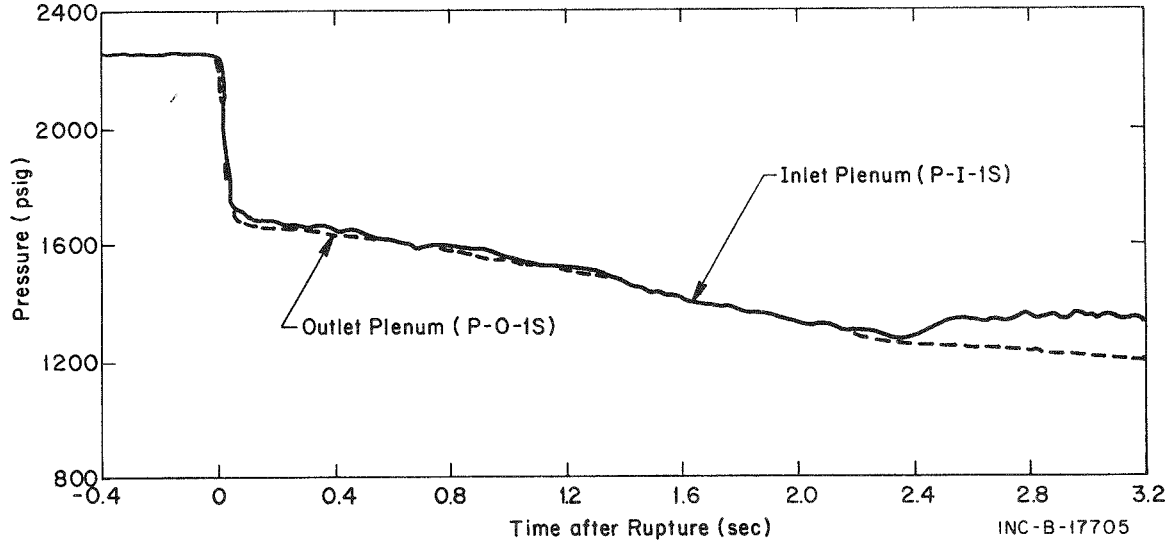

Fig. 10 Vessel pressures during the initial portion of saturated decompression - Test 824.

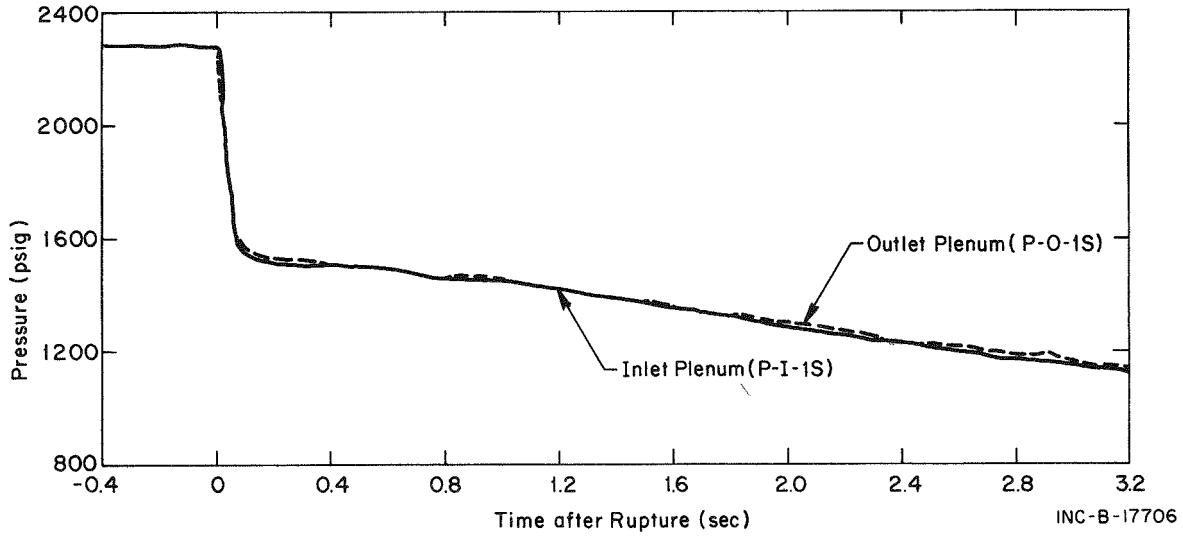

Fig. 11 Vessel pressures during the initial portion of saturated decompression - Test 825.

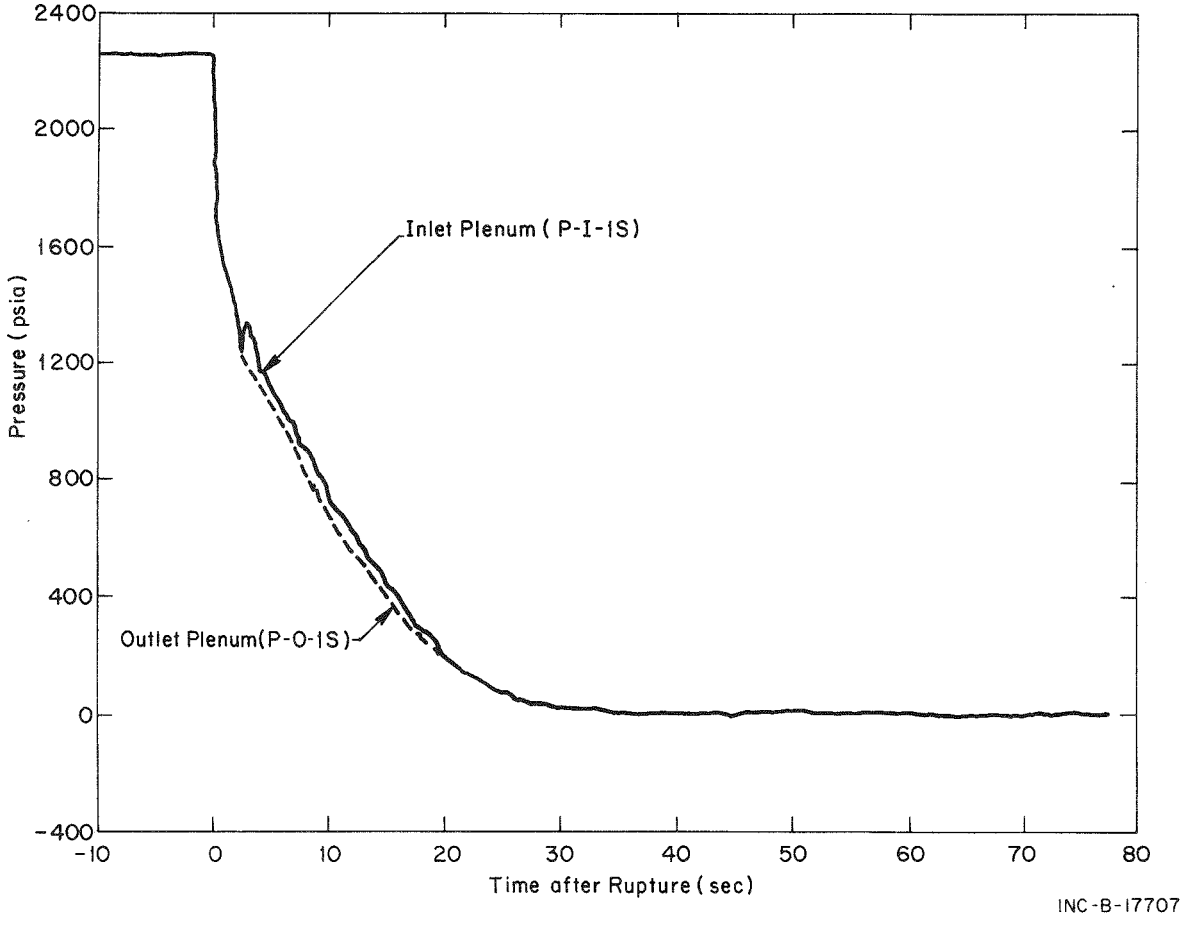

Fig. 12 Vessel pressure history for Test 824.

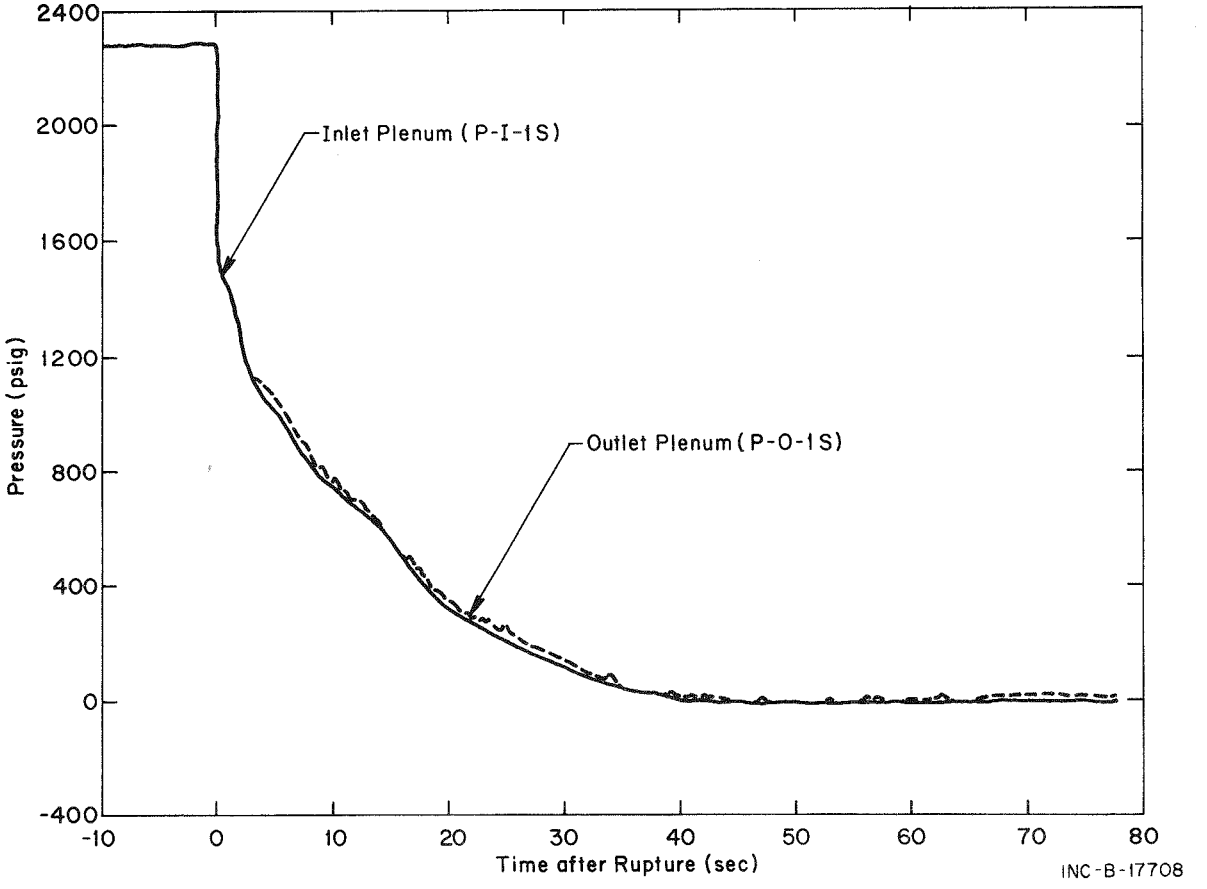

Fig. 13 Vessel pressure history for Test 825.

2. TEMPERATURE

The presentation of measured temperature data is separated into a section on fluid temperatures and a section on material (pin cladding and insulator, vessel internals, and piping) temperatures. All temperatures recorded during the decompression tests were measured with Chromel-Alumel thermocouples. The overall accuracy of these measurements is considered to be within ± 5% of full scale (within ± 30°F).

To improve the accuracy of the initial fluid temperature measurements, resistance temperature bulbs (RTB's), with an accuracy within ± 1°F, were installed at strategic locations in the system. All fluid temperature data have been normalized at the initial test conditions to agree with the initial temperature indicated by the closest RTB. The accuracy of the normalized transient temperatures is estimated to be within ± 1% of full scale, or within ± 6°F.

2.1 Fluid Temperatures

The initial temperatures for Tests 824 and 825, given earlier in Table I, are reproduced here for convenience.

	Test 824	Test 825
Vessel outlet	640°F	600°F
Vessel inlet	590°F	560°F

These temperatures represent, within a few degrees, the hot and cold leg initial temperatures for both tests; initial temperature drops exist across the steam generator comparable to the initial temperature rises across the core.

In general, the fluid temperatures drop slightly upon system rupture and during the subcooled expansion of the fluid. As soon as the fluid near the break (vessel outlet nozzle and outlet plenum) has expanded to near-saturation conditions at the local temperatures, the temperature of fluid in this vicinity decreases with saturation temperatures for the balance of decompression. Figures 14 and 15 present in-vessel temperature measurements for Tests 824 and 825 for the early portion of the blowdown transient. For both tests, the outlet plenum temperature drops rather sharply due to subcooled expansion of the fluid for the first 0.2 sec following rupture. The larger and more rapid temperature drop in Test 824 (Figure 14) is due to a lower initial degree of subcooling (higher initial temperature at comparable pressure). Following the initial temperature drop, the outlet plenum temperature decreases at a reduced rate corresponding to rate of decrease of saturation pressure in the outlet plenum.

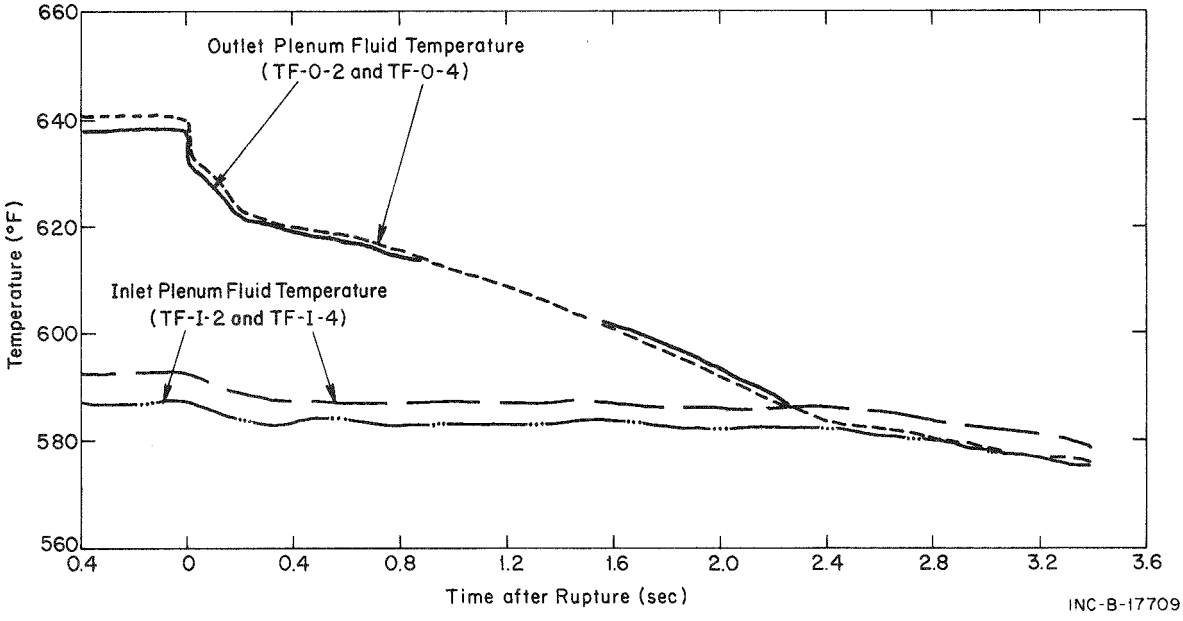

Fig. 14 Vessel plenum temperatures during the initial portion of saturated decompression - Test 824.

The inlet plenum temperatures, also shown in Figures 14 and 15, do not exhibit initial decreases during subcooled fluid expansion comparable to those of the outlet plenum temperatures. Inlet plenum temperatures remain nearly constant for the first 2 to 3 sec of blowdown; during this time, fluid in the inlet plenum (and the cold leg) remains in the subcooled state. Only after the fluid in the outlet plenum and hot leg reaches a state commensurate with saturation conditions for the inlet plenum and cold leg does the inlet plenum temperature start to drop significantly. As mentioned previously in the presentation of pressure data, and as indicated by Figures 14 and 15,

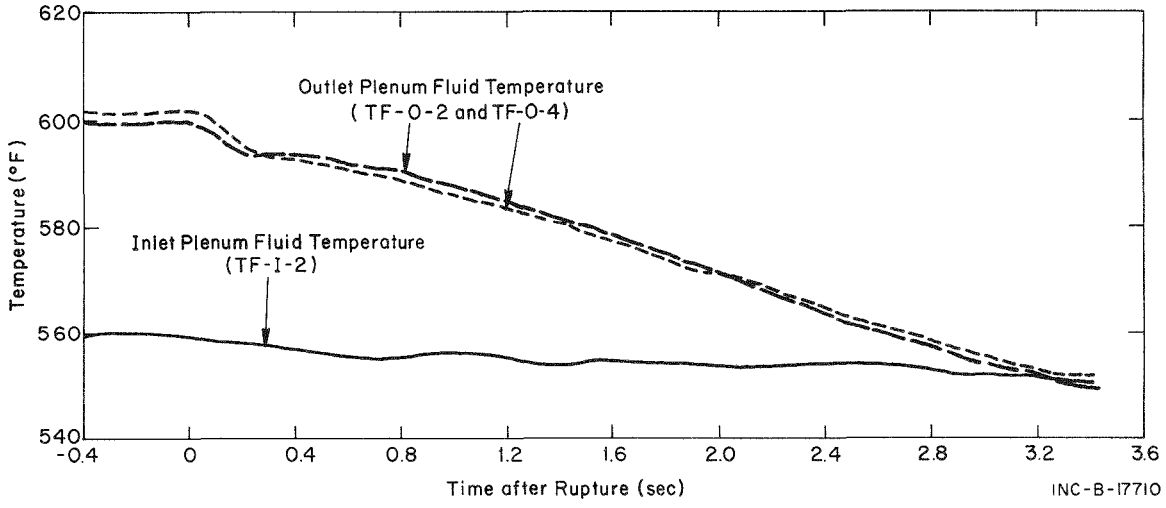

Fig. 15 Vessel plenum temperatures during the initial portion of saturated decompression - Test 825.

this event occurs at 2.3 sec for Test 824 and 3.2 sec for Test 825. Figures 16 and 17 show the entire transient temperature history for in-vessel locations. The rate of vessel fluid temperature decrease was similar for the two tests during the major portion of saturated decompression.

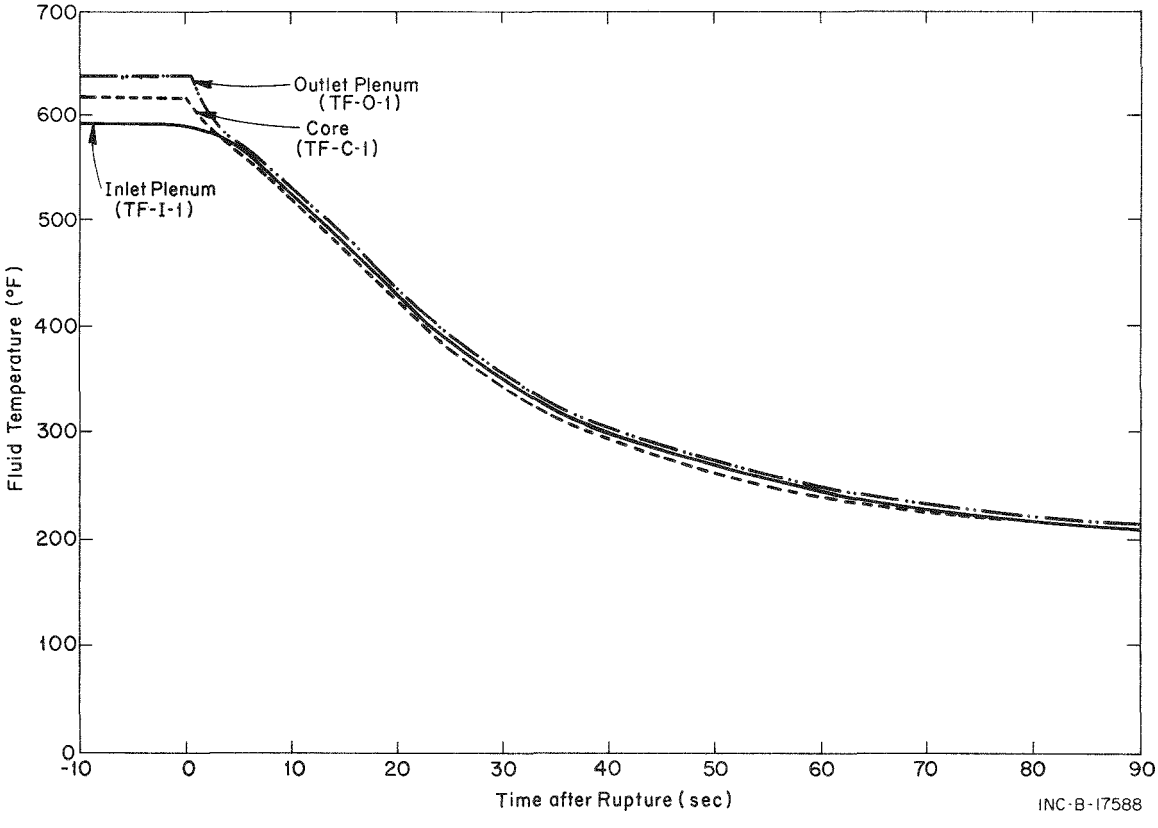

Fig. 16 Vessel fluid temperature history - Test 824.

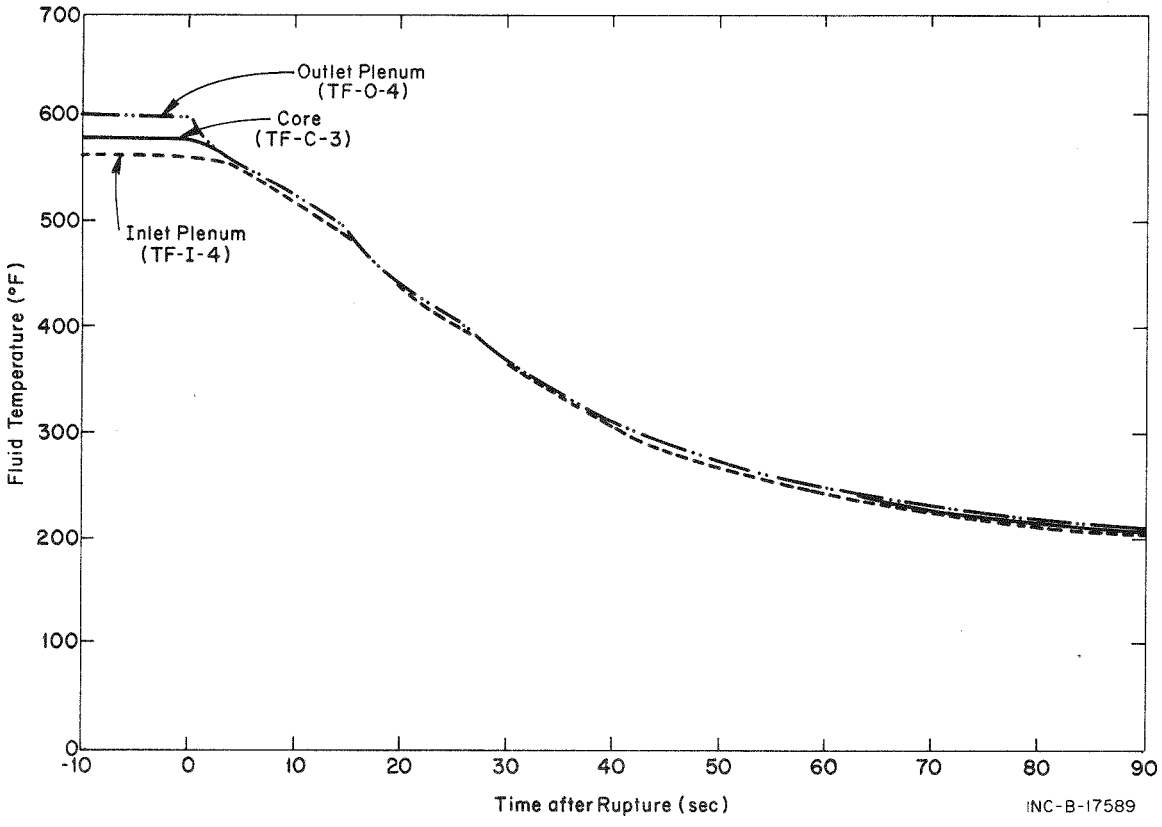

Fig. 17 Vessel fluid temperature history - Test 825.

Figures 18 and 19 present fluid temperature histories recorded at various loop locations for Tests 824 and 825. The temperature at the steam generator inlet, for both tests, dropped momentarily a few seconds after rupture to a value below the cold leg temperature. This temperature dip is a result of colder fluid (500°F), blown down from the auxiliary loop (Figure 1), reaching the steam generator. The real significance of this temperature dip is that it indicates flow is maintained in the normal flow direction around the loop, at least for the first few seconds after rupture. Continuation of flow in the normal direction is supported by the steam generator pressure drop measurements.

As soon as the vessel outlet and hot leg fluid has decompressed to the inlet plenum and cold leg saturation pressure and temperature, all fluid temperatures decrease according to saturation conditions (hot and cold leg saturation temperatures differ by only 10 to 15°F). During later stages of saturated blowdown, when the quality of the fluid in the vicinity of a thermocouple becomes high, the thermocouple receives heat by means of radiation from nearby metal surfaces. As a result, the data from the thermocouple affected shows uncharacteristic increases or other erratic temperature behavior. This phenomenon, referred to in this report as temperature "breakaway", can be used to identify and locate liquid voiding (flow separation or stagnation) within the system during decompression.

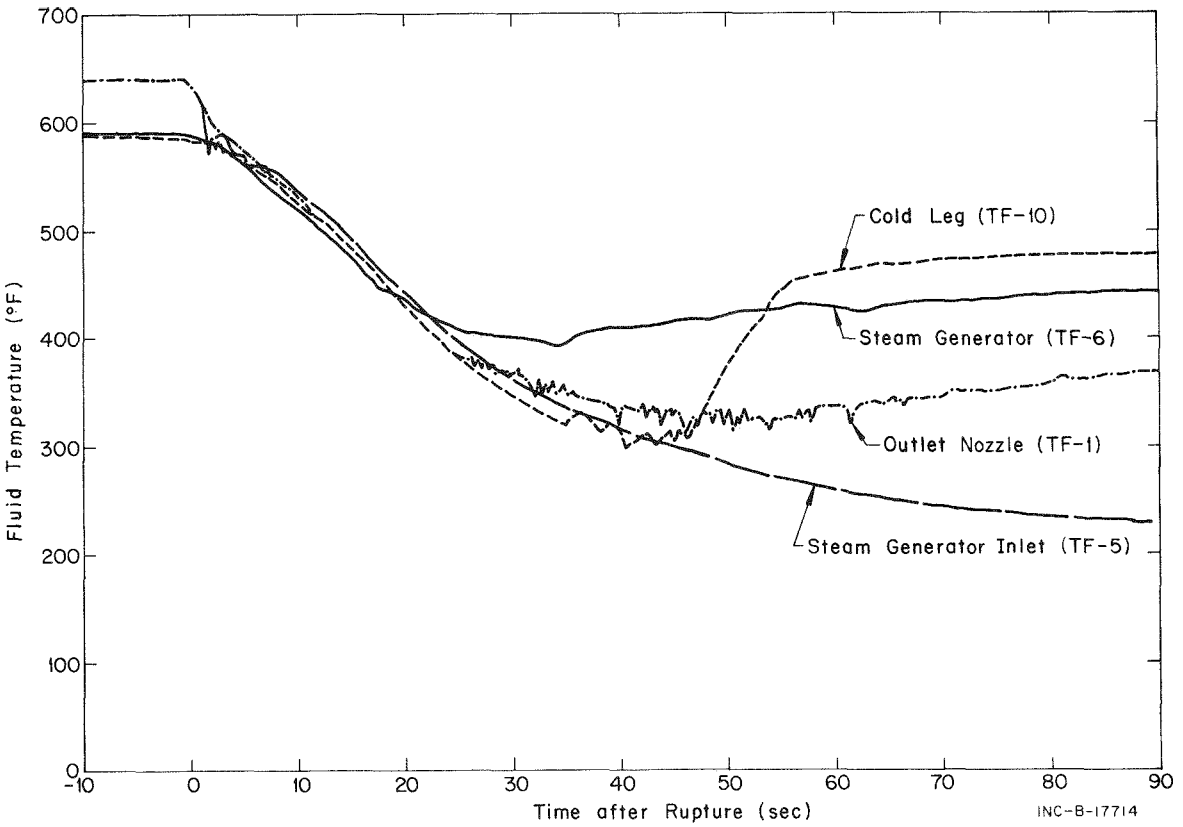

Fig. 18 Loop fluid temperatures - Test 824.

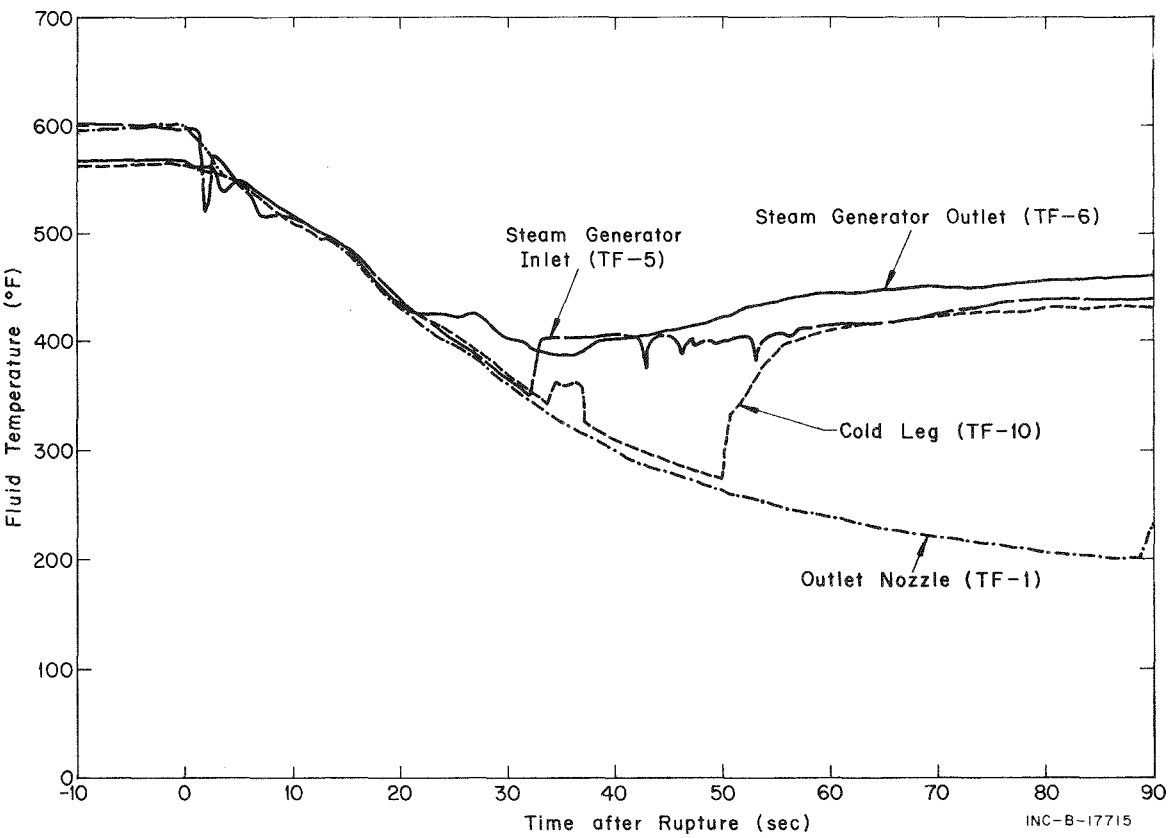

Fig. 19 Loop fluid temperatures - Test 825.

Temperature breakaway first occurs at the steam generator outlet in both tests at about 20 sec after rupture (Figures 18 and 19). An even more striking example of temperature breakaway is the sudden rise in cold leg temperature at 45 to 50 sec after rupture in both tests.

Comparison of the temperature behavior at the steam generator inlet and the vessel outlet nozzle for the two tests reflects the difference in test conditions between Tests 824 and 825. For Test 824, steam generator operation was maintained throughout decompression. Steam generator inlet temperature data in Figure 18 indicate no temperature breakaway suggesting the continued presence at this location of fluid of sufficient quality to limit heat radiation effects. High quality fluid could remain at the steam generator inlet if a stagnation point existed in the pump section leg near the steam generator outlet; such a stagnation point is indicated by steam generator outlet temperature breakaway as noted earlier. For Test 825, steam generator operation was terminated at rupture, and steam generator inlet temperature breakaway is indicated at about 32 sec in Figure 19.

Behavior of vessel outlet nozzle temperature for the two tests reflects the difference in duration of core heat application between the two tests. Core power was shut off at rupture for Test 824; the vessel outlet nozzle temperature data in Figure 18 show erratic (breakaway) behavior. Core power was continued about 14 sec after rupture for Test 825; no erratic behavior is indicated by the outlet nozzle temperature data in Figure 19. Because of the continued core operation in Test 825 and the correspondingly greater steam generation, the fluid velocity at the vessel outlet nozzle is sufficient to adequately cool the thermocouple at that location.

2.2 Material Temperatures

Examples of typical material temperature behavior at various system, vessel, and core locations during the blowdown transient for Tests 824 and 825 are presented in Figures 20 and 21. Included are heater pin cladding temperatures at three elevations along the heated length, temperature of the insulator material temperature at the midelevation, temperature of the core flow skirt, and temperatures both external to and within the pipe wall at the outlet nozzle.

Cladding temperatures in Figures 20 and 21 are for the center pin (Pin 61) of the core and were measured with Chromel-Alumel thermocouples located approximately 0.015 in. below the cladding surface. For Test 824, Figure 20 shows that pin cladding temperatures at all three elevations decrease with coolant saturation conditions for the entire blowdown. However, beyond about 23 sec after rupture the thermocouple (TM-61-T) located 2 in. below the top of the heated length of the pin indicates a slower drop in temperature than that of lower pin elevations. The slower temperature drop at the top elevation is attributed to a decrease in cooling rate resulting from an increase in the fluid quality at this location. Similar temperature behavior is exhibited by data from the core flow skirt thermocouple (TM-CS-1-330) which is located on the inside surface at the top of the flow skirt.

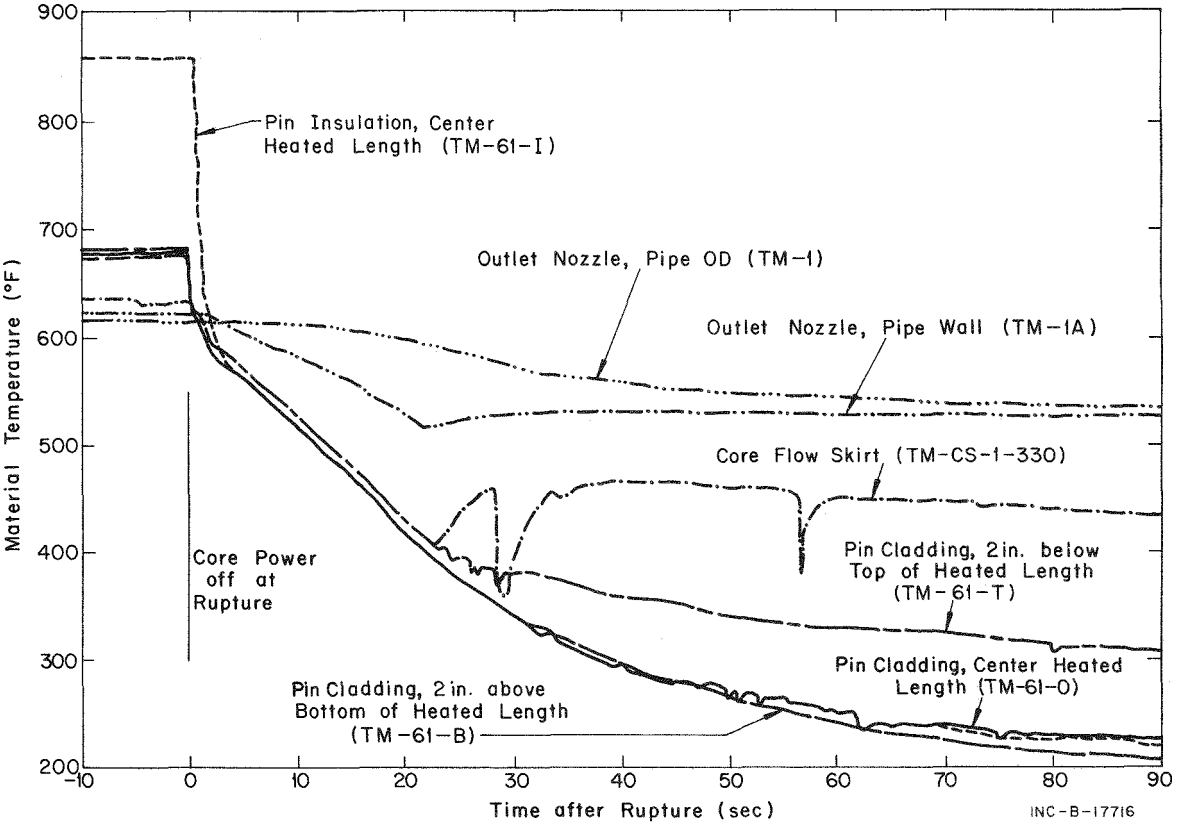

Fig. 20 Typical material temperatures - Test 824.

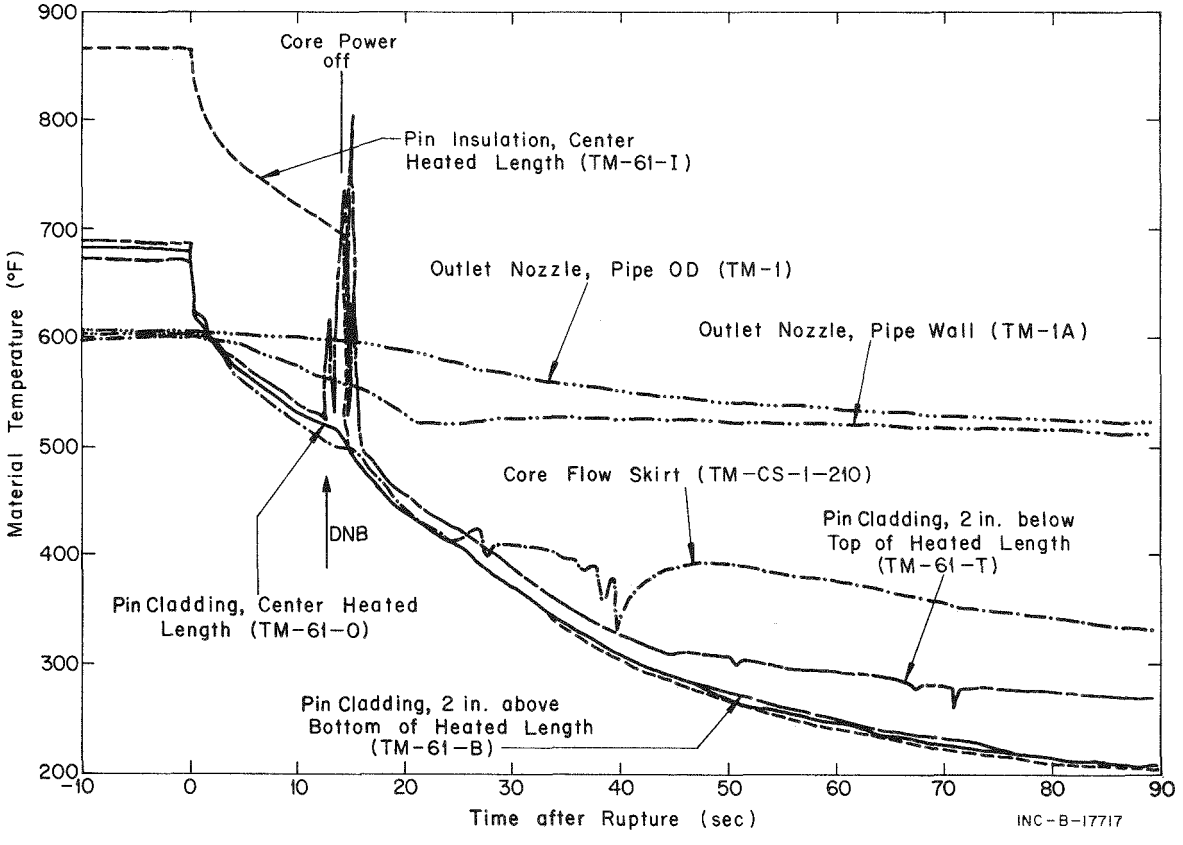

Fig. 21 Typical material temperatures - Test 825.

The effect of continued core power on heater pin material temperatures is evident from the data presented in Figure 21 for Test 825. The cladding temperature data for the top heater rod elevation (TM-61-T) indicate that departure from nucleate boiling (DNB) occurred at 12.5 sec after rupture with subsequent large temperature fluctuations until after core power was turned off and wetting of the heater pin surfaces was reestablished (about 16 sec after rupture).

The data for pin insulator temperatures further reflect continued core heating. For Test 824, the pin insulator temperature (TM-61-I) drops rapidly (within 2.5 sec after rupture) to the corresponding cladding temperature at the midelevation (TM-61-0) and generally follows saturation conditions until ambient saturation temperature is reached. For Test 825, the temperature difference between insulator and cladding remains nearly constant until the power is shut off; only then does the insulator temperature drop to essentially the fluid saturation and cladding temperature.

Heater pin temperature data, along with corresponding fluid temperature data, provide the basis for subsequent discussion (Section V) of core heat transfer. Additional pin temperature data for Tests 824 and 825 are presented in digitized form for various core locations and elevations in Appendix C.

Figures 20 and 21 also include the material temperature history recorded by thermocouples on the outside surface of the outlet nozzle wall (TM-1) and at a point 1/16 in. from the inside surface of the wall (TM-1A). The maximum temperature difference across the wall occurs 22 sec after rupture for both tests. The temperature difference is indicative of the rate at which heat is being absorbed from the piping wall by the fluid and is a measure of the resulting circumferential strain that is induced in the piping wall during decompression.

3. DENSITY

Fluid density data for semiscale tests are obtained by a gamma attenuation technique which provides a measurement of the average density. The normalization and conversion methods used in connection with the measurement technique are discussed in Appendix B. The estimated accuracy of the results is within about ± 2 lb/ft^3.

Density data for Tests 824 and 825 are presented in Figures 22 through 25. Comparison of fluid densities at various locations in the loop (Figures 22 and 23) shows similar behavior for these two tests even though power to the core was continued in Test 825 and was shut off at rupture in Test 824. At 4.5 sec for Test 824 and 6.5 sec for Test 825 fluid density in the hot leg (D-3) increases sharply to values typical of the cold leg density. The increase is attributed to a backflow of cold leg fluid and indicates that flow reversal occurred in the loop for both tests at about 4 to 6 sec following rupture. Even though the hot leg location, Station 3, is relatively close to the break, a high fluid density is maintained for a relatively long time during the decompression process. The significance of this behavior is discussed later with flow rates.

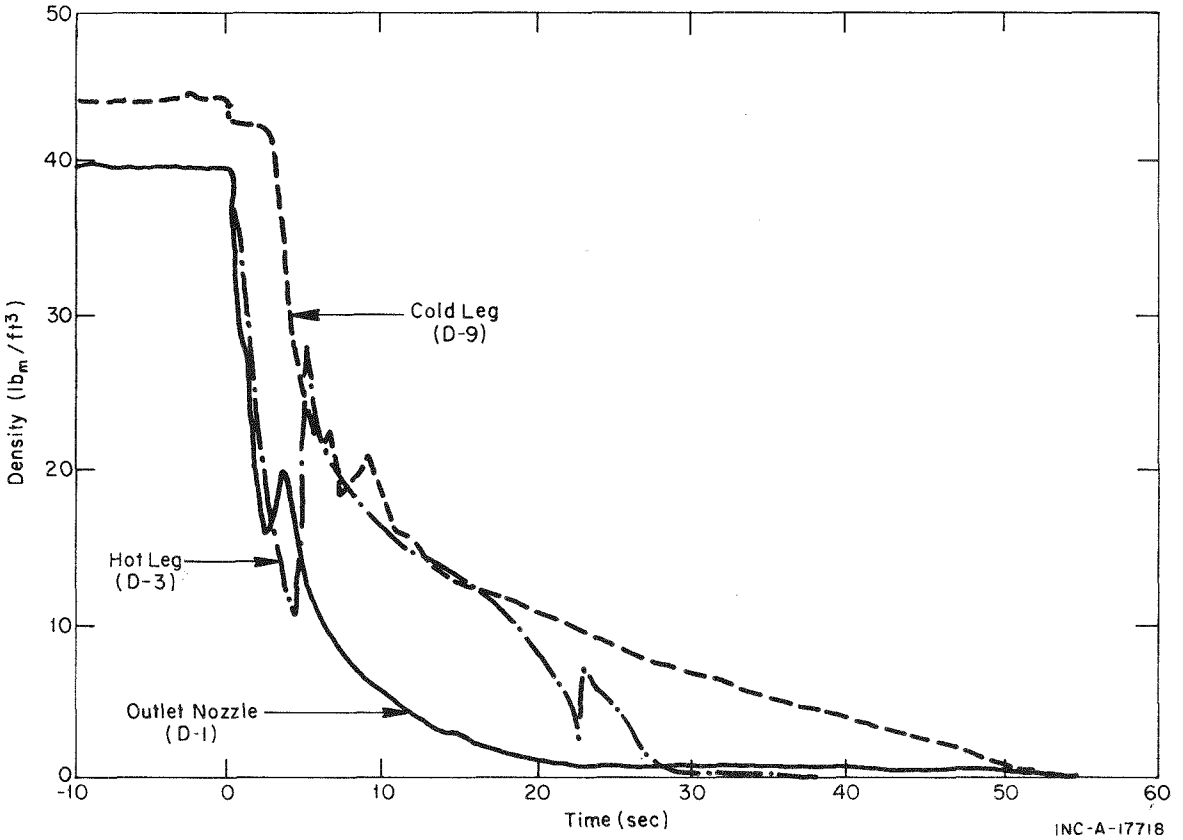

Fig. 22 Loop fluid density - Test 824.

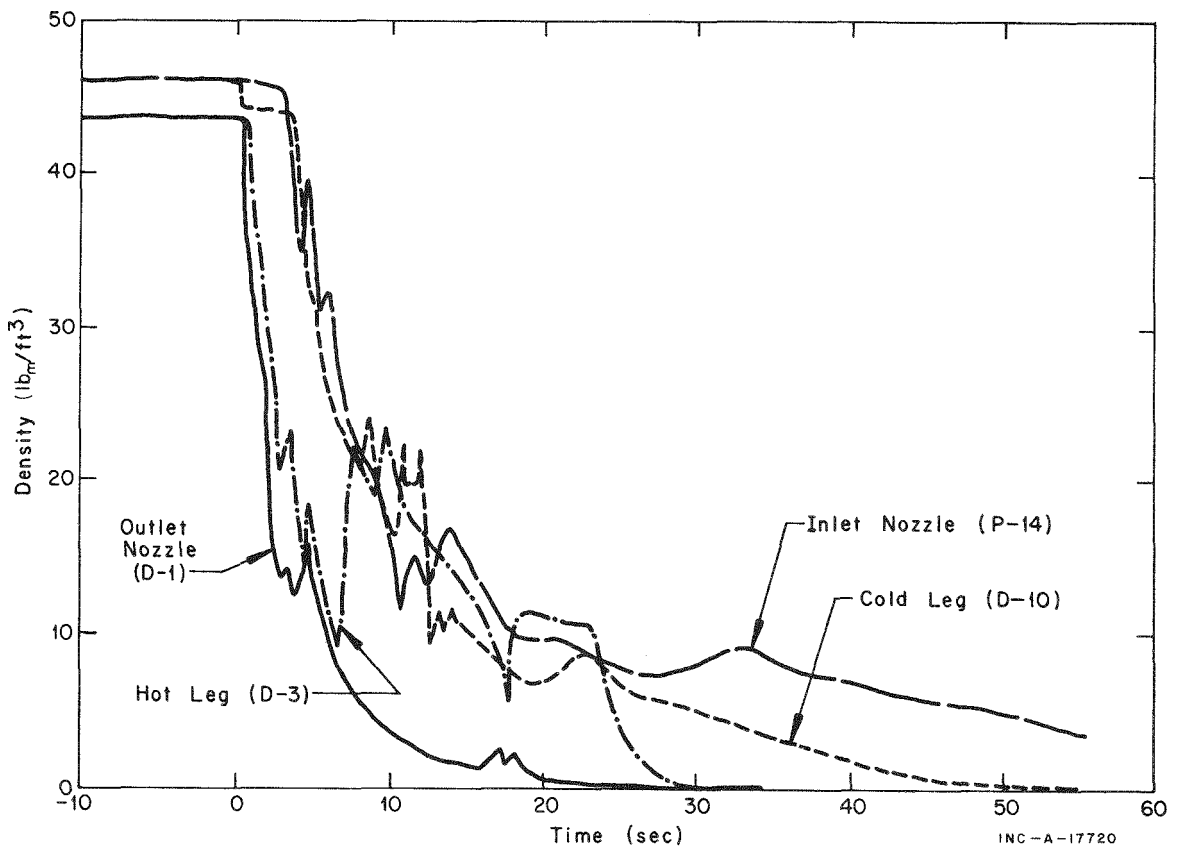

Fig. 23 Loop fluid density - Test 825.

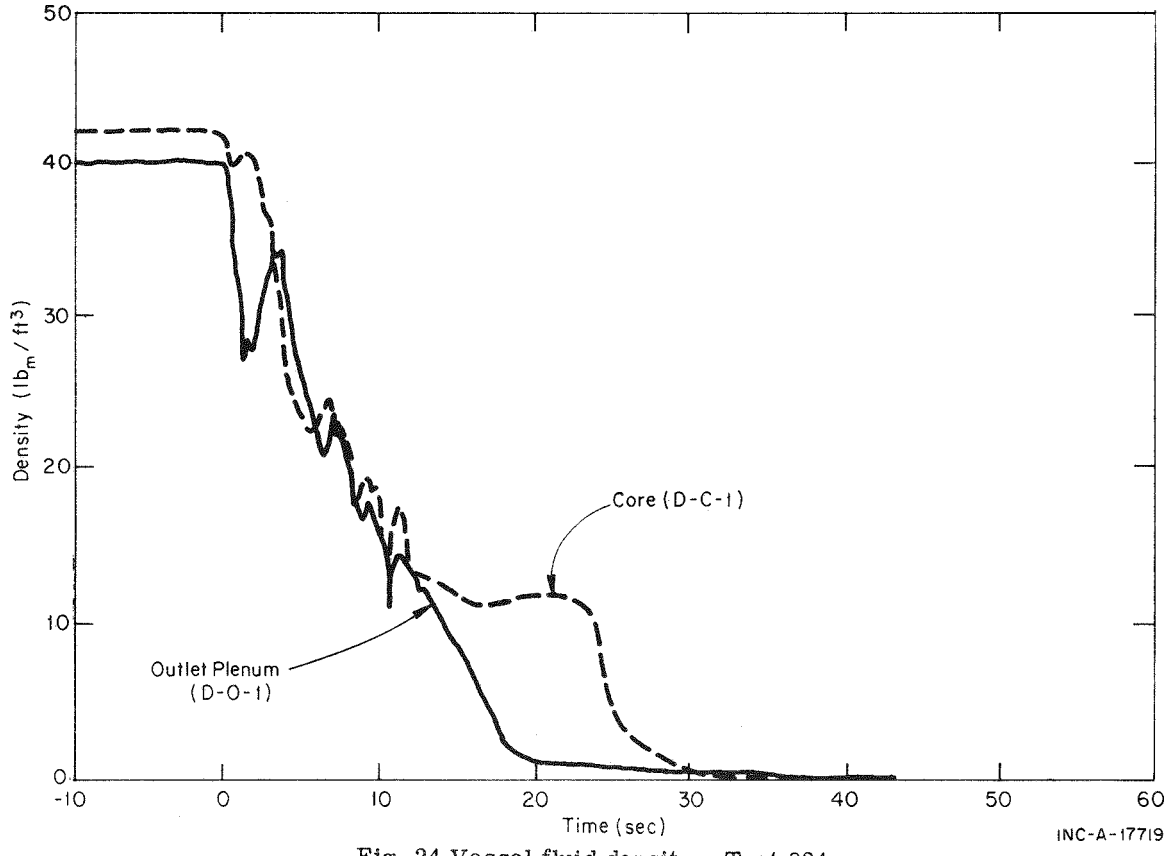

Fig. 24 Vessel fluid density - Test 824.

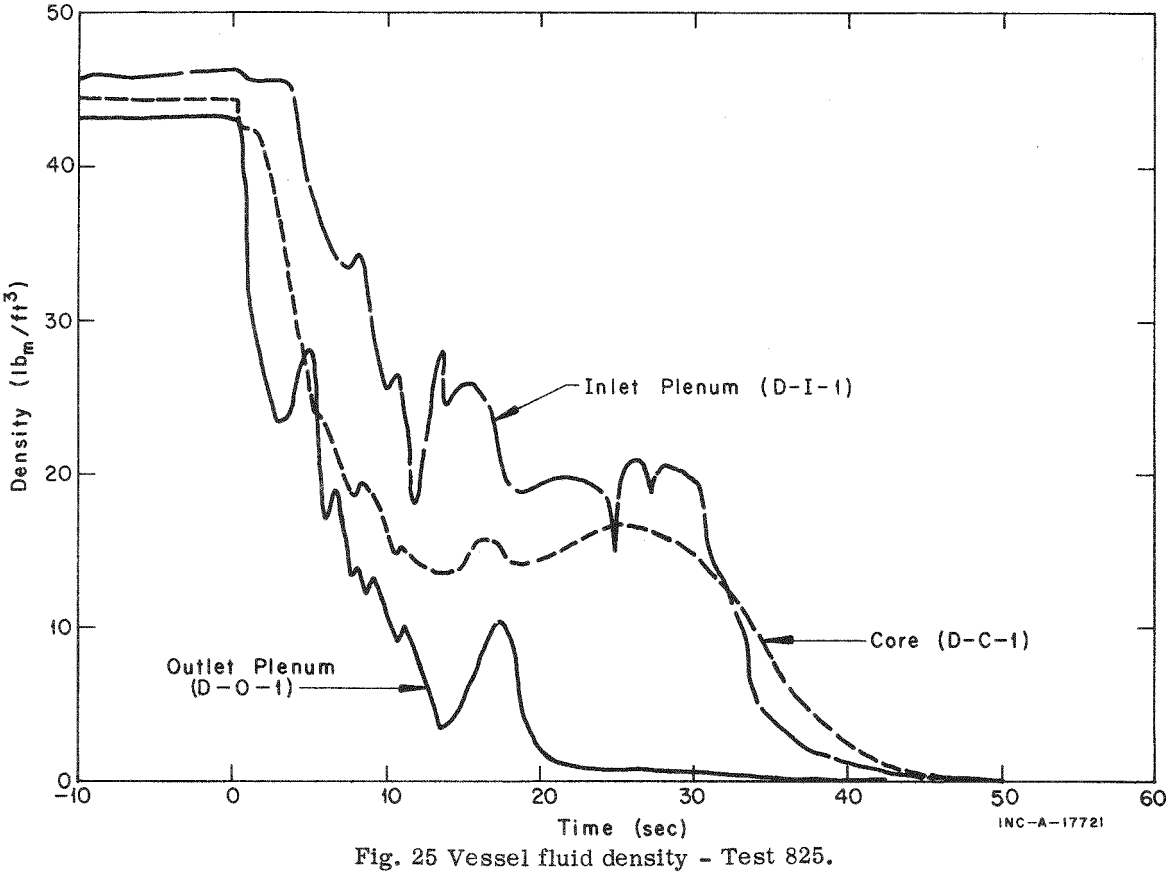

Fig. 25 Vessel fluid density - Test 825.

For both tests, the density of fluid flowing through the outlet nozzle past Station 1 (D-1) drops to less than 5 lb/ft^3 within 11 sec after rupture whereas the density in the balance of the loop remains relatively high for at least the first 20 sec of decompression.

Examination of the fluid densities measured at various locations in the vessel, Figures 24 and 25, shows that the fluid density in the core dropped immediately upon rupture to the density of fluid in the outlet plenum but promptly recovered to somewhat greater values for the first 3 or 4 sec of the blowdown transient. Densities in the core and outlet plenum are again similar from 3 to 12 sec in Test 824 and 4 to 7 sec in Test 825 and indicate that the fluids in these two sections of the vessel are undergoing a similar decompression process during this time interval.

Fluid densities in the core and outlet plenum decrease more rapidly than the density in the inlet plenum. As is evident in Figure 25 for Test 825, the inlet plenum density remains comparatively high for the first 20 sec of blowdown; the data indicate a lack of coupling between the inlet plenum fluid and fluid in the core and outlet plenum for this time period. For the final portion of the blowdown in Test 825, the core fluid density becomes similar to the fluid density in the inlet plenum; for this portion of decompression, the outlet plenum fluid does not exhibit strong coupling to other vessel fluid.

4. THRUST

Figure 26 presents horizontal thrust data for Tests 824 and 825. The plotted thrust is the sum of measurements from Load Cells 3 and 4 incorporated in the two horizontal trunnion supports on the vessel opposite the break location.

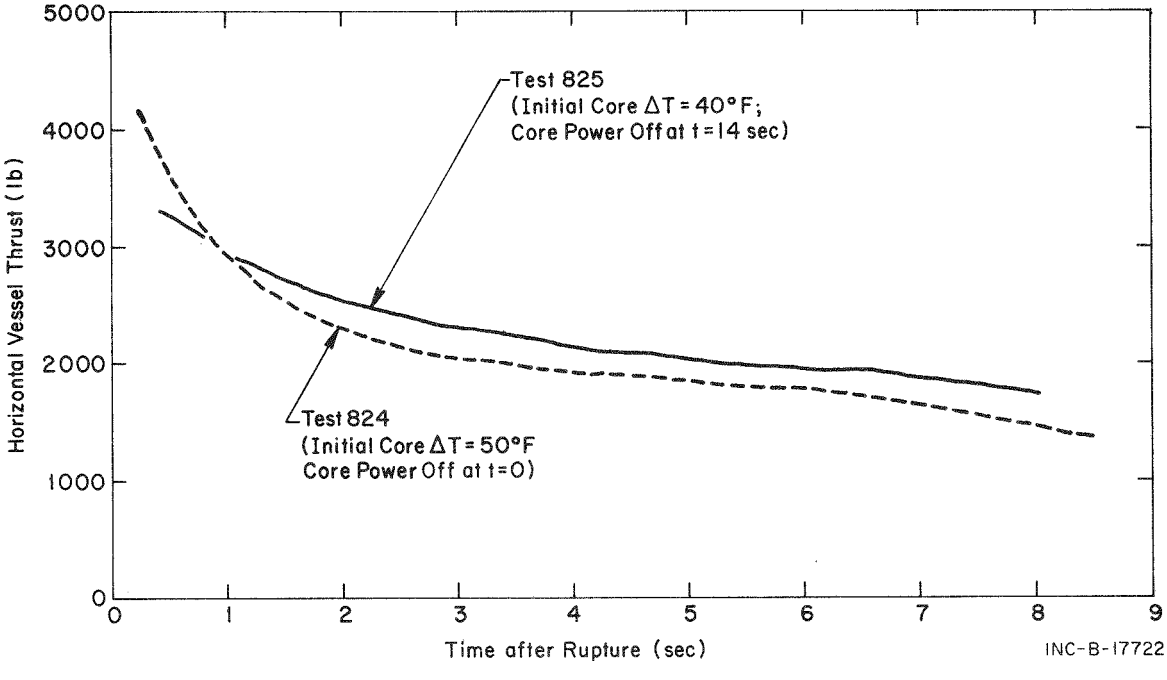

Fig. 26 Horizontal vessel thrust - Tests 824 and 825.

The data given are only for the early portion of the decompression process because large temperature changes in system piping later in blowdown and thermally-induced piping reactions distort the thrust data. A comparison of the measured horizontal thrust data with values calculated from pressure, density and flow rates is included in the discussion of test results (Section V). Examples of the uncorrected load cell data are included in Appendix C. Normalization of these data to obtain thrust values is discussed in Appendix B.

5. LOOP STRAIN

Strain gages are located on the outside of the piping at various locations in the loop. Measured circumferential strains resulting from the subcooled decompression are about 20 to 60 μin./in. (compressive). These values are as expected for a pressure decrease of 900 to 1000 psi. The largest strains, about 200 to 600 μin./in. (compressive), occur well into saturated blowdown and are, for the most part, thermally induced. A summary of the measured strains in the loop occurring during Tests 824 and 825 is given in Table II. The normalization process applied to the data is discussed in Appendix B. An example of the digitized loop strain data is included in Appendix C.

TABLE II

LOOP STRAIN MEASUREMENTS -- SEMISCALE TESTS 824 AND 825

		Test 824 Indicated Strain[a] (μin./in.)		Test 825 Indicated Strain[b] (μin./in.)	
Detector	Station[a]	Subcooled	Saturated	Subcooled	Saturated
S-1A	1	-30 (A)	-440 (A)	-25 (A)	-370 (A)
S-1C	1	-50 (C)	-590 (C)	---	---
S-14A	14	-20 (A)	-180 (A)	---	---
S-14C	14	-50 (C)	-315 (C)	-65 (C)	-375 (C)
S-23-A2	23	---	---	-15 (A)	-175 (A)
S-23-B1	23	-20 (A)	-395 (A)	-15 (A)	-265 (A)
S-36-A1	36	-20 (A)	-230 (A)	-20 (A)	-215 (A)
S-36-B1	36	-20 (A)	-225 (A)	-20 (A)	-225 (A)
S-36-B2	36	-20 (A)	-235 (A)	-15 (A)	-250 (A)
S-36-C	36	---	---	-60 (C)	-345 (C)

[a] The station designation refers to the location in the loop as given by Figure 1 or Appendix A.

[b] Axial strain indicated by (A) and circumferential strain indicated by (C).

6. WATER REMAINING IN SYSTEM

Posttest determination was made of water remaining in the system. About 6 min after system rupture (decompression is complete in less than 1 min), drains were opened at low points in the loop (steam generator inlet, pump inlet, and piping low point) and in the vessel (bottom head) to collect residual water. Table III presents the water remaining in pounds and as a percent of initial system fluid (about 530 lb) for Tests 824 and 825. Continuation of steam generator operation during decompression (Test 824) seems to have affected the amount of water remaining in that section of the system.

TABLE III

WATER REMAINING IN SYSTEM AFTER DECOMPRESSION -- SEMISCALE TESTS 824 AND 825

Location	Test 824	Test 825
Low loop point	0	0
Pump inlet	0	0
Steam generator inlet	4.5 lb (0.85%)	0
Vessel bottom head	8.75 lb (1.65%)	17 lb (3.2%)
Total water remaining	13.25 lb (2.5%)	17 lb (3.2%)

V. DISCUSSION OF TEST RESULTS

The previous section of this report has dealt primarily with variables that were measured directly in Tests 824 and 825 and which required a minimum of mathematical processing for presentation. These test data have, in turn, been used to calculate additional variables such as fluid flow rates, fluid quality, and heat tranfer coefficients which aid in understanding fluid behavior during decompression. The additional test discussion in this section includes the methods and techniques used in calculations.

1. FLUID FLOW RATES

Calculation of the fluid flow rate during the blowdown transient is accomplished by combining two measured quantities: momentum flux (ρv^2) and density (ρ). The density measurements made during Tests 824 and 825 were presented and discussed previously (Section IV-3). The momentum flux measurements were made with devices which employ a drag disc placed in the flowing fluid. The force exerted on the disc is proportional to the momentum flux and essentially supplies the velocity component required for calculation of the fluid flow rate from the equation

$$\dot{m} = [\rho(\rho v^2) A^2]^{1/2} \text{ or } \dot{m} = \rho v A \qquad (1)$$

where

$\dot{m}$ = fluid flow rate (lb/sec)

ρ = measured density (lb/ft^3)

ρv^2 = measured momentum flux ($lb/sec^2\text{-}ft$)

A = cross-sectional flow area (ft^2).

An example of the output signal (volts) from one of the drag disc flowmeters is presented in Appendix C. The meter output is converted to momentum flux through a calibration curve for the instrument.

The accuracy of the fluid flow rate calculations is dependent on the accuracy of the momentum flux and density measurements. As mentioned in the discussion of density measurements, estimated accuracy is within $\pm$ 2 lb/ft^3. The results of flow rate calculations based on very low densities (less than 2 lb/ft^3) thus must be used with caution. In addition, the drag disc flowmeters are temperature sensitive and are subject to considerable thermal drift during the approximately 400°F fluid temperature drop encountered during the blowdown transient. The thermal drift is particularly pronounced for tests involving small breaks and long blowdown times. As outlined in Appendix A, compensation for thermal drift consists of applying a linear correction with time to the measured momentum flux data. Experience gained in performance of system mass balances[3] has demonstrated that this correction process yields acceptable results.

For Tests 824 and 825, detectors to measure the density, momentum flux, pressure, and fluid temperature, were located at stations in the system such that a mass balance could be performed for the system or across desired components. To obtain a mass balance for the system, appropriate detectors were located in the hot leg (Station 3) and the vessel outlet nozzle (Station 1). Additional detectors were located in the inlet nozzle (Station 14) and inlet plenum (to measure fluid conditions at the core inlet) and the pump suction leg (Station 6 or 7).

Due to an inordinately large number of detector failures during Test 824, only the flow through the vessel outlet nozzle could be calculated; the desired mass balances for the system and vessel could not be obtained. The flow past the outlet nozzles is presented in Figure 27 and indicates that approximately 55% of the 530 lb total initial system mass was ejected from the system through the vessel outlet nozzle. A maximum flow rate of 85 lb/sec occurred shortly after rupture for Test 824.

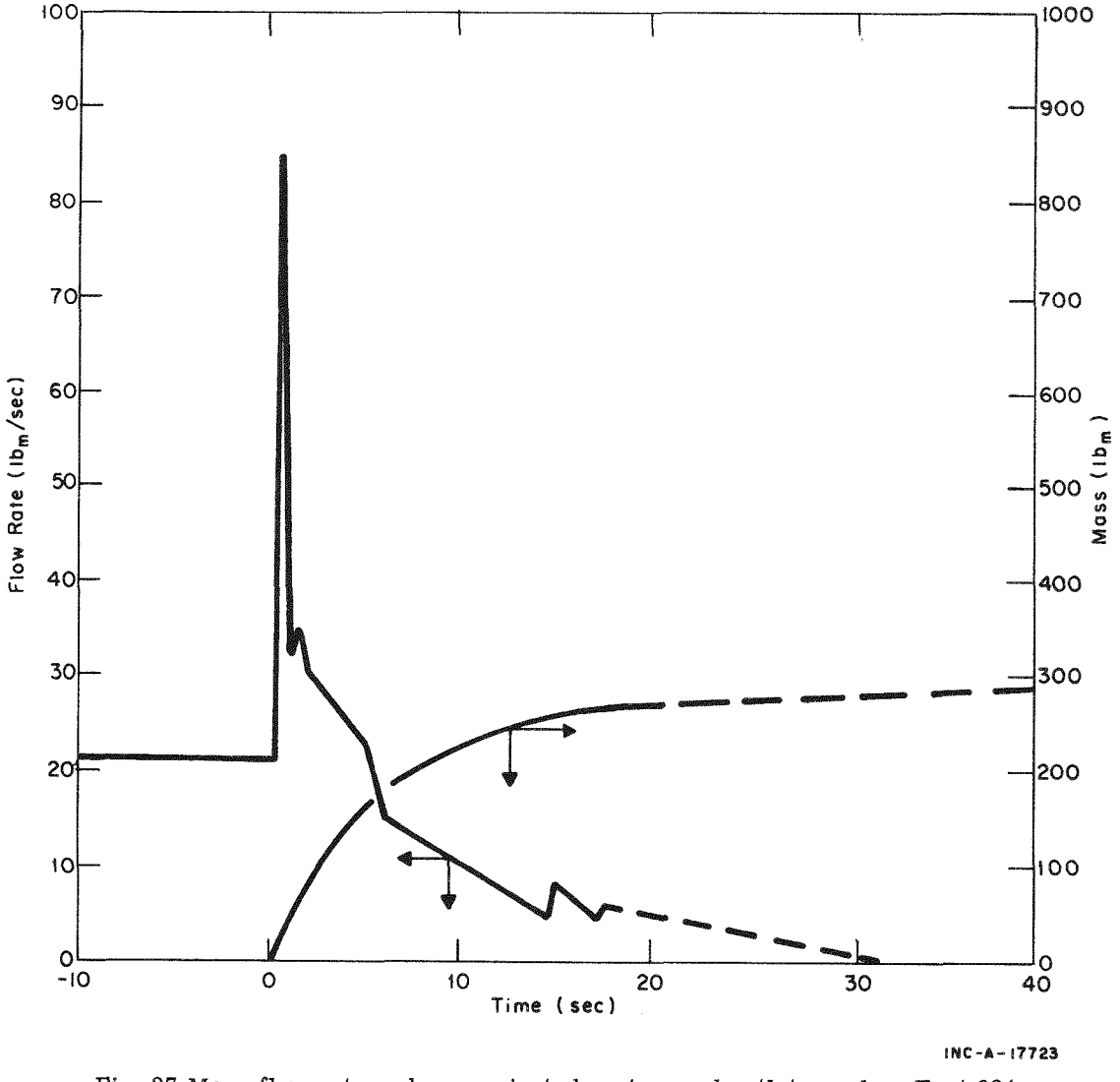

Fig. 27 Mass flow rate and mass ejected past vessel outlet nozzle - Test 824.

The calculated fluid flow rates from the system through the vessel outlet nozzle and the hot leg for Test 825 are shown in Figure 28. The maximum flow rate through the vessel outlet nozzle (88 lb/sec) occurred shortly after rupture and is about four times the flow rate prior to rupture. Comparison of outlet nozzle flow rates for the two tests shows close agreement.

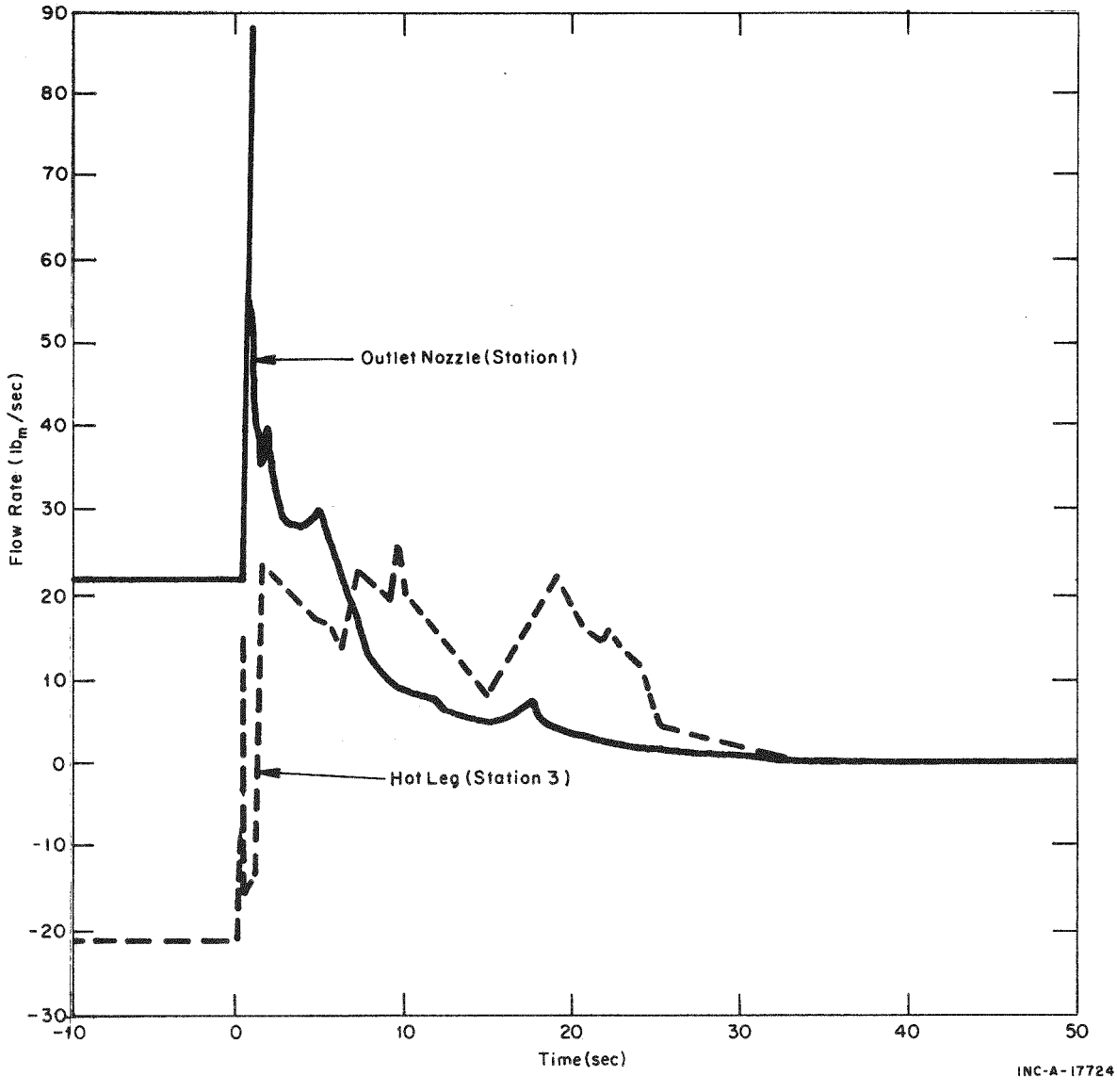

Fig. 28 Mass flow rate from system - Test 825.

Figure 29 presents the mass ejected from the system through the vessel outlet nozzle (Station 1) and from the hot leg (Station 3) for Test 825. A total mass ejected of approximately 690 lb, or 130% of the initial fluid mass, is indicated. The error is reflected in the total fluid mass remaining in the system for Test 825, included in Figure 29.

The major source of error in the total mass ejected in Test 825 is thought to be thermal drift of the drag-disc flowmeter located in the hot leg (Station 3). Examination of the flow rate from the hot leg (Figure 28) indicates that,

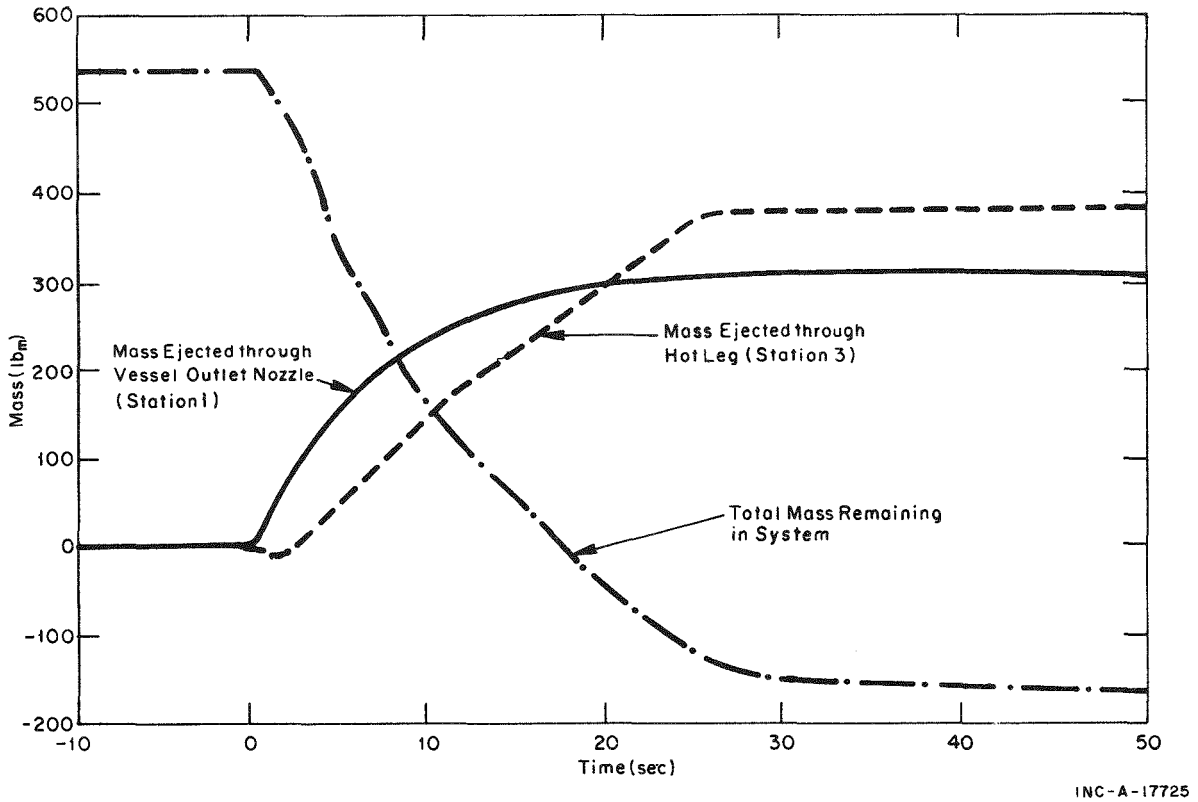

Fig. 29 Mass ejected from system and total mass remaining - Test 825.

after an initial surge at rupture, the flow continued into the loop for about 1 sec after rupture (the initial hot leg flow past Station 3 is in a direction opposite the flow during blowdown, hence the negative sign for the initial flow) and then reversed to be ejected from the system, at a rate varying from approximately 10 to 20 lb/sec for most of the remainder of blowdown. The high fluid flow rate from the hot leg indicated from 15 to 25 sec after rupture is thought to be due to thermal drift of the drag-disc flowmeter rather than to actual flow.

Due to the thermal drift problem associated with the hot leg flowmeter and the resulting data, additional mass balances, based on the vessel outlet nozzle flow and the change of mass calculated from the measured densities in various segments of the system were made throughout the system. The integrated masses flowing through the inlet nozzle and the hot leg resulting from these mass balance calculations are shown in Figure 30 and a comparison of the calculated fluid flow rate through the vessel inlet nozzle and core inlet is shown in Figure 31. Comparison of the curve for the integrated flow through the hot leg past Station 3, as measured, and the integrated flow based on the mass balance calculations (Figure 30) indicates good agreement for the first 5 sec of blowdown when the fluid temperature is not greatly different from the initial temperature. After this time, however, the effects of the meter temperature sensitivity become predominant and the deviation between the curves for the measured and calculated flow increases with time for the remainder of the blowdown. The mass ejected from the system as determined from a mass balance of the calculated hot leg fluid flow rate (Station 3) and the vessel outlet nozzle flow (Station 1) is 480 lb, or 92% of

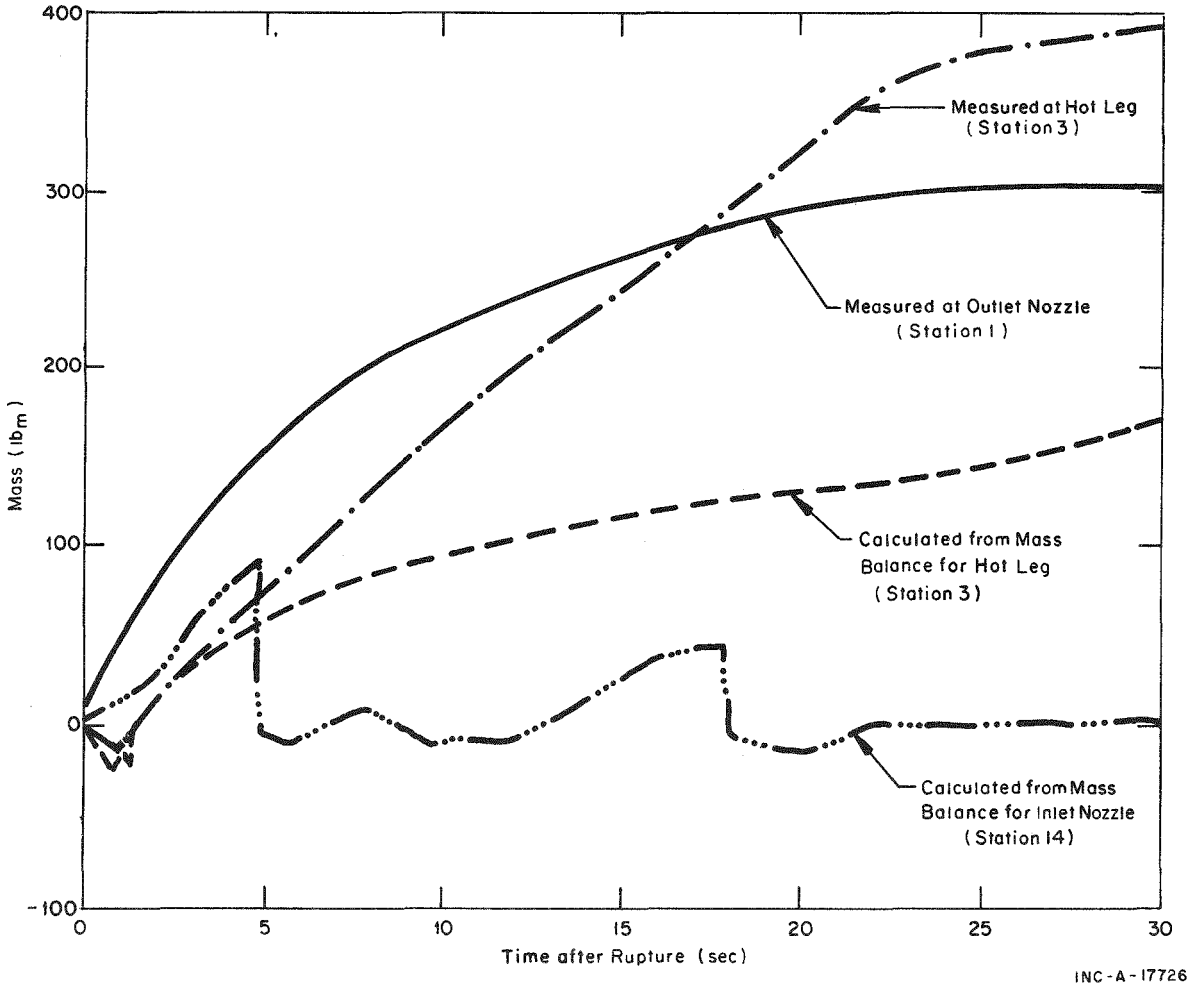

Fig. 30 Integrated mass flow - Test 825.

the initial 530 lb system mass. In addition, this mass balance indicates that about 58% of the available loop fluid mass and 41% of the vessel fluid mass are expelled from the system in the first 6 sec of blowdown.

The inlet nozzle and core flow rates, based on the mass balance calculations, and shown in Figure 31, indicate that the flow remained primarily in the normal flow direction (up through the core) for about the first 6 sec of blowdown. After this time these flow rates decreased to a very low value (approximately 7 lb/sec or less) and indicate that little or no fluid flow was available for core cooling until 14 sec after rupture when the power to the core was terminated. The calculated flow through the inlet nozzle and core increases in the normal flow direction from 14 to 16 sec and drops back to approximately zero flow at 18.5 sec. The power to the pump was terminated at 16.5 sec after rupture and the increase in flow rate from 14 to 16.5 sec may reflect the effects of the pump head after termination of core power and prior to the termination of pump power.

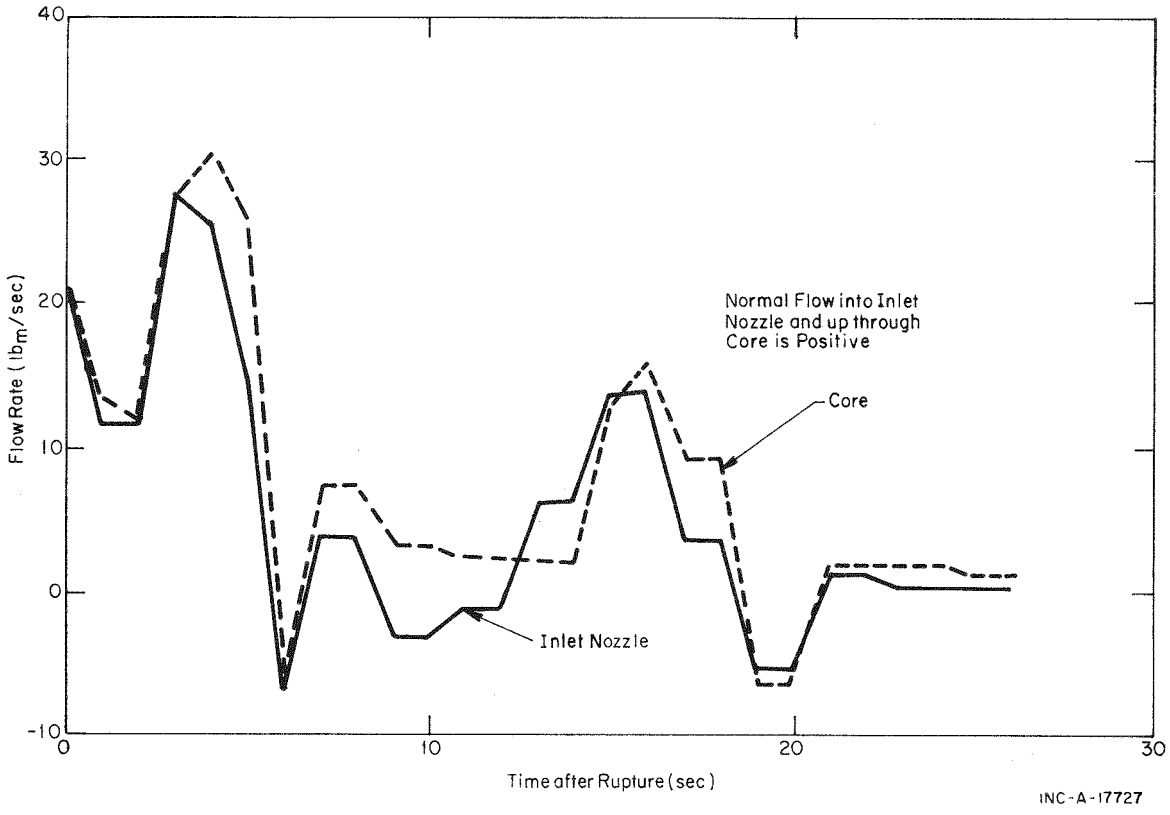

Fig. 31 Calculated flow rate in the core and inlet nozzle - Test 825.

2. CALCULATED THRUST

For Test 825 the horizontal thrust generated by the blowdown fluid as it was expelled through the break was calculated, using the calculated system fluid flow rates and measured pressures, temperatures, and densities. The equation used to calculate the thrust is:

$$T = \left(\frac{G^2}{g\rho_e} + P_e\right) A_e \qquad (2)$$

where

G = mass flux ($lb_m/sec\text{-}ft^2$)

g = gravitational constant

ρ_e = exit density (lb_m/ft^3)

P_e = exit pressure (psi)

A_e = exit pipe area (0.09 ft^2).

The measured pressure at the rupture disc assembly (Station 18) was used for the exit pressure (P_e), and the exit density (ρ_e) was calculated on the basis of an isenthalpic process after mixing of the flows from the vessel outlet nozzle (Station 1) and the hot leg (Station 3). The enthalpy at the vessel outlet nozzle and at the hot leg was determined from the system temperature and density at these points by assuming a saturated homogeneous mixture.

A comparison of the calculated thrust and measured thrust (Section IV-4) is given in Figure 32. This comparison is limited to the early portion of blowdown because thermally-induced piping reactions due to the large temperature changes in the pipe during the latter portions of blowdown distort the measured thrust data.

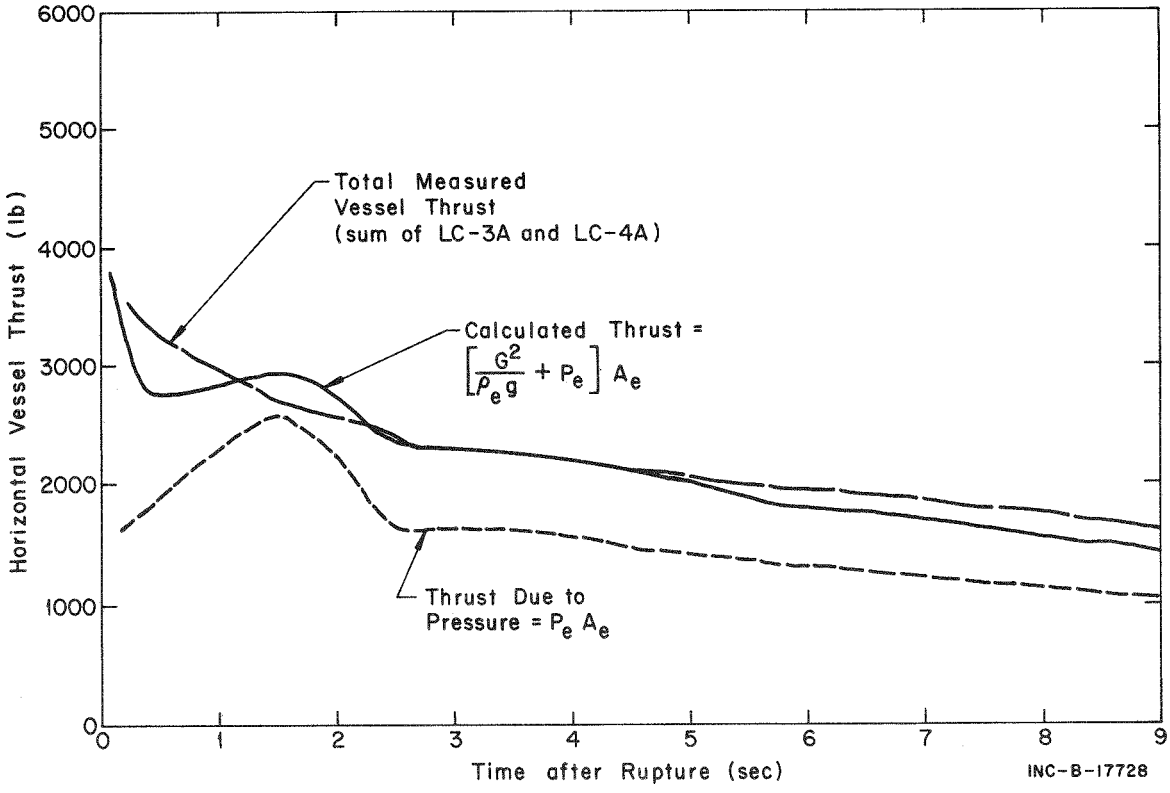

Fig. 32 Comparison of calculated and measured horizontal vessel thrust - Test 825.

The good agreement between the measured and calculated thrust supports the accuracy of the data for both the calculated flow rates presented in Section V-1, and the measured thrust data presented in Section IV-4, at least for the first 8 to 10 sec of blowdown.

The calculated contribution of the pressure term to the total thrust is also shown in Figure 32, and is about two-thirds of the total calculated thrust, whereas the remaining one-third is due to the momentum, or flow, term.

3. FLUID QUALITY AND THERMODYNAMIC PROPERTIES

The density data have been used in conjunction with the pressure and temperature data to determine the fluid quality in the vessel and at various locations in the loop piping. As mentioned in Section IV-3, the densities were measured through use of a gamma attenuation technique and are representative of the average fluid density at each specific location. The accuracy of the density measurements below 2 lb/ft^3 is questionable and, therefore, the fluid quality data reported above 30 to 40% must be used with caution.

The in-vessel and loop piping fluid qualities for Test 824 are shown in Figures 33 and 34 and for Test 825 in Figures 35 and 36. For both tests the fluid quality in the vessel outlet nozzle and plenum increased rapidly after rupture whereas the quality of the fluid in the cold leg (Test 824) and the inlet nozzle (Test 825) remained low well into blowdown. For both tests the quality of the fluid flowing from the hot leg (past Station 3) remained below 15% until 25 sec after rupture. The quality then rapidly rose to 100%, indicating that little phase separation occurred in the flowing fluid and that once the supply of system fluid from the steam generator and pressurizer flowed out of the system all that remained to flow from the hot leg was steam.

In marked contrast to the cold and hot leg fluid quality, the quality of the fluid in the vessel outlet plenum and nozzle rose rapidly after system rupture for both tests, indicating a large amount of phase separation. As shown in Figure 35, the quality of the fluid in the core and outlet plenum for Test 825 remained low much longer than that in the outlet plenum, indicating a distinct fluid separation or lack of coupling between the fluid in the outlet plenum and the remainder of the vessel. This lack of coupling is also evident in the results for Test 824 (Figure 33).

Of particular significance is the behavior of the fluid quality in the vessel outlet plenum for both tests. For the first 10 sec after rupture the fluid quality in the outlet plenum is similar for both tests, but at 14 sec for Test 825, the fluid quality decreases abruptly until about 18 sec. This decrease can be attributed to the fact that core power, which was terminated at rupture for Test 824, was continued for 14 sec after rupture for Test 825; the sudden change in heat input to the fluid in Test 825 momentarily allowed coupling between the fluid in the outlet plenum and the low density fluid in the core and inlet plenum. The same sudden drop in fluid quality in Test 825 is also apparent at the vessel outlet nozzle (Figure 36).

To aid in visualizing the process which the fluid follows during blowdown while going from a subcooled liquid to a saturated vapor at ambient conditions, the pressure, temperature, and density data were used to prepare temperature-entropy diagrams as shown in Figures 37 and 38 for Tests 824 and 825, respectively. With the exception of the fluid in the vessel outlet plenum and nozzle, the fluid remains at low quality during most of the fluid discharge at a given location and then abruptly changes to a high quality fluid. The results of Test 824 for locations at the outlet plenum and outlet nozzle indicate a rather smooth steady process of decreasing fluid density at these locations due to phase separation between the core region and the outlet plenum. Results for Test 825 indicate a more rapid and erratic fluid density decrease due to a combination of phase separation and steam generation by the hot core.

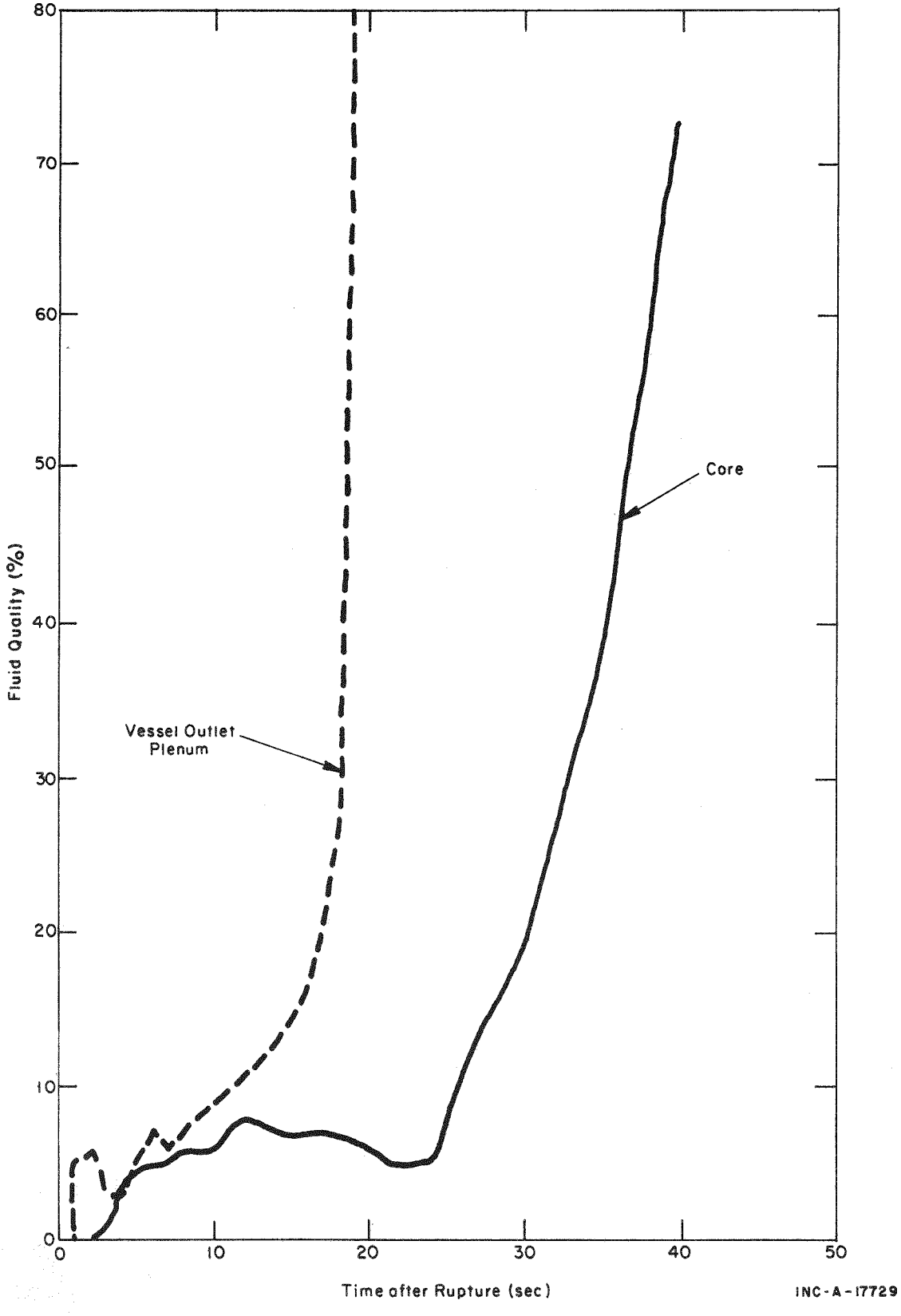

Fig. 33 Vessel fluid quality - Test 824.

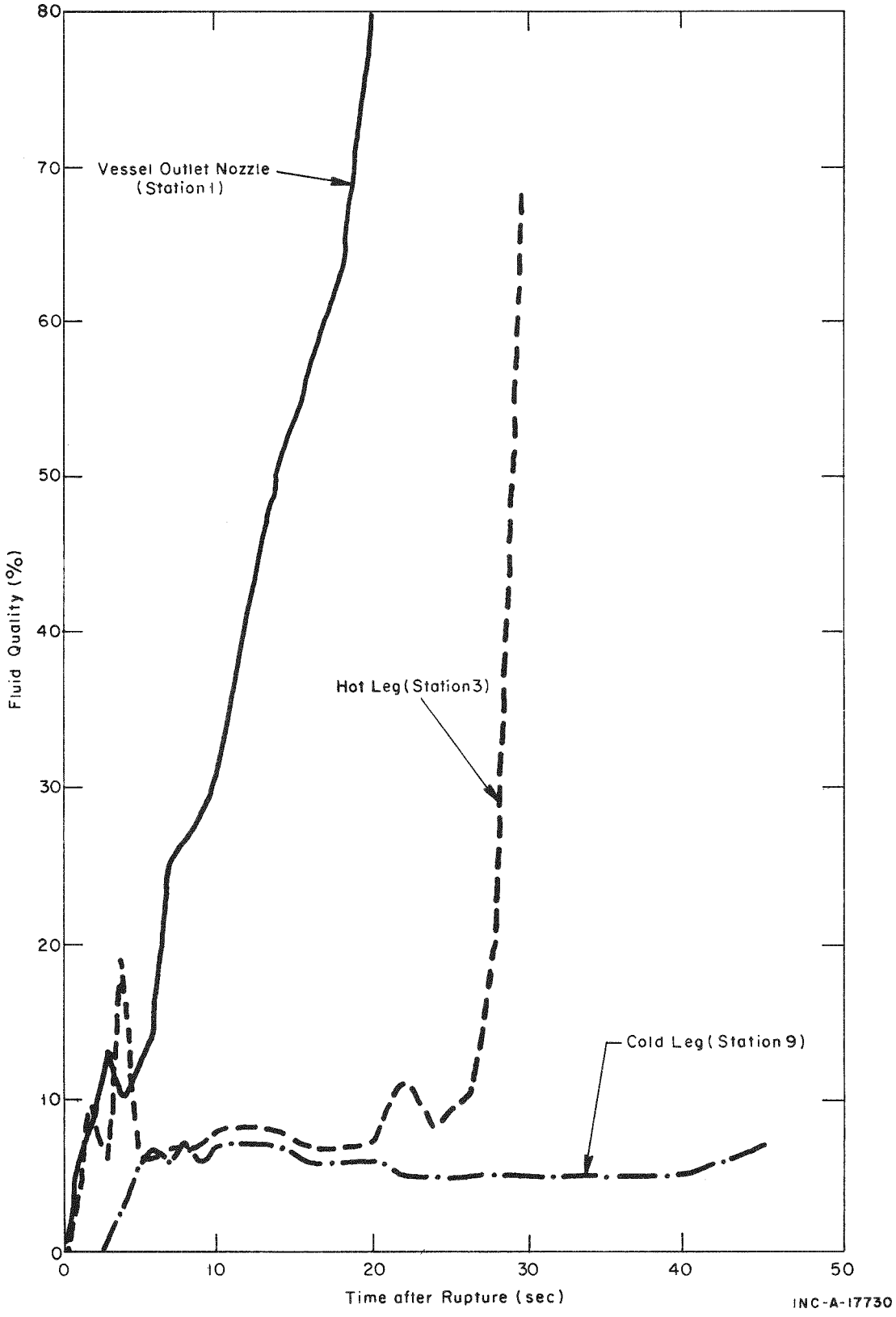

Fig. 34 Loop fluid quality - Test 824.

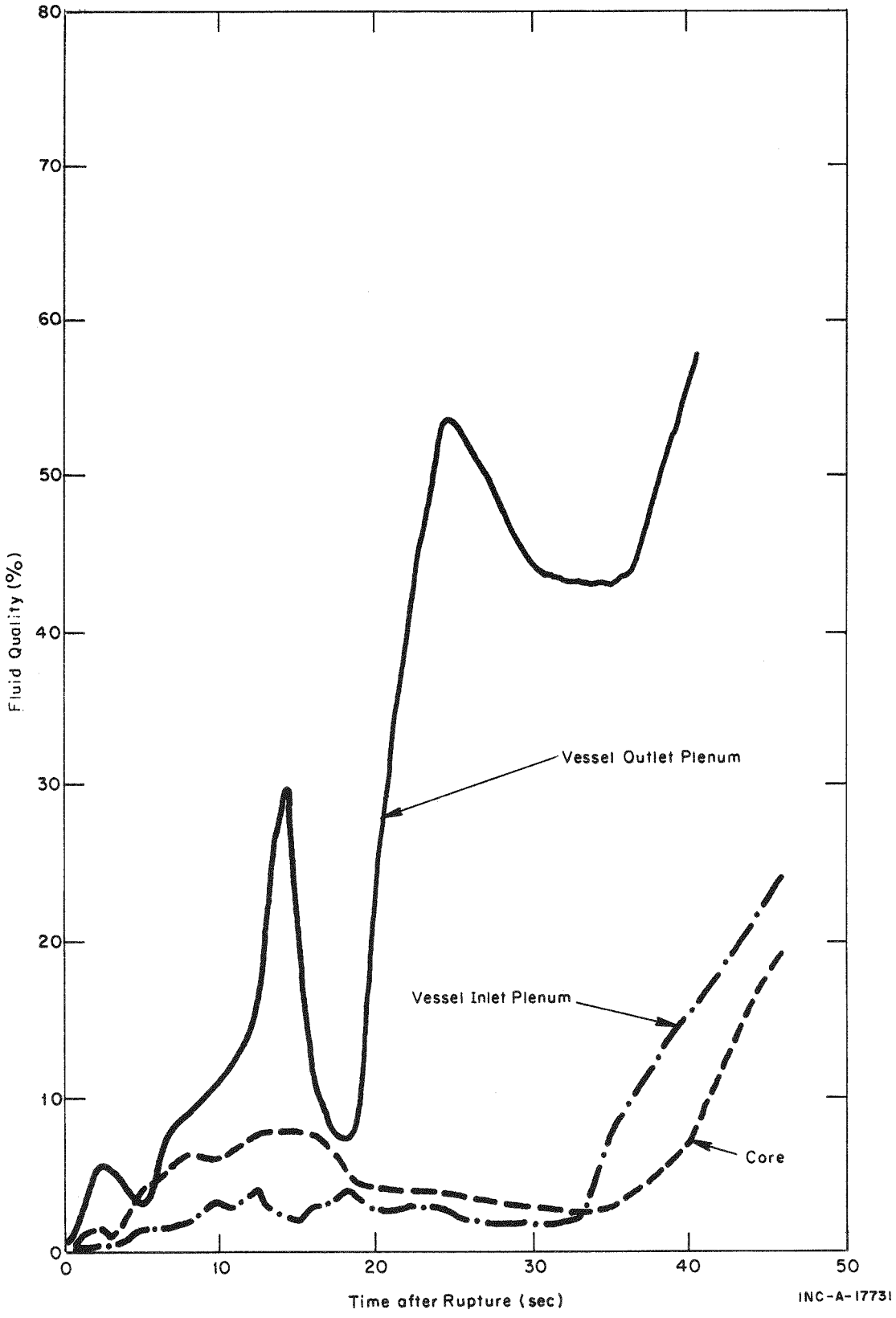

Fig. 35 Vessel fluid quality - Test 825.

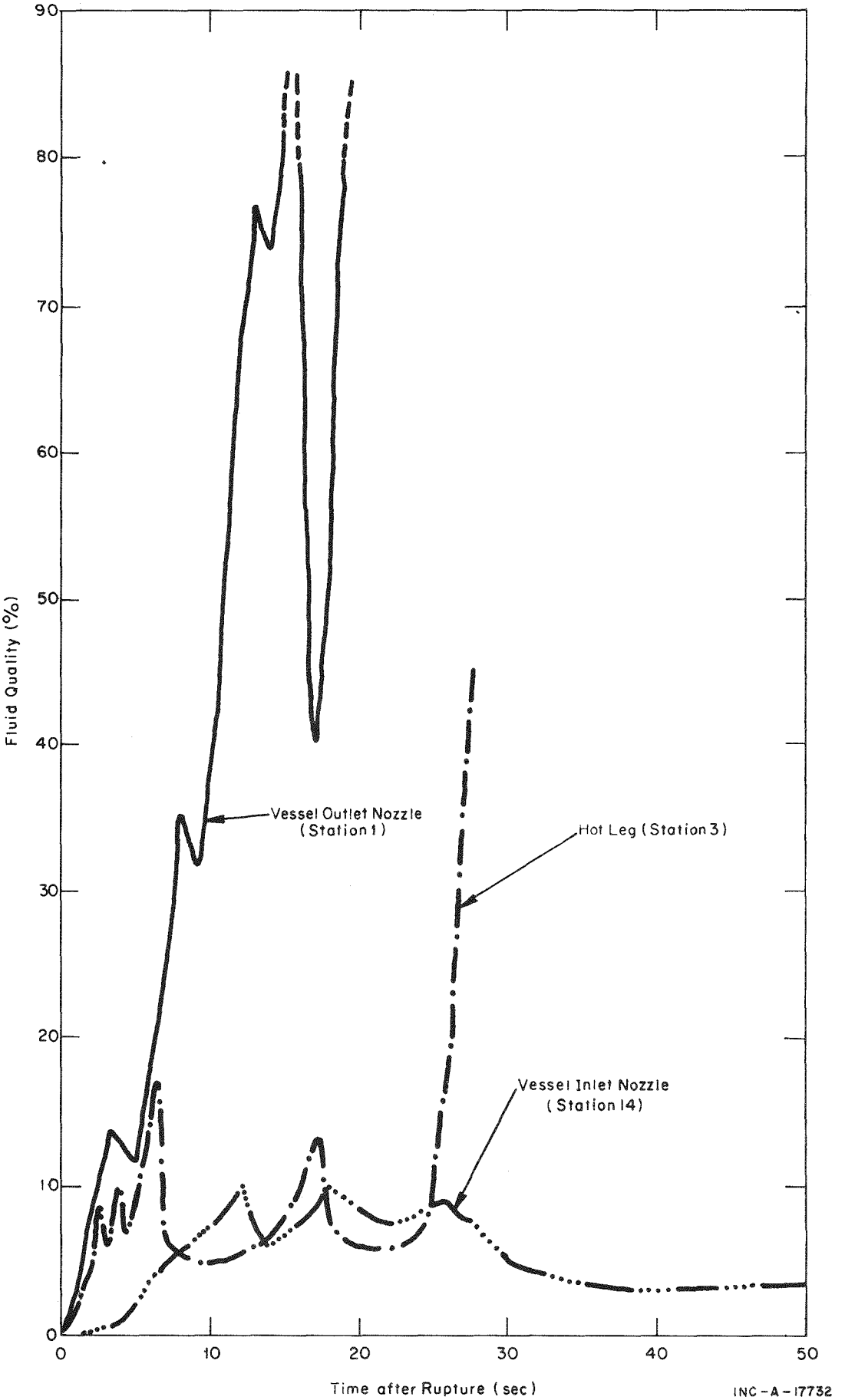

Fig. 36 Loop fluid quality - Test 825.

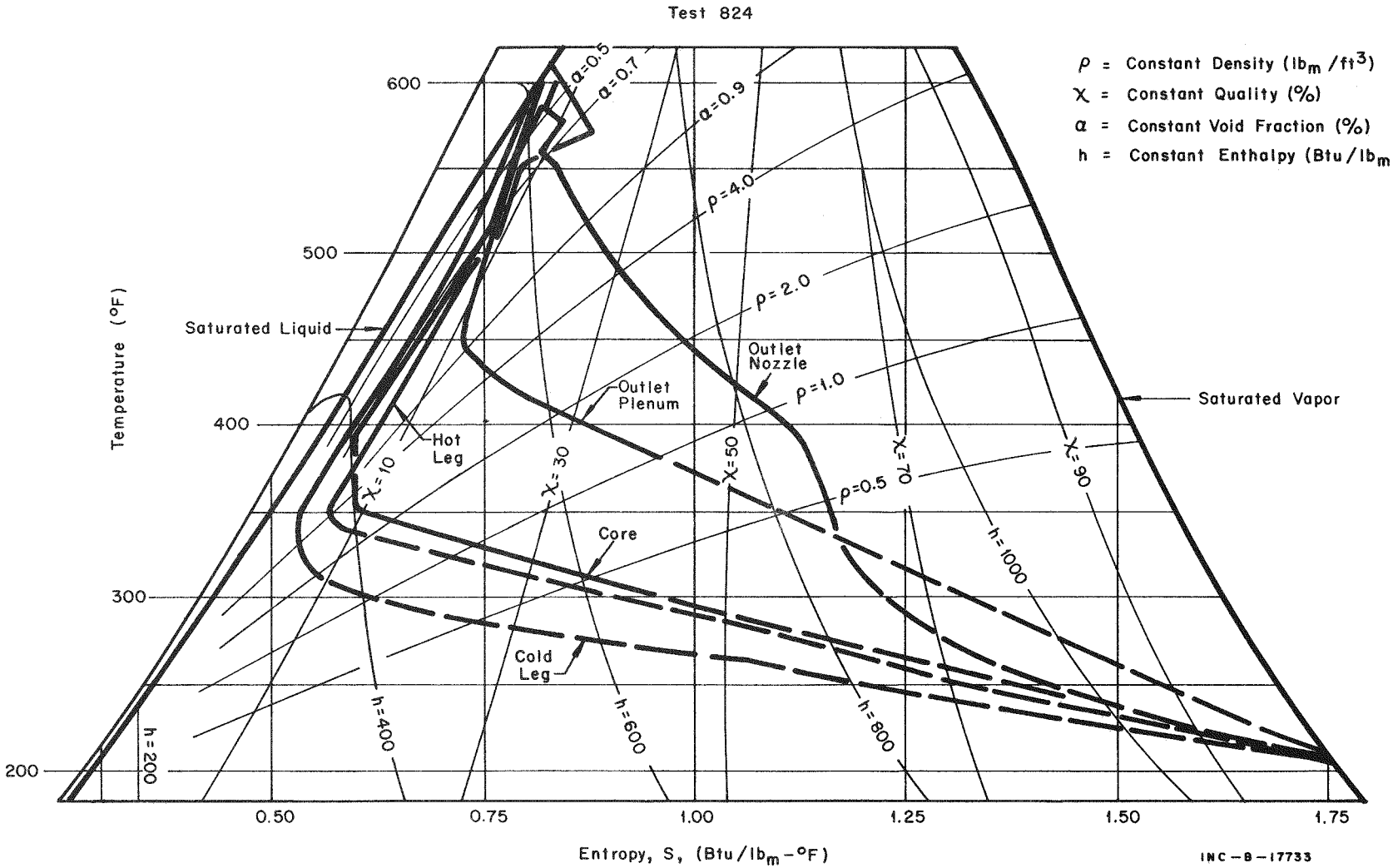

Fig. 37 Temperature-entropy diagram - Test 824.

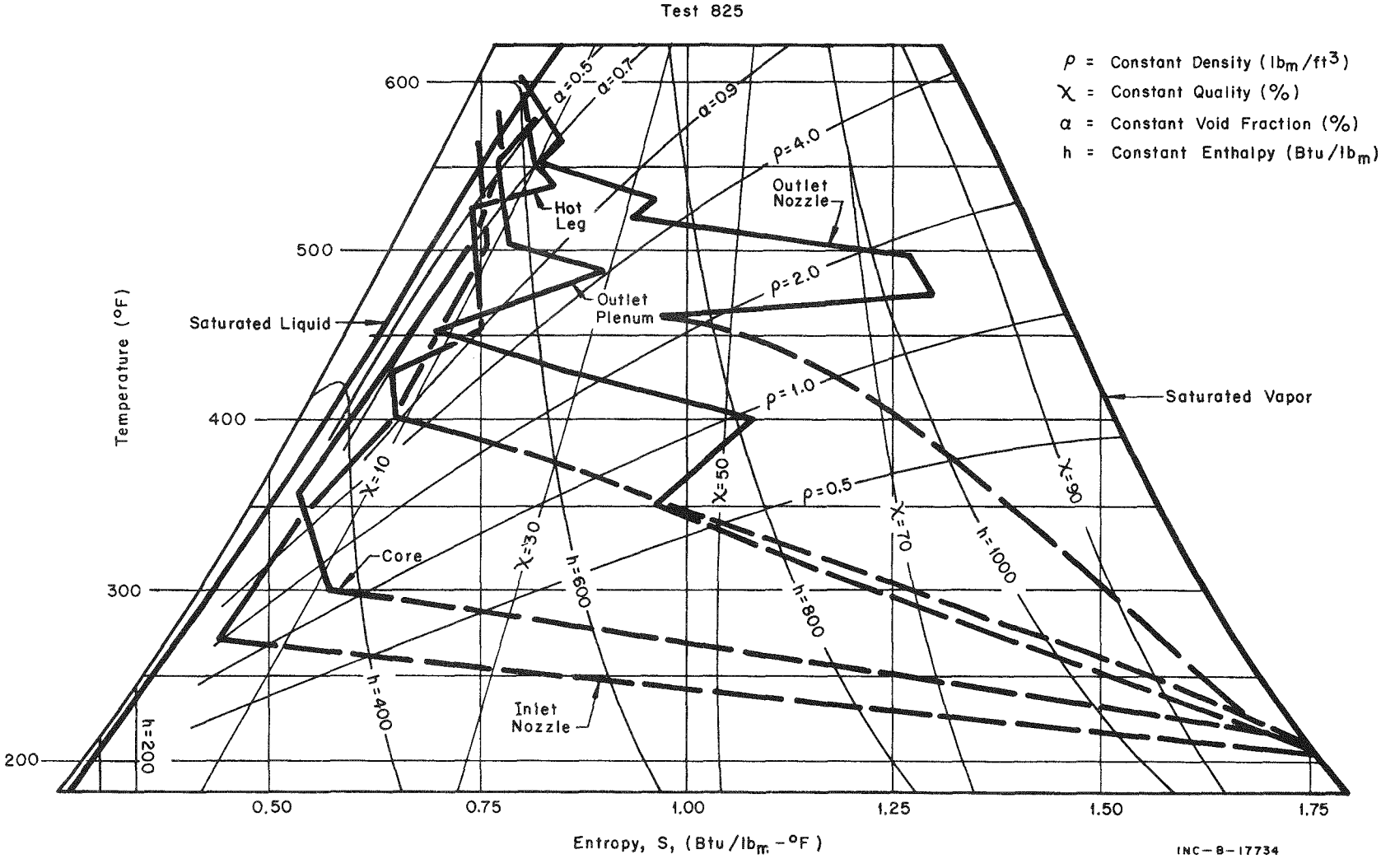

Fig. 38 Temperature-entropy diagram - Test 825.

4. CORE HEAT TRANSFER

The discussion of core heat transfer presented here is based on calculations and analysis involving temperature data taken at representative locations for Test 825 only. No attempt was made to determine heat transfer coefficients for Test 824 because of the detector failures noted earlier.

The calculations were made using a version of the DATAR (DATA Reduction) computer code developed by Westinghouse Electric Corporation for the PWR-FLECHT Project[7]. The modified version, DATAR-S (DATA Reduction-Semiscale), is designed to solve for one-dimensional heat transfer in a cylindrical rod by computing the rod surface temperature and heat transfer coefficients from the temperature data obtained from thermocouples imbedded in the heater rod cladding, the fluid temperatures measured by thermocouples located in adjacent fluid channels, and the power history of the heater rod. Material thermal conductivities and volumetric heat capacities are additional input to the code in the form of temperature-dependent functions. The resulting calculational analysis should be considered as representative of general trends only. Figures 39 through 54 show the calculated rod surface temperatures and heat transfer coefficients as functions of time for selected rod elevations and locations during Test 825.

During steady state operation prior to rupture the value of the heat transfer coefficient, h, varies from 3300 to 6000 Btu/hr-ft^2-°F. The heat transfer regime during steady-state operation prior to rupture is subcooled forced convection.

Examination of Figures 39 through 54 show that all rod surface temperatures decrease by 50 to 60°F and that at rupture the heat transfer coefficient increases rapidly over the length of the core. The increase in surface heat flux associated with the high heat transfer coefficients is a result of the violent flashing of the liquid which reduces the temperature of the rod surfaces during and immediately after subcooled decompression. This conclusion is supported by Figure 55 which presents the degree of subcooling for the fluid in the outlet and inlet vessel plenums as a function of time. The fluid at the top of the core is 50°F subcooled prior to rupture but reaches saturation within 0.1 sec after rupture, whereas the fluid at the bottom of the core is 92°F subcooled prior to rupture and is still subcooled up to 3 sec after rupture. As the system reaches saturation temperatures, pool boiling heat transfer prevails. In addition, the high rate of heat transfer from the rod surfaces is enhanced by the sudden increase in flow which occurs immediately after rupture (Section V-1).

Within 0.1 sec after rupture the heat transfer coefficient, h, increases by a factor of between 2 and 7-1/2 times the steady state value at all locations. In all cases, the value of h then generally remains above 10,000 Btu/hr-ft^2-°F for at least 12 sec after rupture and the major heat transfer regime is saturated forced convection in the bulk free stream with nucleate boiling at the rod surfaces.

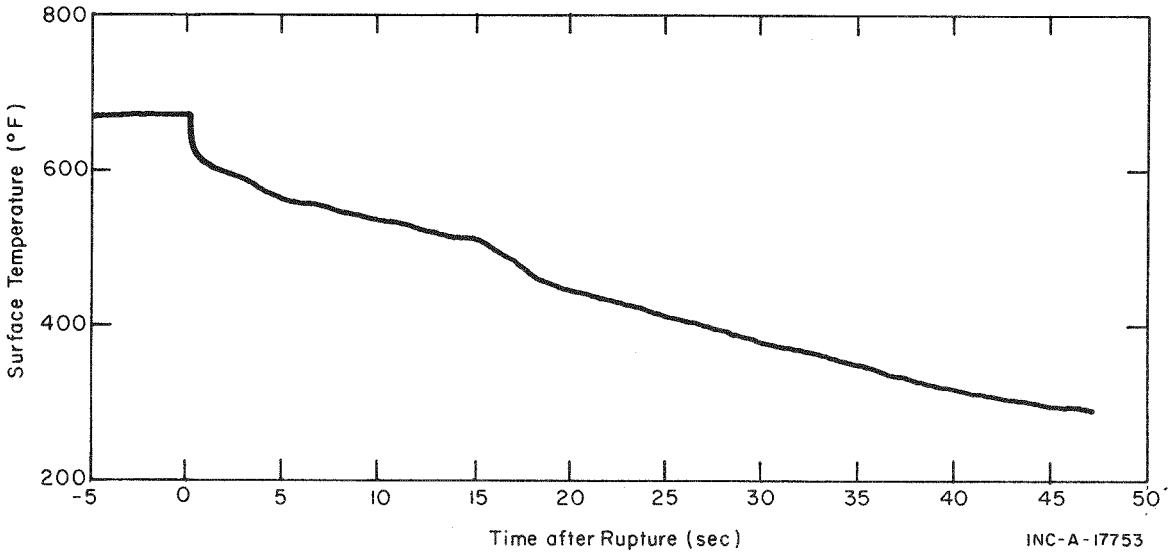

Fig. 39 Calculated surface temperature for bottom of Pin 13 - Test 825.

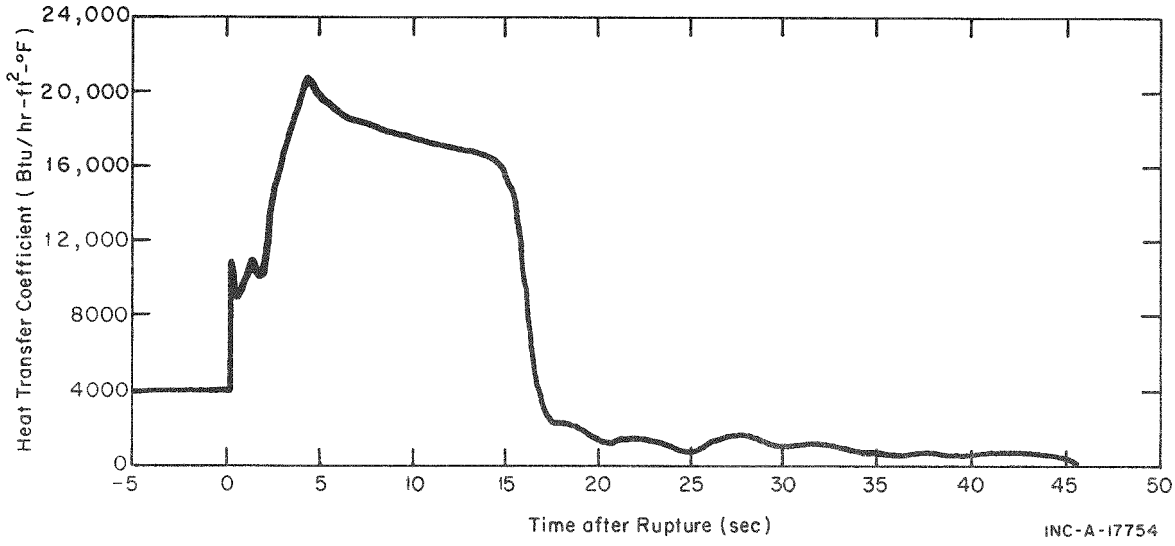

Fig. 40 Heat transfer coefficient for bottom of Pin 13 - Test 825.

Cladding temperature data indicate that departure from nucleate boiling (DNB) occurred at approximately 12.5 sec after rupture and at this time the value of h at the high core elevation drops to a value between 5 and 10 Btu/hr-ft^2-°F and remains at this value for approximately 2 sec after the power was reduced to zero. The power was reduced to zero when the temperature of the cladding of the monitored pin exceeded 900°F to insure core integrity. The heat transfer coefficient increases to a value in excess of 13,000 Btu/hr-ft^2-°F at 17 sec after rupture or approximately 3.5 sec after core power was terminated.

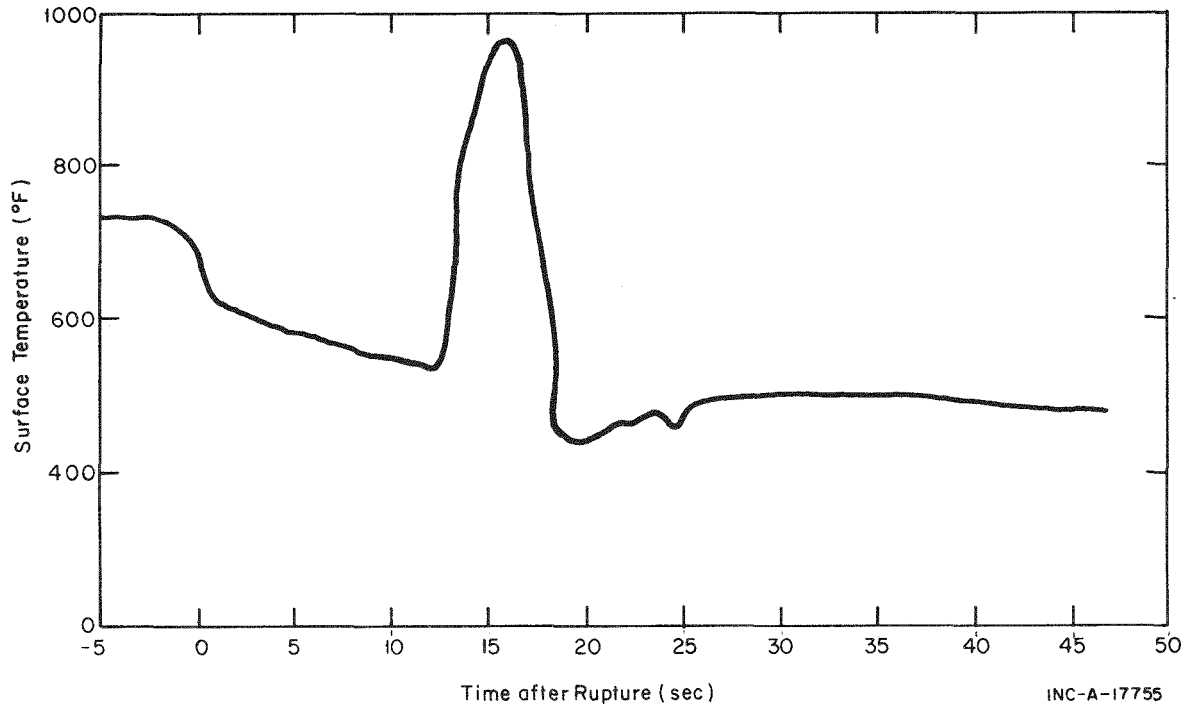

Fig. 41 Calculated surface temperature for top of Pin 13 - Test 825.

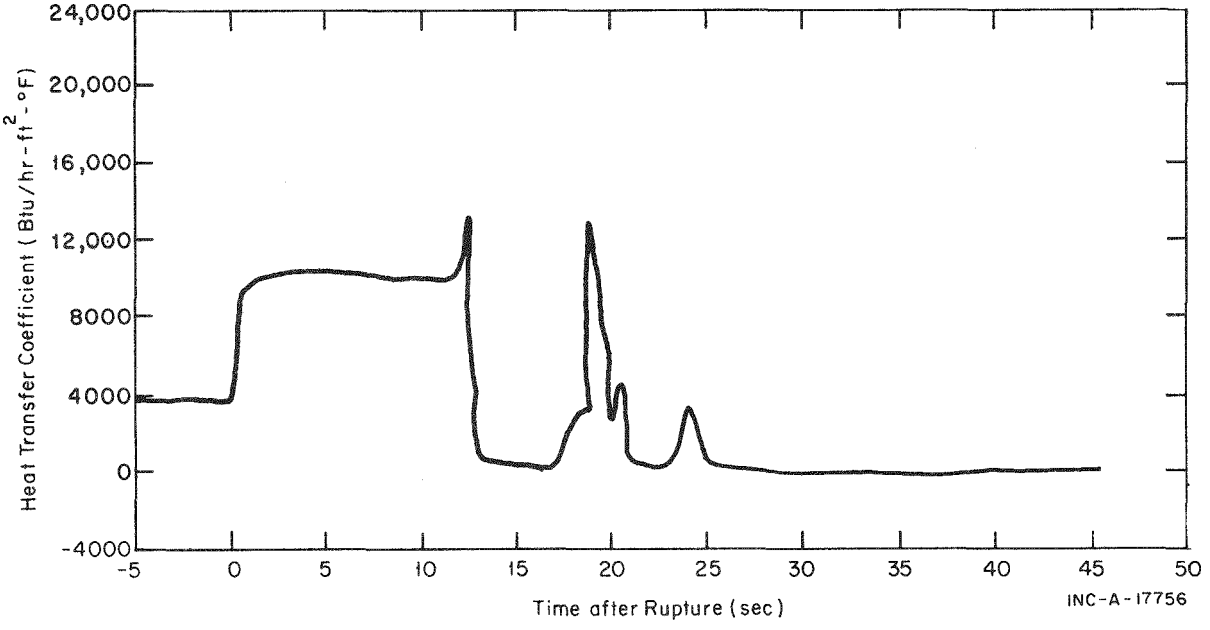

Fig. 42 Heat transfer coefficient for top of Pin 13 - Test 825.

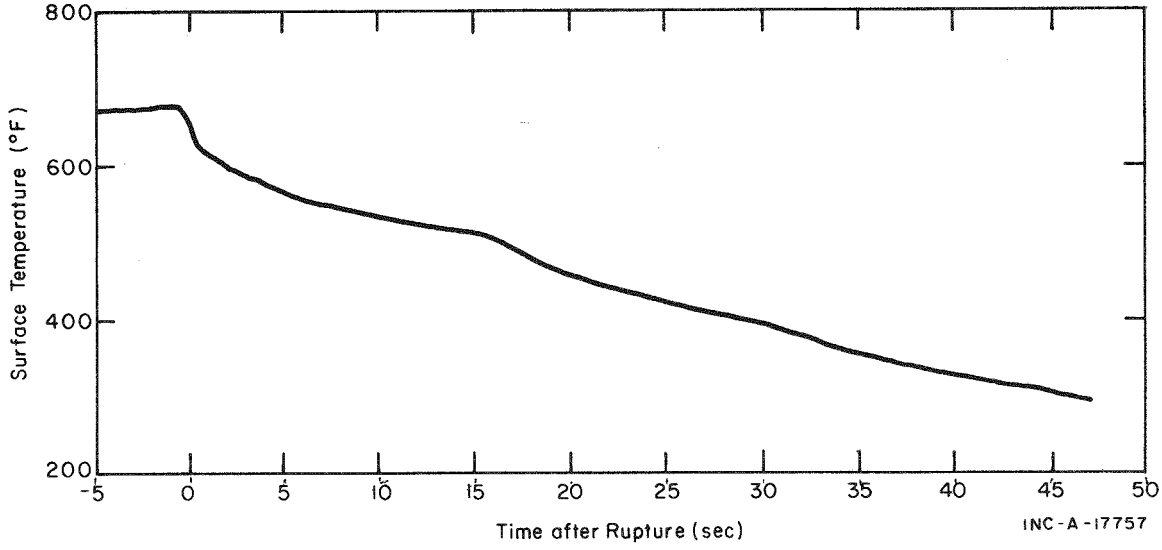

Fig. 43 Calculated surface temperature for bottom of Pin 30 - Test 825.

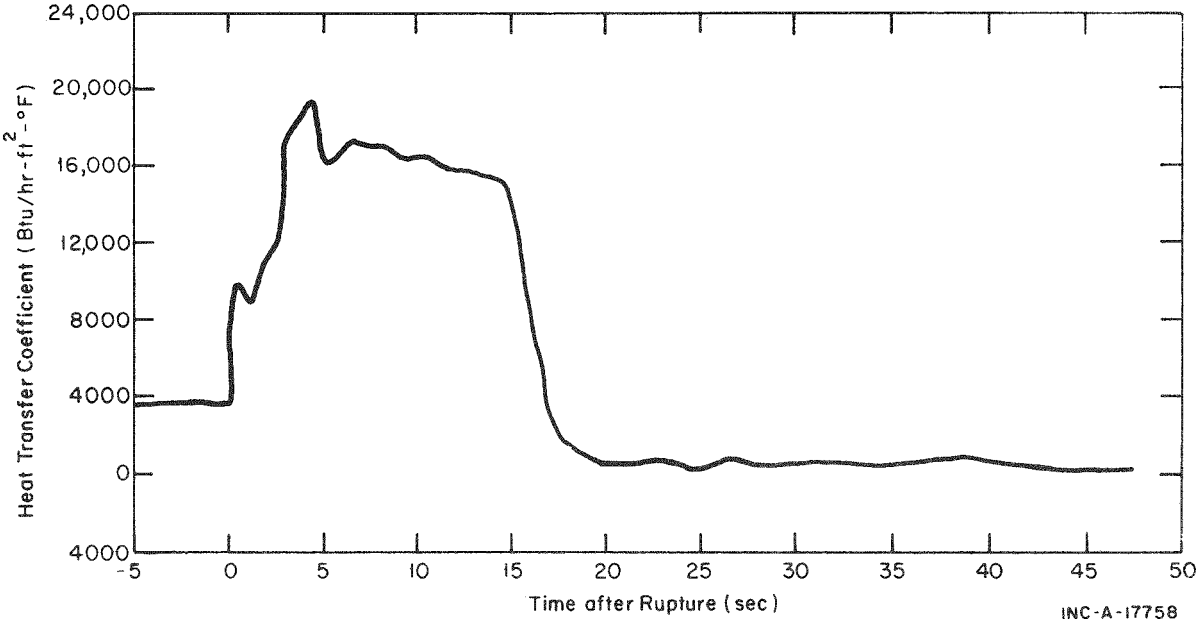

Fig. 44 Heat transfer coefficient for bottom of Pin 30 - Test 825.

For the time period just prior to and immediately after DNB, the upper portion of the core probably progresses through several heat transfer and flow regimes. The heat transfer coefficients at the upper core elevations (Figures 42, 48, and 54) increase by as much as 4,000 Btu/hr-ft^2-°F just prior to DNB. This increase in surface heat flux indicates that the liquid

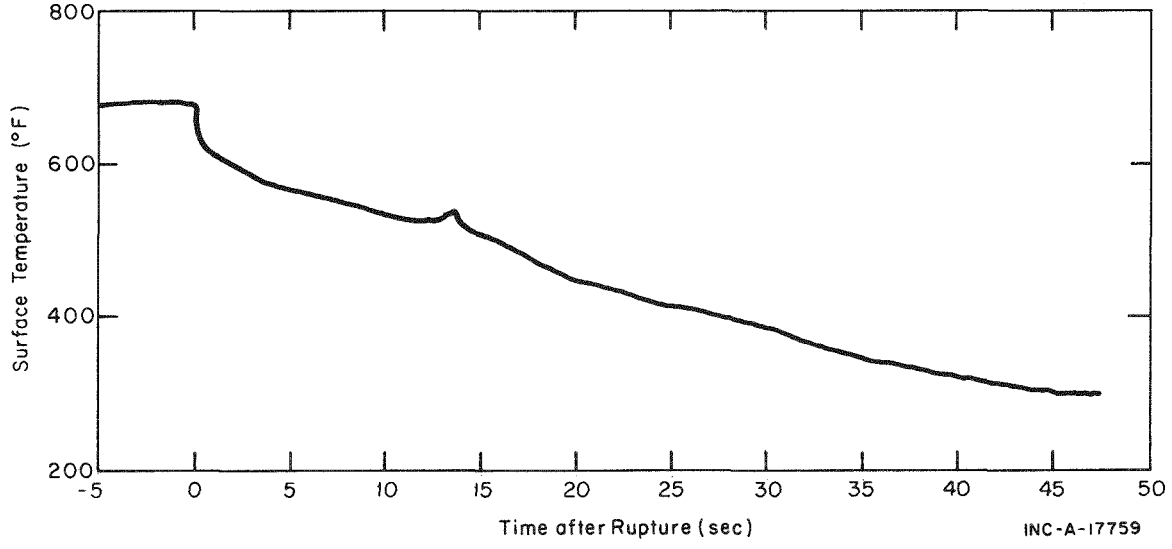

Fig. 45 Calculated surface temperature for center of Pin 30 - Test 825.

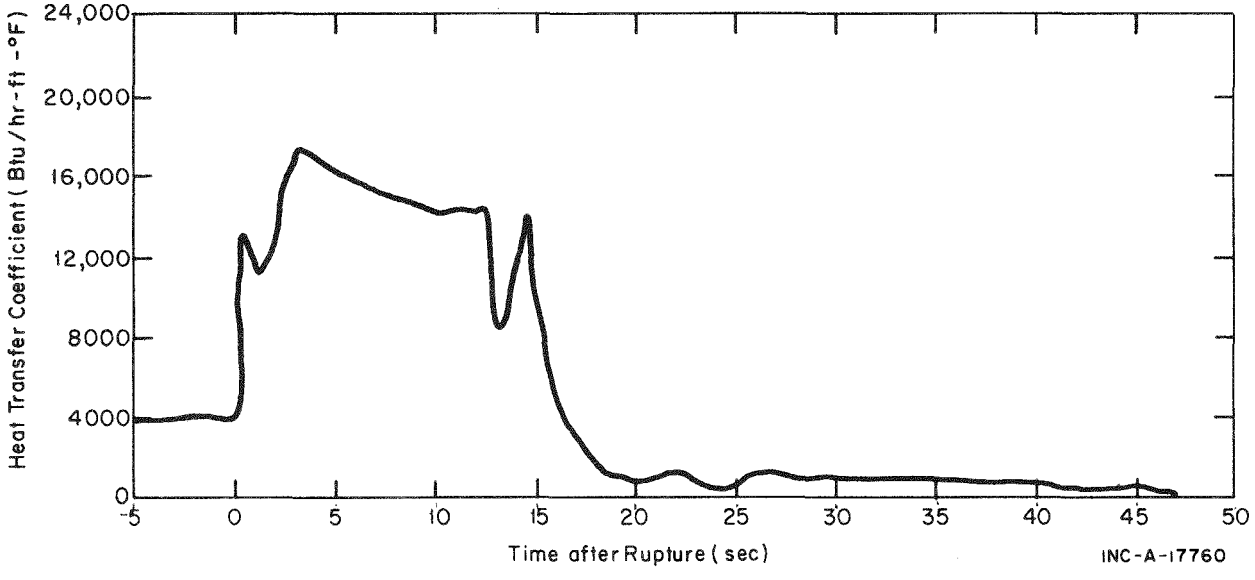

Fig. 46 Heat transfer coefficient for center of Pin 30 - Test 825.

superheating at the rod surface increases to the point at which nucleate boiling is resumed momentarily. Within the nucleate boiling regime, the effect is at first to enhance the heat transfer coefficients. But this process is limited when the critical heat flux is reached. A transition to film boiling takes place and the coefficients are drastically reduced.

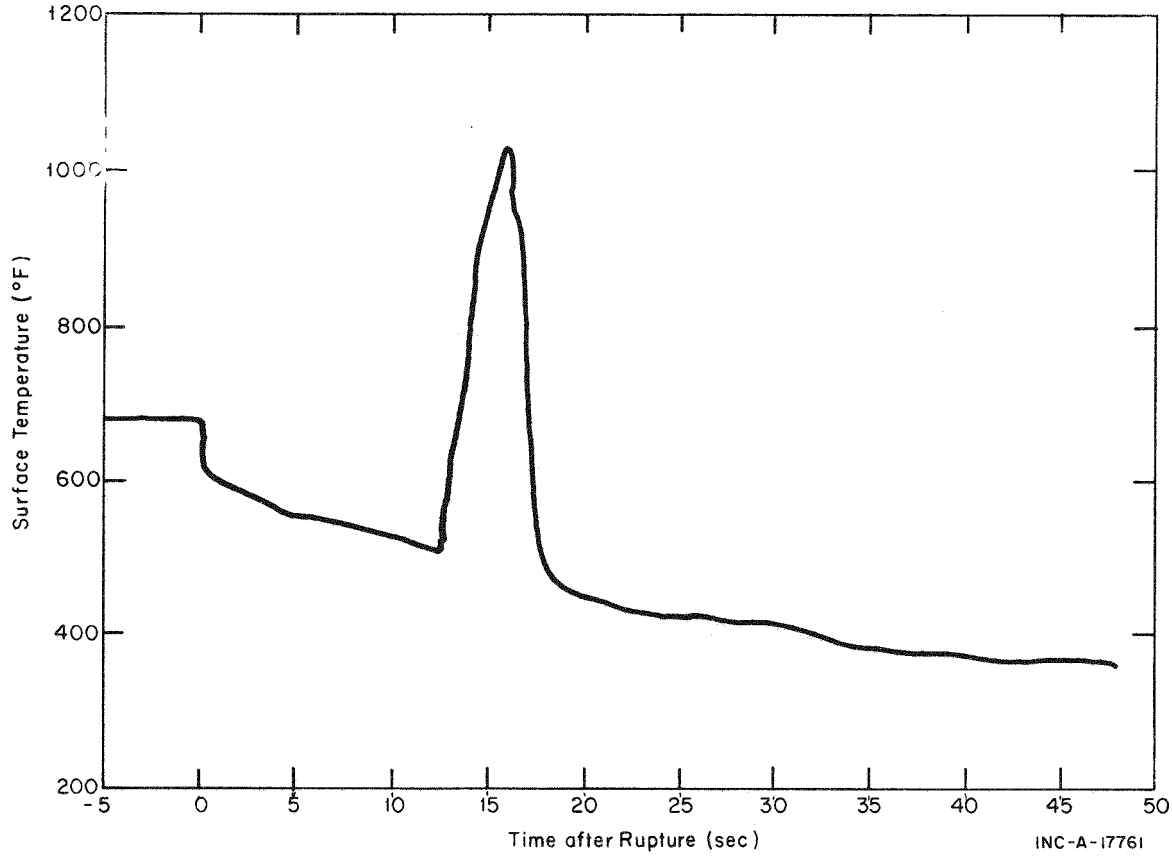

Fig. 47 Calculated surface temperature for top of Pin 30 - Test 825.

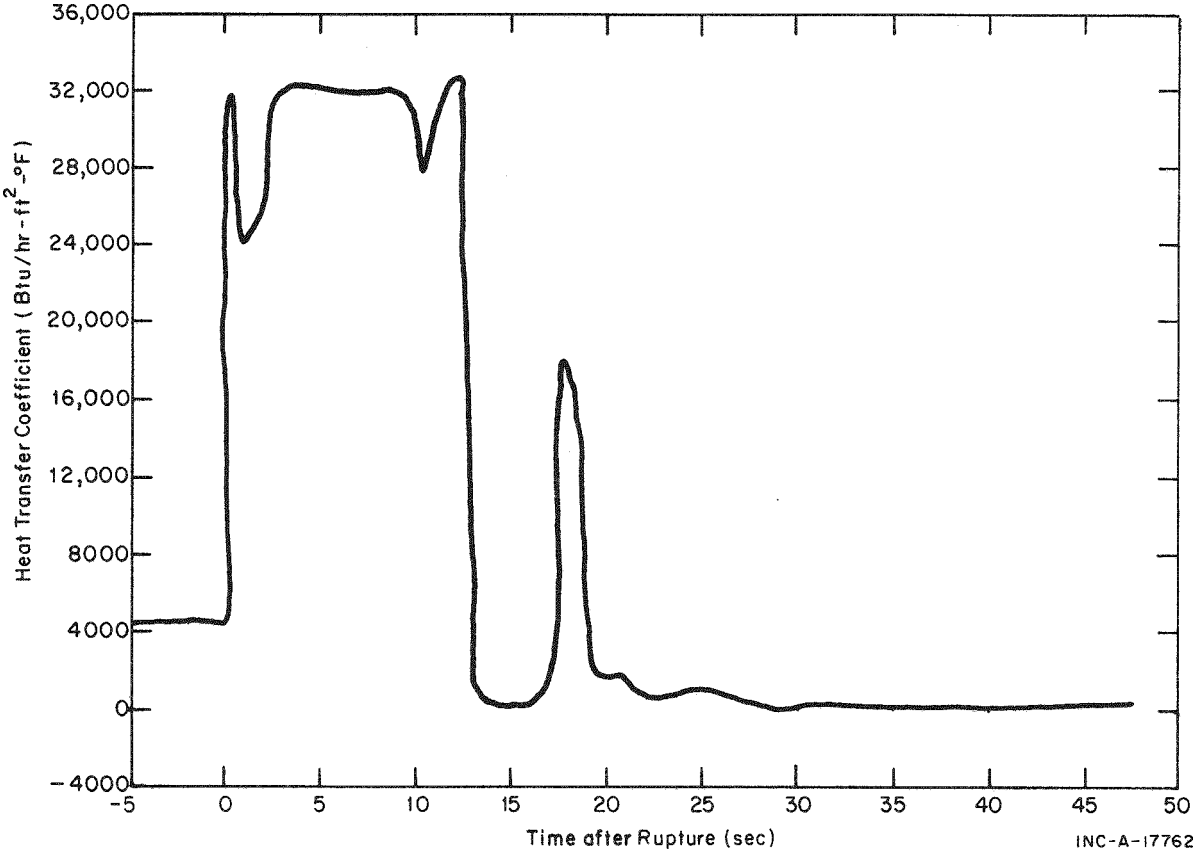

Fig. 48 Heat transfer coefficient for top of Pin 30 - Test 825.

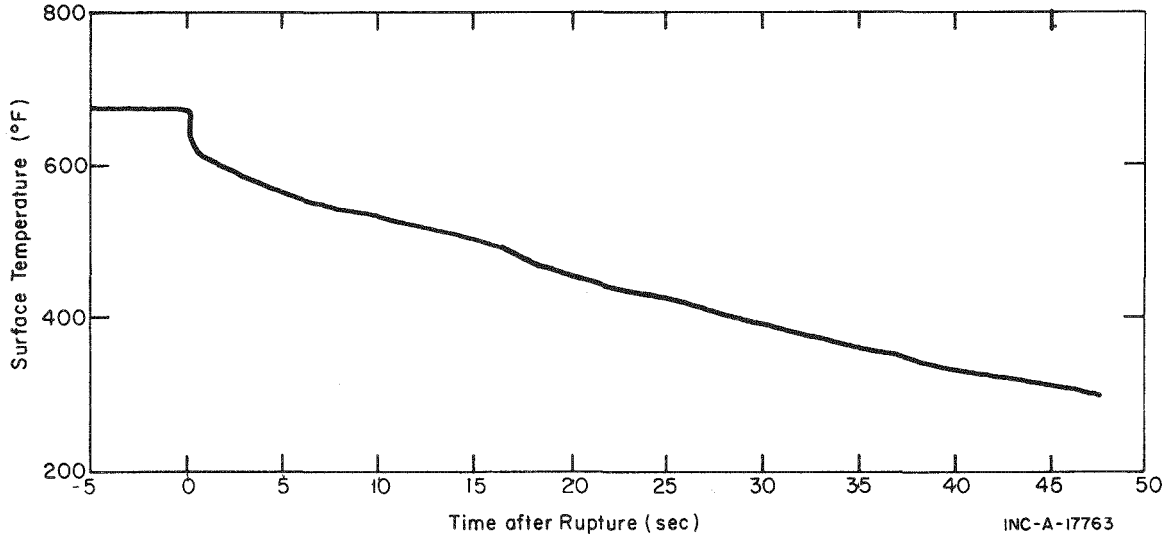

Fig. 49 Calculated surface temperature for bottom of Pin 116 - Test 825.

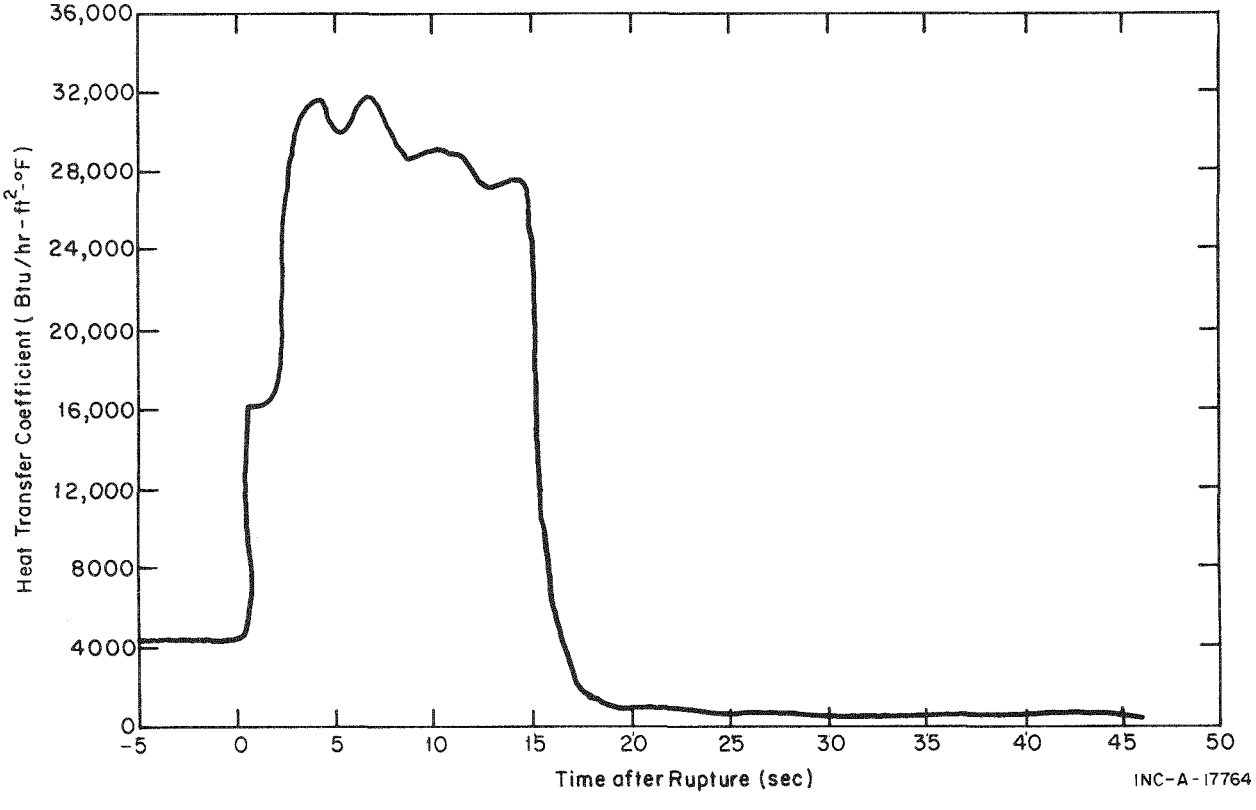

Fig. 50 Heat transfer coefficient for bottom of Pin 116 - Test 825.

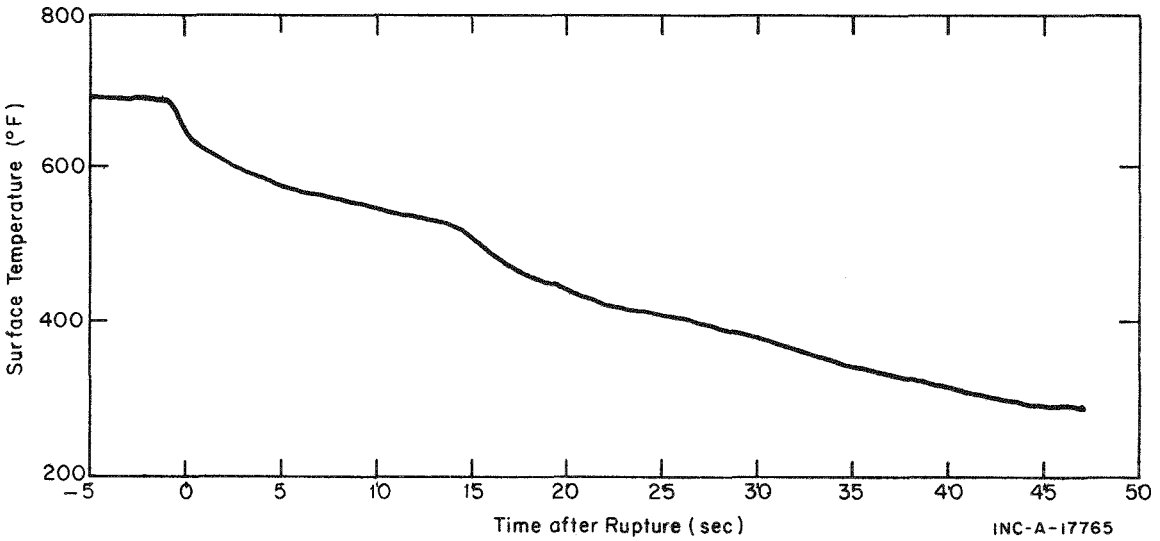

Fig. 51 Calculated surface temperature for center of Pin 116 - Test 825.

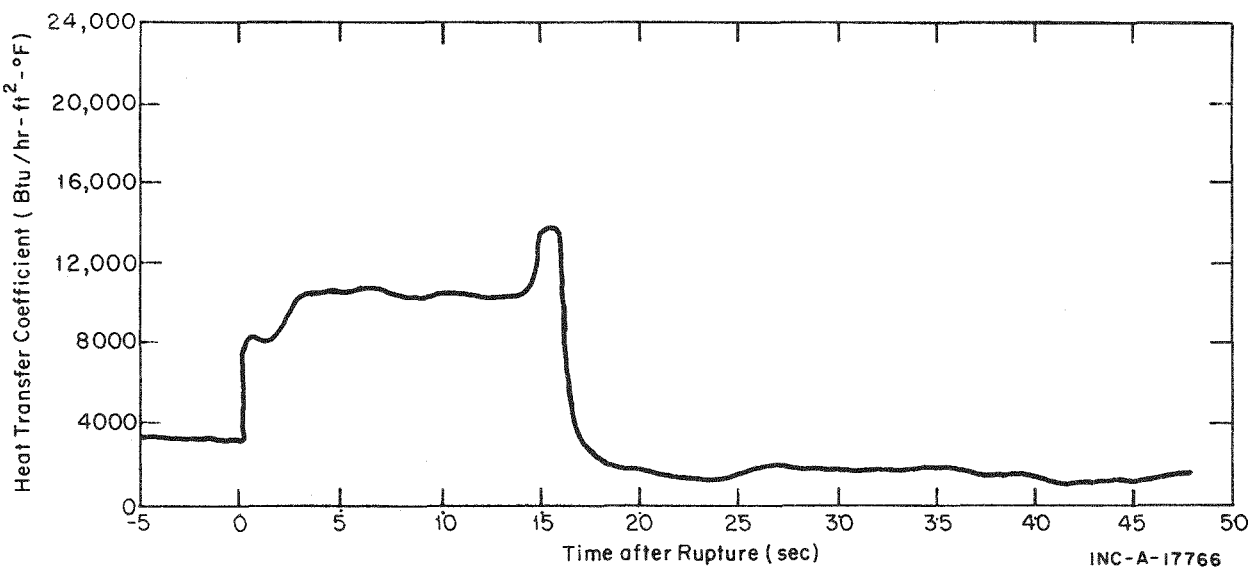

Fig. 52 Heat transfer coefficient for center of Pin 116 - Test 825.

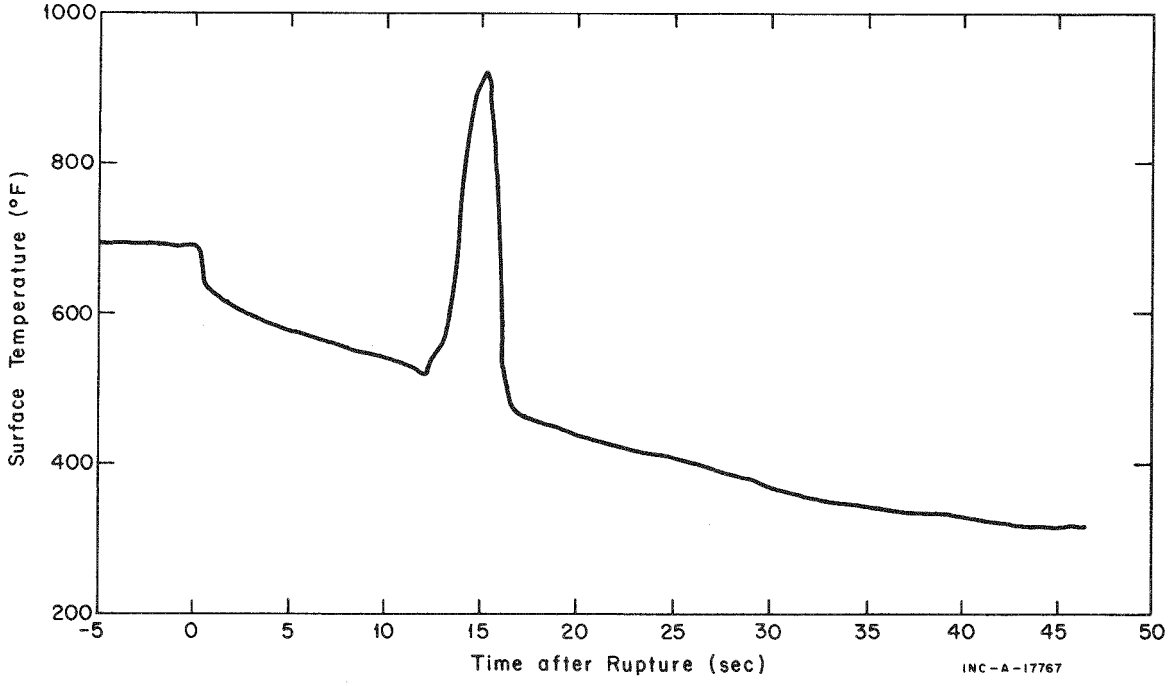

Fig. 53 Calculated surface temperature for top of Pin 116 - Test 825.

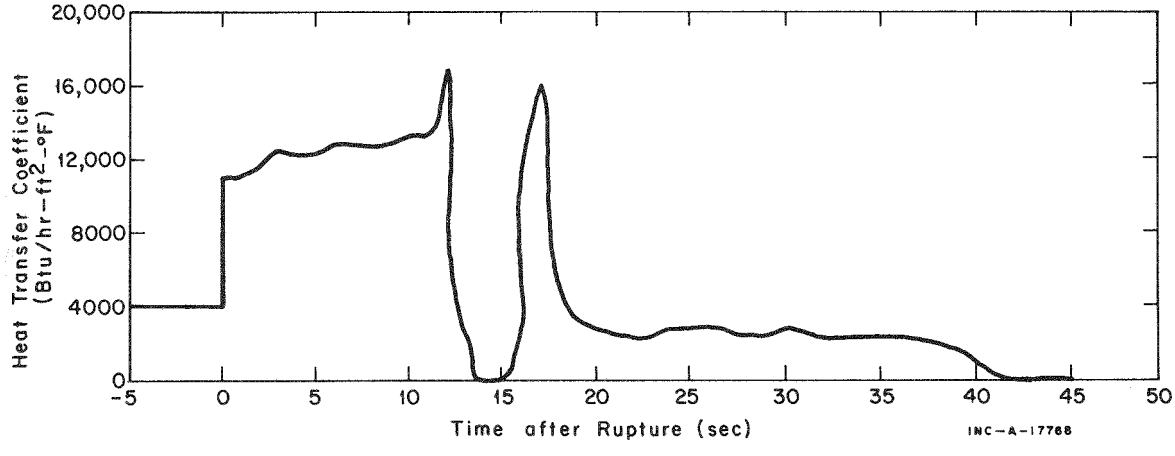

Fig. 54 Heat transfer coefficient for top of Pin 116 - Test 825.

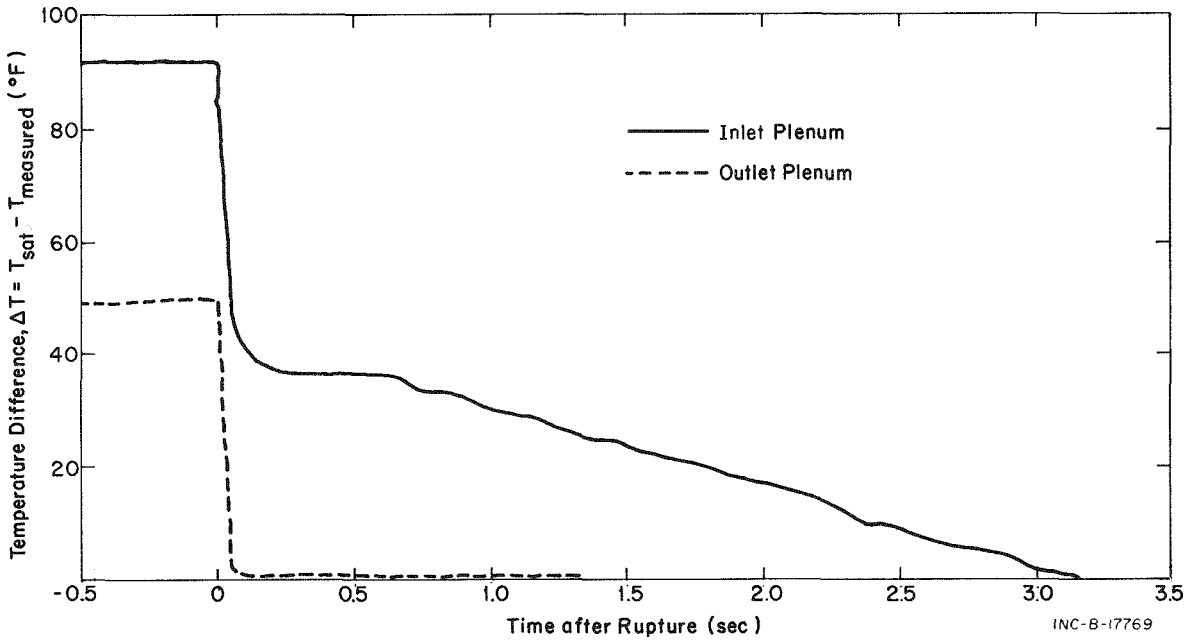

Fig. 55 Subcooling in upper and lower plenums - Test 825.

Table IV summarizes the changes in fluid properties in the vessel outlet plenum from 10 to 14 sec after rupture. Figures 41, 45, 47, and 53 show that DNB occurred when the rod surface temperatures were between 505 and 530°F.

The heat transfer coefficient remains high at the bottom elevations and midelevations for 15 to 16 sec after rupture and decreases to values less than 2,000 Btu/hr-ft^2-°F 20 sec after rupture. As shown in Figure 45, the surface temperature at the midelevation thermocouple for Pin 30 (TM-30-0) indicates that DNB was initiated at this location at 12.5 sec and that nucleate boiling was reestablished by 14 sec. This small temperature excursion was noted on several other rods at the midelevation.

TABLE IV

TEST 825-FLUID PROPERTY CHANGES BETWEEN 10 AND 14 SECONDS AFTER RUPTURE -- TEST 825

Time (sec)	Outlet Plenum Pressure (psig)	Outlet Plenum Density (lb/ft^3)	Core Flow Rate (lb/sec)	Outlet Plenum Steam Quality (%)	Outlet Plenum Fluid Void Fraction
10	780	11	3.5	11.5	0.75
12	690	7	2.5	15	0.87
14	600	3	2.0	30	0.94

VI. SUMMARY OF OBSERVATIONS

On the basis of the data presented in Sections IV and V, the following observations can be made:

(1) Although significant pressure fluctuations occurred at locations near the break at the time of rupture, the severity of the pressure fluctuations was significantly reduced in the vessel inlet and outlet plenum due to the reduction in the magnitude of the pressure waves traveling from a small pipe to the large plenum. The maximum pressure difference across the core measured in the semiscale system for Tests 824 and 825 was 70 to 140 psi and occurred during the initial portion of saturated blowdown. The maximum pressure difference recorded across the core during subcooled blowdown was 40 to 70 psi.

(2) The transport time for the subcooled decompression waves in the semiscale system closely agreed with the calculated transport time based on isentropic sonic velocity.

(3) Large pressure oscillations occurred across the semiscale steam generator during the subcooled portion of blowdown for Tests 824 and 825 (both hot leg breaks). A maximum pressure difference of ± 400 psi occurred immediately after rupture. The pressure difference diminished to ±100 psi within 30 to 40 msec.

(4) Subcooled expansion of the liquid was complete about 70 to 80 msec after system rupture. The fluid at the lower initial temperature remained subcooled, however, until the system decompressed to a pressure corresponding to the saturation pressure for a local temperature.

(5) The fluid temperature drop during the subcooled expansion of the fluid was dependent on the degree of subcooling of the fluid at the initial steady state conditions.

(6) During the saturated portion of blowdown the fluid temperatures followed saturation temperatures provided the system had decompressed to the pressure corresponding to saturation conditions for the lowest initial temperature.

(7) During the latter stages of saturated blowdown, when the fluid quality was high, the thermocouples which measured the fluid temperature indicated high temperatures due to radiation from the hot piping walls.

(8) DNB occurred at the top elevation of the center heater rod at 12.5 sec after rupture for the test in which core power was maintained after rupture (Test 825). The temperature

of the heater subsequently increased at a rate of approximately 150°F/sec. Wetting of the cladding surface was quickly reestablished after core power was terminated.

(9) The temperatures of the piping wall and vessel internals remained significantly higher than the fluid temperatures throughout the blowdown transient.

(10) The density of the fluid in the loop was not greatly affected by continuation of core power after rupture.

(11) The density of the fluid in the hot and cold legs remained higher for a longer period of time than the densities of the fluids in the vessel outlet plenum and nozzle.

(12) The subcooled piping decompression strains were small and corresponded to the decrease in fluid pressure.

(13) The maximum piping strains were thermally induced circumferential compressive strains.

(14) The amount of water remaining in the system was only a few percent of the initial water inventory. The operation of the steam generator during blowdown (Test 824) seems to have affected the amount of water remaining in that section of the system.

(15) For Semiscale Tests 824 and 825, the fluid flow rate through the vessel outlet nozzle increased to about four times the steady state flow rate immediately after rupture.

(16) The calculated fluid flow rate indicates that the core flow during the transient is affected by the duration of core power after system rupture.

(17) For the early stages of saturated blowdown the measured horizontal thrust agreed closely with the thrust calculated on the basis of pressure density and flow data. The pressure component of the thrust data was about two-thirds of the total thrust and the thrust due to flow momentum accounted for the balance.

(18) The fluid quality in the vessel outlet nozzle and plenum increased progressively during blowdown. Quality in the hot and cold leg remained essentially constant until blowdown was effectively completed and then abruptly increased.

(19) The fluid quality in the vessel outlet plenum and nozzle decreased rapidly at the time core power was terminated in Test 825.

(20) The heat transfer coefficient at the heater pin surfaces increased immediately after rupture to a value 2 to 7-1/2 times the steady state value.

(21) At DNB the heat transfer coefficients at the heater pin surfaces dropped to essentially zero.

(22) After core power was terminated the heat transfer coefficient at the heater pin surfaces rapidly increased as wetting was reestablished.

VII. REFERENCES

1. H. W. Heiselmann and J. O. Zane, Semiscale Blowdown and Emergency Core Cooling (ECC) Project, IN-1384 (July 1970).

2. D. J. Olson and J. F. Whitbeck, Semiscale Blowdown and Emergency Core Cooling (ECC) Project Test Report - Test 821, IN-ITR-203 (July 1970). (limited distribution)

3. D. J. Olson and J. F. Whitbeck, Semiscale Blowdown and Emergency Core Cooling (ECC) Project Test Report - Tests 822 and 823, IN-1393 (October 1970).

4. G. F. Brockett, H. D. Curet, H. W. Heiselmann, Experimental Investigation of Reactor System Blowdown, IN-1348 (September 1970).

5. H. W. Heiselmann, D. J. Olson, J. F. Whitbeck, Semiscale Blowdown and Emergency Core Cooling (ECC) Project Test Report - Tests 803 through 820, IN-1404 (October 1970).

6. D. J. Olson and J. G. Van Haverbeke, Description of Facility and Data Acquisition and Processing System for the Heated Core Portion of the 800 Test Series of the Semiscale Blowdown and Emergency Core Cooling (ECC) Project, IN-ITR-202 (July 1970). (limited distribution)

7. J. O. Cermak, A. S. Kitzes, F. F. Cadek, R. H. Leyse, D. P. Dominicis, PWR Full Length Emergency Cooling Heat Transfer (FLECHT) Group I Test Report, WCAP-7435 (January 1970).

APPENDIX A
DATA RECORDED -- SEMISCALE TESTS 824 AND 825

APPENDIX A

DATA RECORDED -- SEMISCALE TESTS 824 AND 825

Table A-I summarizes the 159 channels of data recorded during Test 824 and the 152 channels of data recorded during Test 825. The techniques applied to the data to account for instrument drift and thermal sensitivity are presented in Appendix B and selected examples of test data from both tests are given in Appendix C.

TABLE A-I

SUMMARY OF RECORDED DATA FOR SEMISCALE TESTS 824 AND 825

Variable	Detector Identification	Quantity Test 824	Quantity Test 825	Figure Reference
Pressure				
Loop	P	10	10	A-1
Vessel				
Outlet plenum	P-O-1S, P-O-1D	2	2	A-2
Inlet plenum	P-I-1S, P-I-1D	2	2	A-2
Temperature				
Loop				
Fluid	TF-	9	9	A-1
Material	TM-	12	12	A-1
Vessel				
Fluid	TF-	14	16	A-2
Material				
Internals	TM-	5	5	A-2
Pins		36	35	A-3
Differential Temperature				
Core	DT-C-3	1	1	
Steam generator	DT-C-2	1	1	
Loads				
Piping hangers	S-1L, 2L, 3L	3	3	
Vessel				
Horizontal	LC-3A, LC-4A	4	4	
Vertical	LC-1A, LC-2A	2	2	
Displacement				
Vessel, internal	M-UG-1	1	2	A-2
Vessel, vertical	M-37Z	1	1	A-2
Nozzle, horizontal	M-17X	1	1	

TABLE A-I (Contd.)

SUMMARY OF RECORDED DATA FOR SEMISCALE TESTS 824 AND 825

Variable	Detector Identification	Quantity Test 824	Quantity Test 825	Figure Reference
Acceleration				
Vessel, vertical	AC-37Z, AC-38A	2	2	A-2
Break Time, Rupture Disc	R-18	1	1	A-1
Density				
Loop	D-1, D-2. ...	6	6	A-1
Core	D-C-1	1	1	A-2
Plenums	D-O-1, D-I-1	2	2	
Pressure Drop				
Core	DP-C-3	1	1	A-2
Loop	DP-C-2	1	1	A-2
Loop Strain		19	17	A-1
Drag Force (Fluid ρV^2)				
Loop	V-1, V-3, ...	6	3	A-1
Vessel	V-I-1, ...	1	2	
Power	PWR-	3	3	
Voltage	ET, E-	8	8	
Current	IT	1	1	
Miscellaneous		4	6	

The location of the measurement instrumentation can be determined from Figures A-1, A-2, and A-3. Detector identification is accomplished by the following alpha-numeric characterizations:

(1) The first one or two letters define the variable being measured (for example: P = pressure and TF - fluid temperature).

(2) The second character, if it is a numeral, defines either a station number (Figure A-1) or a heater pin number; if it is a letter(s), it designates a location within the vessel (for example, I = inlet) or a specific part of the internal structure (for example, CS = core structure).

(3) Detectors located within the vessel are generally identified by third and fourth characters which are specific in regard to the locations (angular, vertical, horizontal) of the detector on the core structure, as shown in Figures A-2 and A-3.

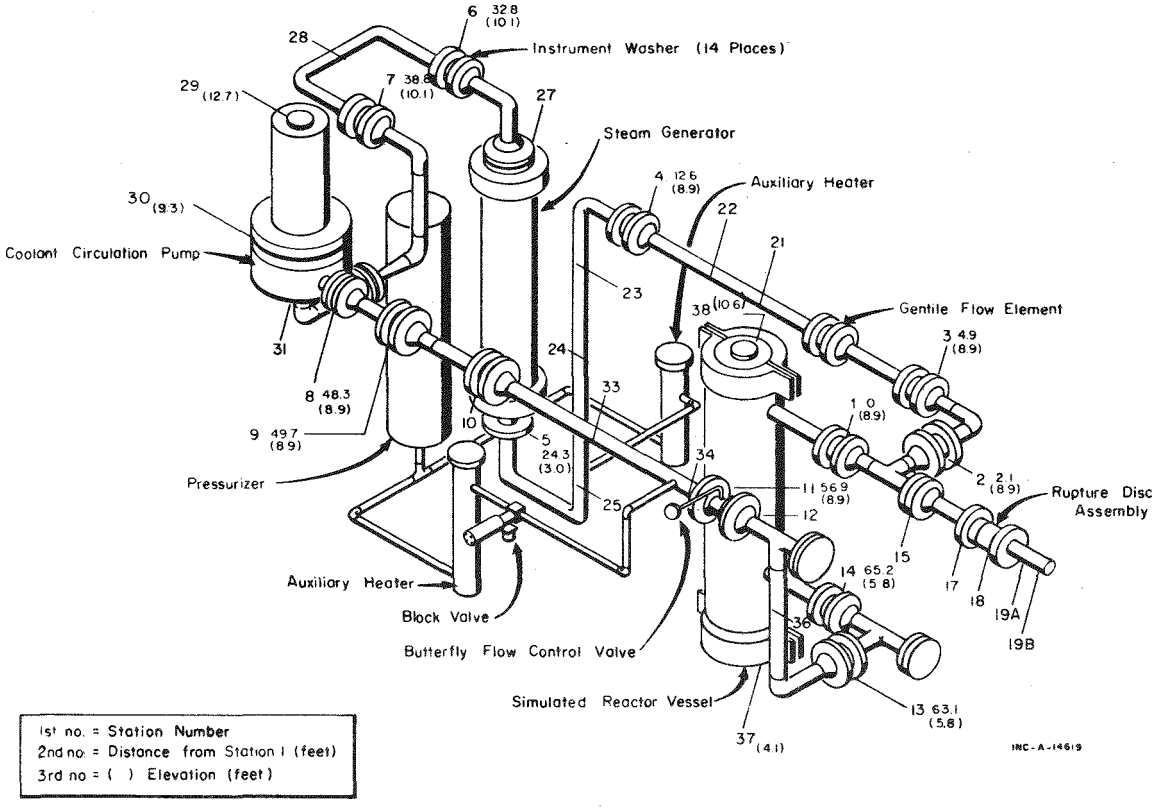

Fig. A-1 Single-loop semiscale - loop instrumentation station locations.

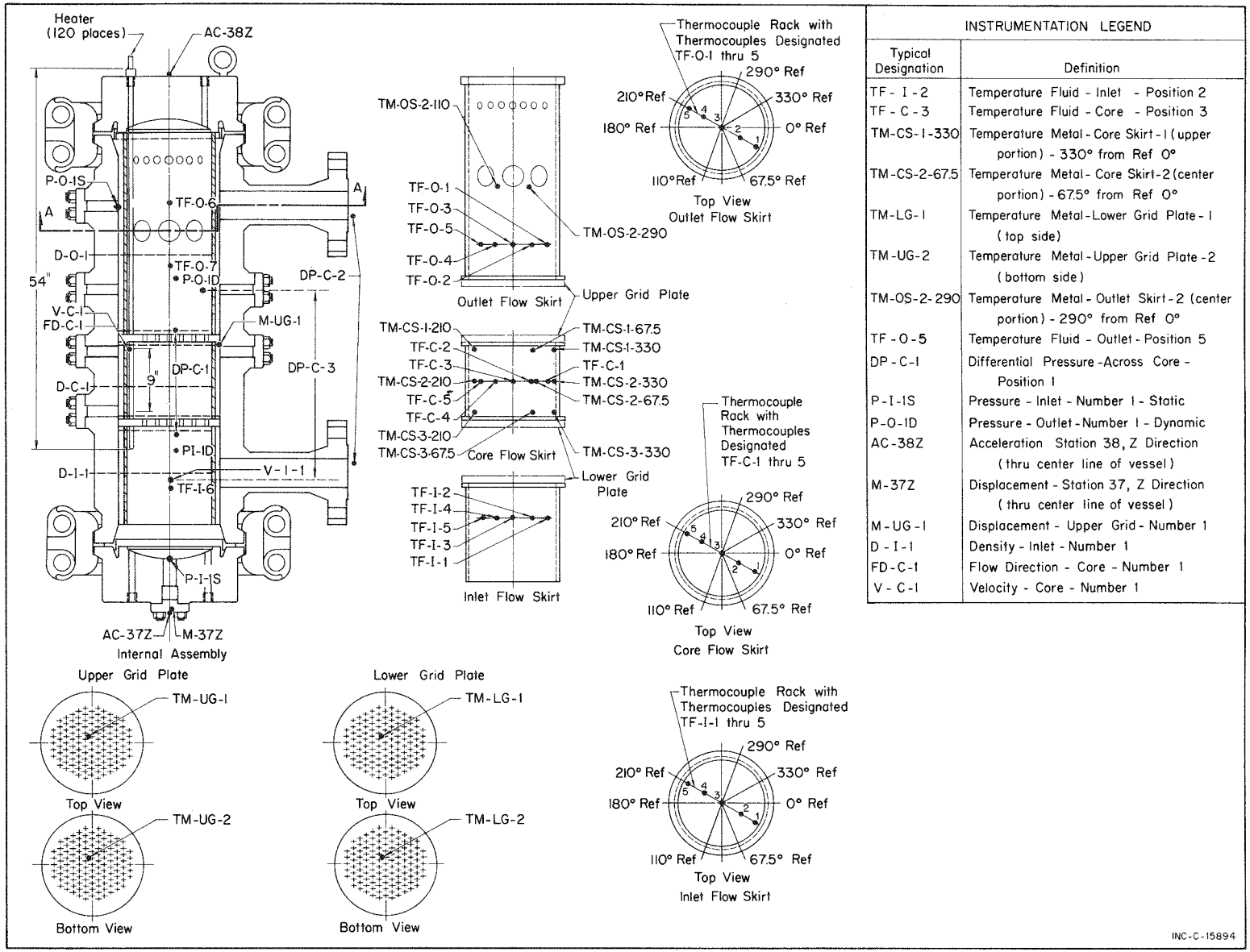

INSTRUMENTATION LEGEND	
Typical Designation	Definition
TF - I - 2	Temperature Fluid - Inlet - Position 2
TF - C - 3	Temperature Fluid - Core - Position 3
TM-CS-1-330	Temperature Metal - Core Skirt - 1 (upper portion) - 330° from Ref 0°
TM-CS-2-67.5	Temperature Metal - Core Skirt-2 (center portion) - 67.5° from Ref 0°
TM-LG-1	Temperature Metal - Lower Grid Plate - 1 (top side)
TM-UG-2	Temperature Metal - Upper Grid Plate - 2 (bottom side)
TM-OS-2-290	Temperature Metal - Outlet Skirt - 2 (center portion) - 290° from Ref 0°
TF - O - 5	Temperature Fluid - Outlet - Position 5
DP - C - 1	Differential Pressure - Across Core - Position 1
P - I - 1S	Pressure - Inlet - Number 1 - Static
P - O - 1D	Pressure - Outlet - Number 1 - Dynamic
AC - 38Z	Acceleration Station 38, Z Direction (thru center line of vessel)
M - 37Z	Displacement - Station 37, Z Direction (thru center line of vessel)
M - UG - 1	Displacement - Upper Grid - Number 1
D - I - 1	Density - Inlet - Number 1
FD - C - 1	Flow Direction - Core - Number 1
V - C - 1	Velocity - Core - Number 1

INC-C-15894

Fig. A-2 In-vessel instrumentation.

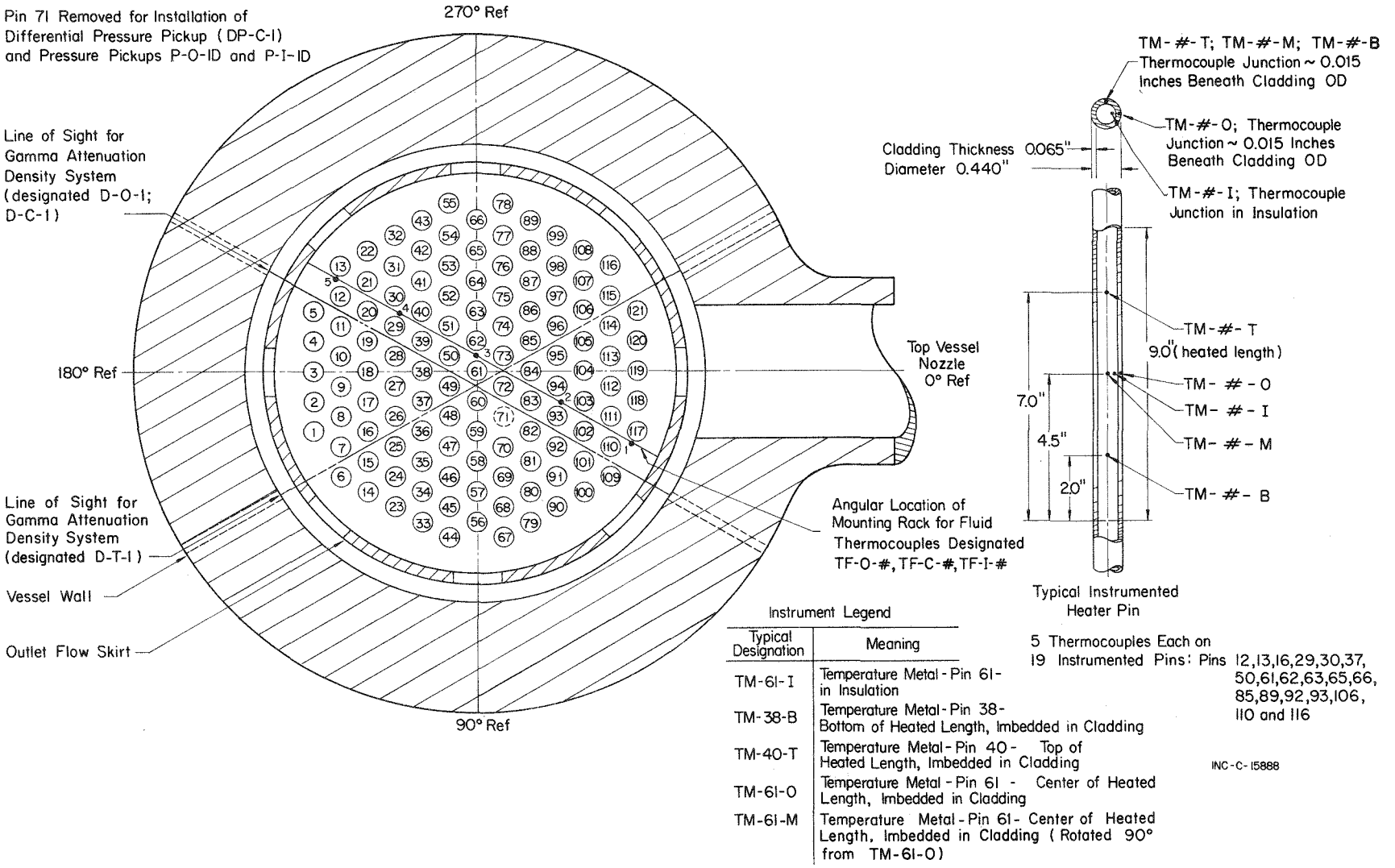

Fig. A-3 Heater pin and thermocouple locations.

APPENDIX B

METHODS USED TO NORMALIZE TEST DATA TO ACCOUNT FOR INSTRUMENT DRIFT AND THERMAL EFFECTS

APPENDIX B

METHODS USED TO NORMALIZE TEST DATA TO ACCOUNT FOR INSTRUMENT DRIFT AND THERMAL EFFECTS

The data reported for Tests 824 and 825 have, in many cases, been corrected to account for instrument drift and detector thermal sensitivity. The purpose of this appendix is to explain the methods used to normalize the test data.

I. PRESSURE

The majority of the pressure transducers used for Tests 824 and 825 are of the strain-gage type with a 3000-psi range. On the basis of the manufacturer's specifications, at constant temperature, the absolute value of the pressure measurements are within ±5% of full scale. In addition, the manufacturer's specifications indicate that for a 400°F temperature change the error for a full scale reading is less than 480 psig, and for a zero pressure reading the error is less than 60 psig.

In a typical decompression experiment, starting at 2250 psig, the pressure drops about 1,000 psi during subcooled blowdown in less than 100 msec and is accompanied by a fluid temperature change of about 5 to 6°F. For the remainder of the decompression (saturated blowdown), the pressure changes relatively slowly down to atmospheric pressure; fluid temperatures, however, decrease about 400°F during the time required to reach atmospheric conditions. The information obtained from the pressure transducers was modified in the following manner:

(1) With the semiscale system at steady state pretest conditions (approximately 2250 psi and 580°F), each pressure transducer output was normalized to agree with pretest pressures obtained from a precision pressure gage located on the vessel head, with appropriate corrections made for the fluid pressure drop around the loop.

(2) The total pressure change measured for each transducer as the system pressure drops from the saturation pressure to atmospheric pressure was modified by use of a linear correction factor to obtain the required total pressure drop. For example, if a pressure transducer indicated a pressure of -50 psi at the end of the transient (pressure at atmospheric conditions), the entire pressure history would be modified to decrease the measured drop from saturation to atmospheric pressure by 50 psi in a manner linear with time.

II. TEMPERATURE

The only modification of the temperature data for Tests 824 and 825 consisted of assigning the initial condition temperature to all temperature data at the time of rupture (amounting to as much as 30°F correction). For piping materials in which heat loss from the piping was evident, this modification of the temperature data was not made.

III. DENSITY

Fluid density measurements are processed using a computer data conversion program. Initial output from density detectors is in volts which must be converted to lb/ft^3 based on the detector sensitivity.

With the semiscale system at pretest steady state conditions, the initial voltage output from the detectors is assigned the appropriate initial density value. The final voltage recorded is assigned a value of 0.03 lb/ft^3 (essentially zero) and a linear (with time) calibration factor is applied between these two points. The estimated accuracy of the density measurements is within ± 5% of full scale or within approximately ± 2.2 lb/ft^3.

IV. MOMENTUM FLUX

Momentum flux measurements are made using calibrated drag disc devices which give an output in volts. On the basis of the initial density and the calibration curve for a particular detector, the initial voltage from the detector is assigned a value commensurate with initial pretest steady state flow conditions. To compensate for thermal sensitivity of the detector, a computer data-conversion program applies a linear (with time) correction to the data based on the detector calibration curve and on the initial and final conditions.

V. THRUST

The vessel horizontal load cell data must be corrected for the loading imposed on the vessel due to thermal expansion of the piping during the warmup period. The thrust loads during blowdown are thus represented by the change from the initial value, assuming a negligible temperature change of the piping during blowdown (that is, the measured load at the time of rupture is set equal to zero). The assumption of negligible temperature change in the piping is valid only for the early portion of decompression; larger changes in pipe temperature occur during the later portions of saturated blowdown and thrust data are not reliable beyond this point.

VI. STRAIN

The magnitude of the strains measured during blowdown was recorded with compressive strains referred to as negative strains and tensile strains as positive strains. The thermal sensitivity of the full bridge installations was monitored during system warmup. Strain values were determined by normalizing all strain data to zero at the initial test conditions. In general, the apparent strain due to instrument temperature sensitivity was less than 0.3 μin./in.-°F for strain gages installed in the loop piping.

APPENDIX C

SELECTED EXAMPLES OF DIGITIZED DATA -- SEMISCALE TESTS 824 AND 825

APPENDIX C

SELECTED EXAMPLES OF DIGITIZED DATA -- SEMISCALE TESTS 824 AND 825

The 33 figures included in this appendix are intended to illustrate, in general, the type of information provided by Tests 824 and 825. Unless otherwise indicated, this information is as received directly from the digitized analog data prior to application of any initialization or corrective process.

I. PRESSURE HISTORIES

Figures C-1 through C-12 represent the total pressure histories at four loop and two vessel locations for both Tests 824 and 825. The corrective process outlined in Section I of Appendix B has been applied in all cases to account for zero shift and thermal sensitivity.

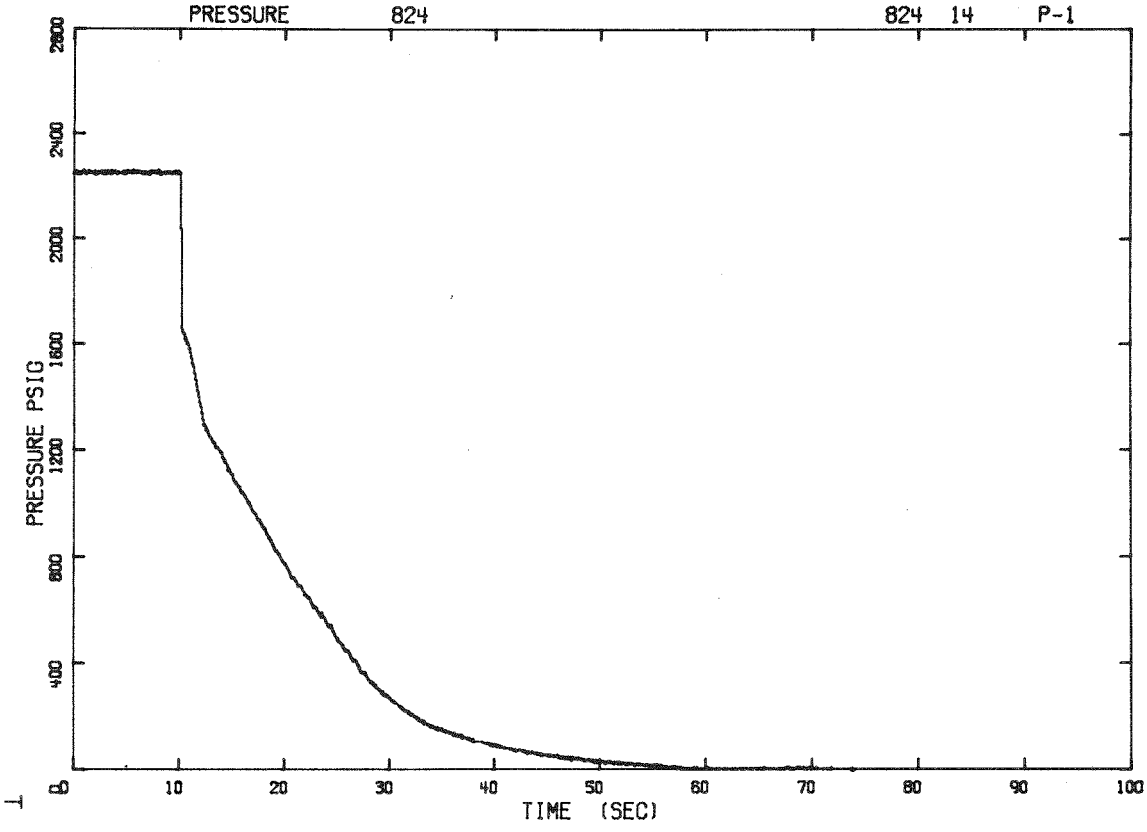

Fig. C-1 Pressure at vessel outlet - Test 824.

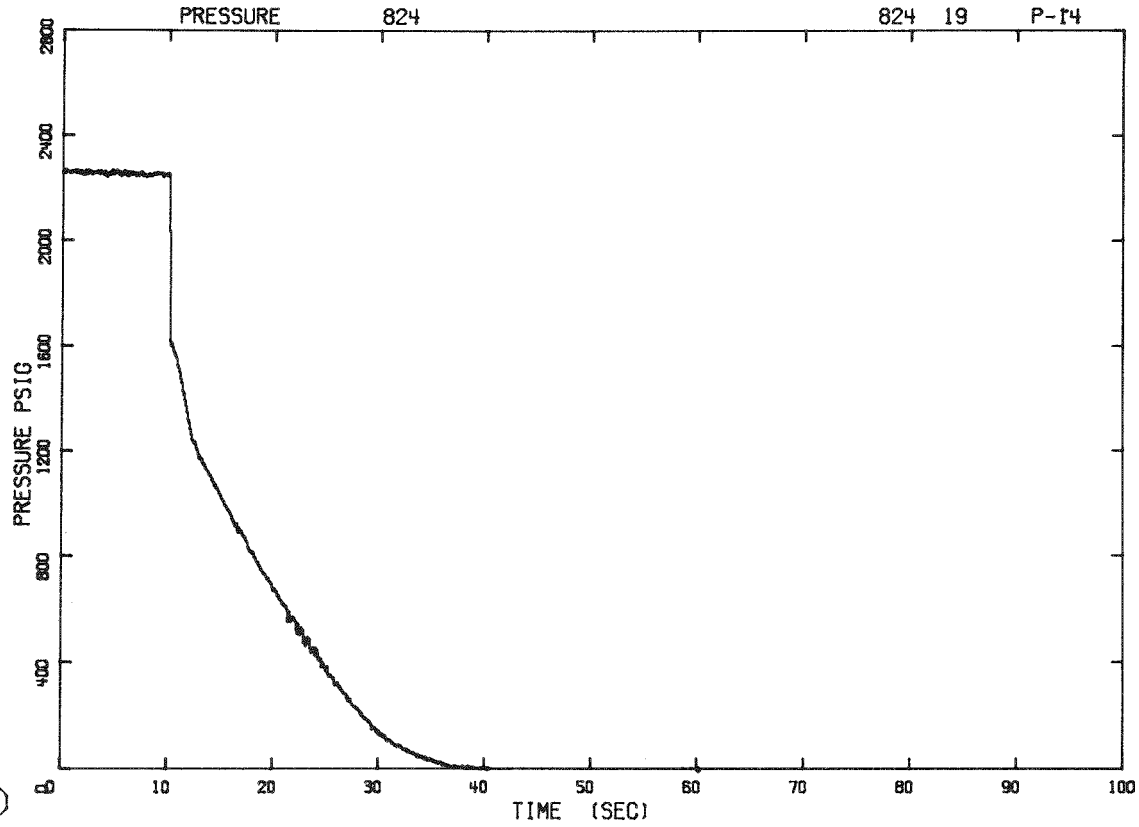

Fig. C-2 Pressure at vessel inlet - Test 824.

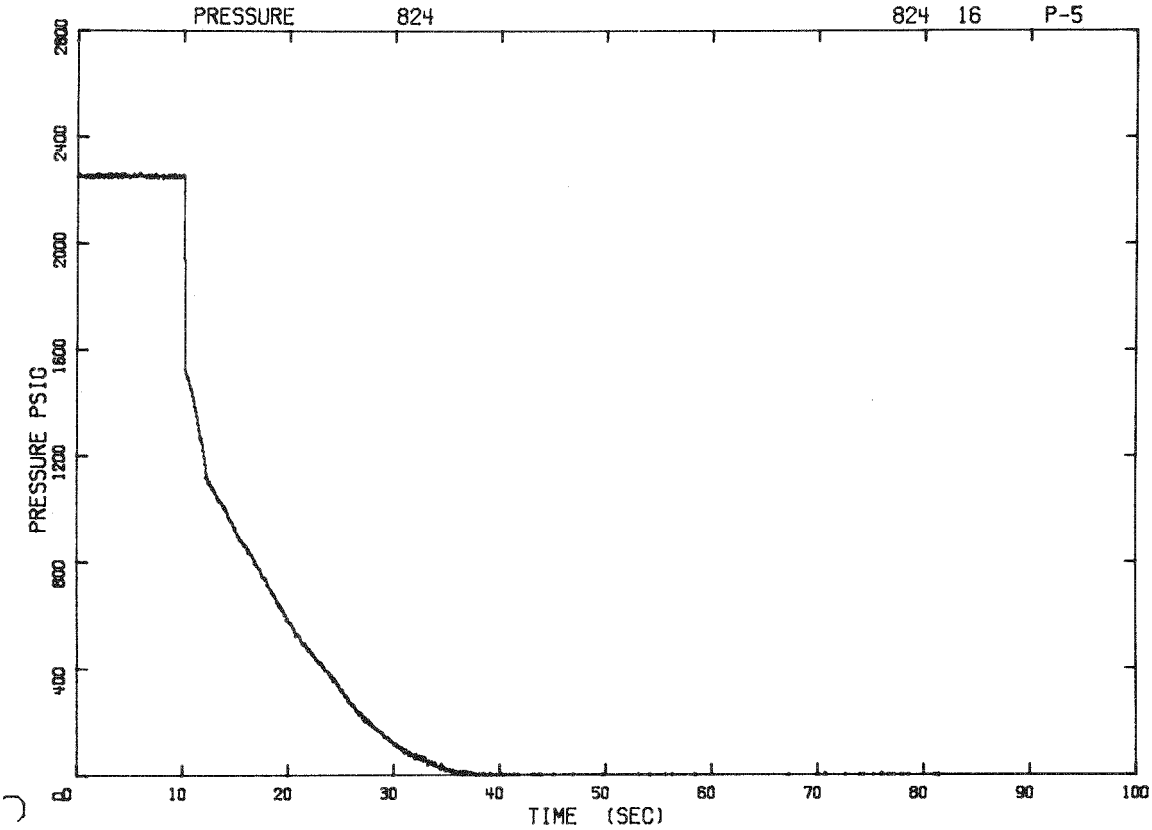

Fig. C-3 Pressure at steam generator inlet - Test 824.

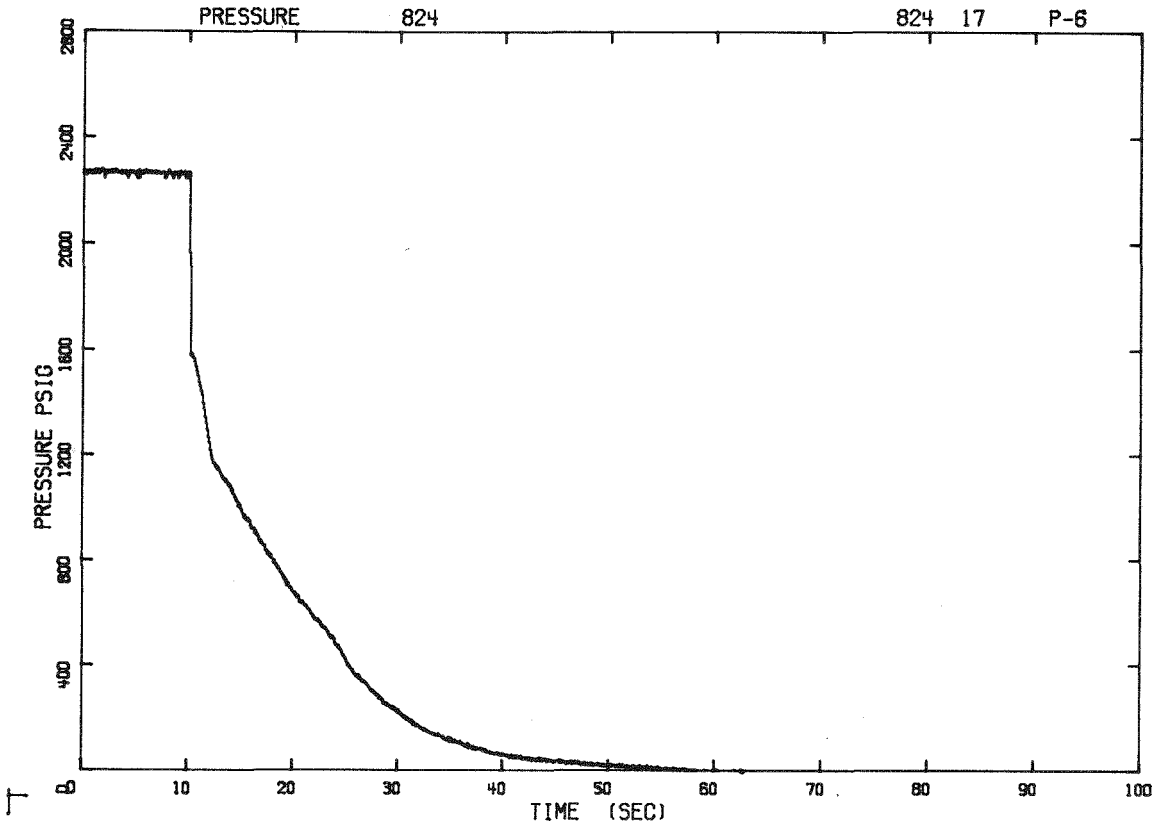

Fig. C-4 Pressure at steam generator outlet - Test 824.

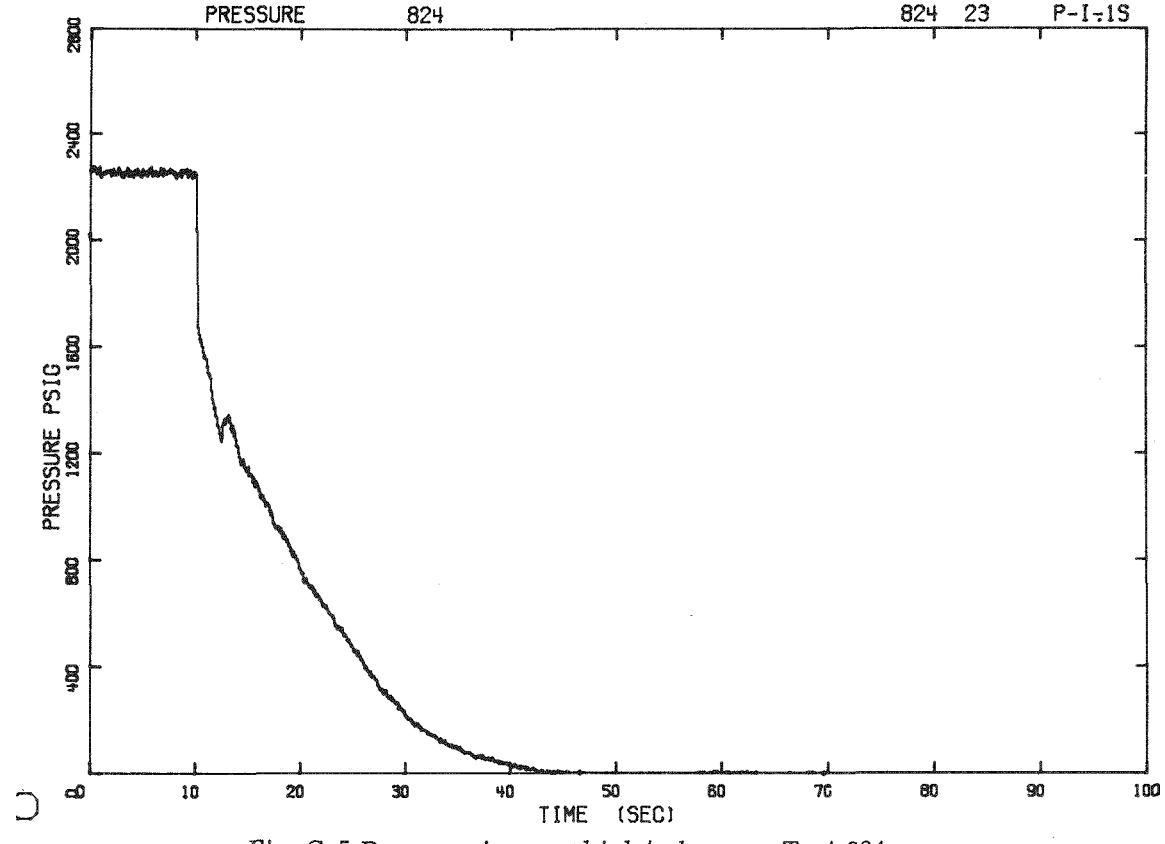

Fig. C-5 Pressure in vessel inlet plenum - Test 824.

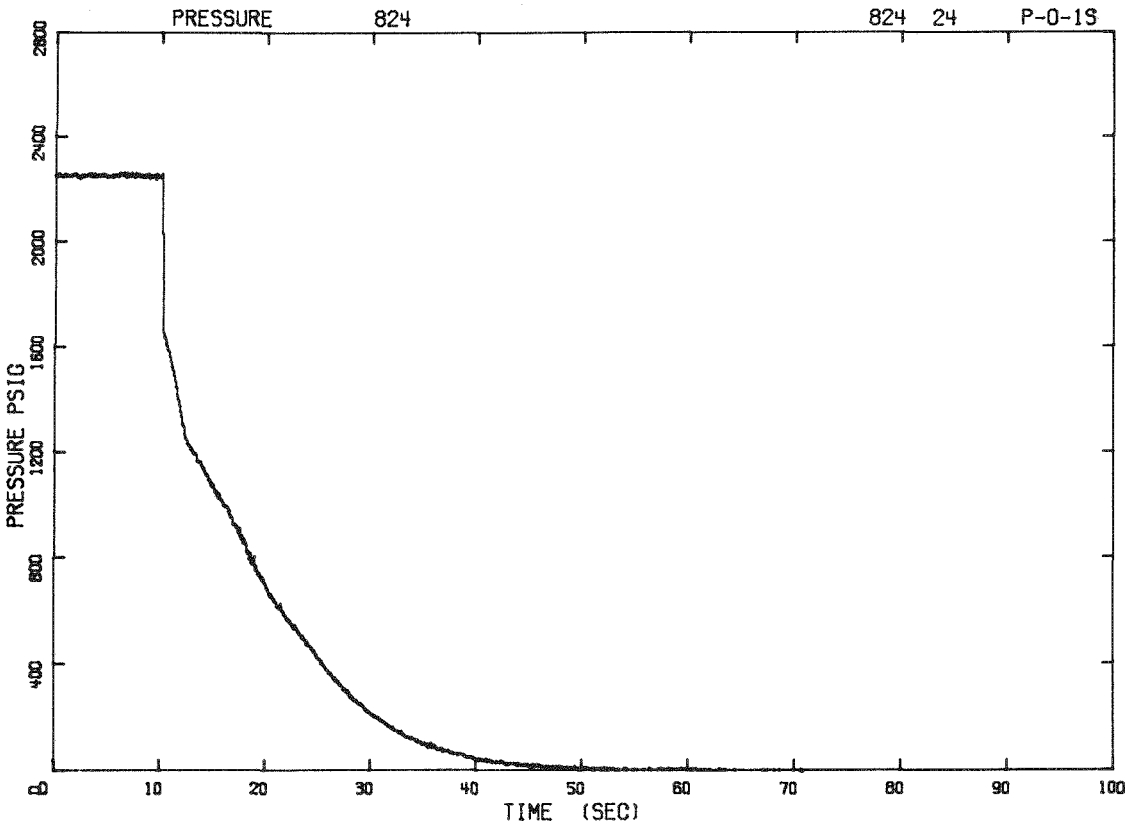

Fig. C-6 Pressure in vessel outlet plenum - Test 824.

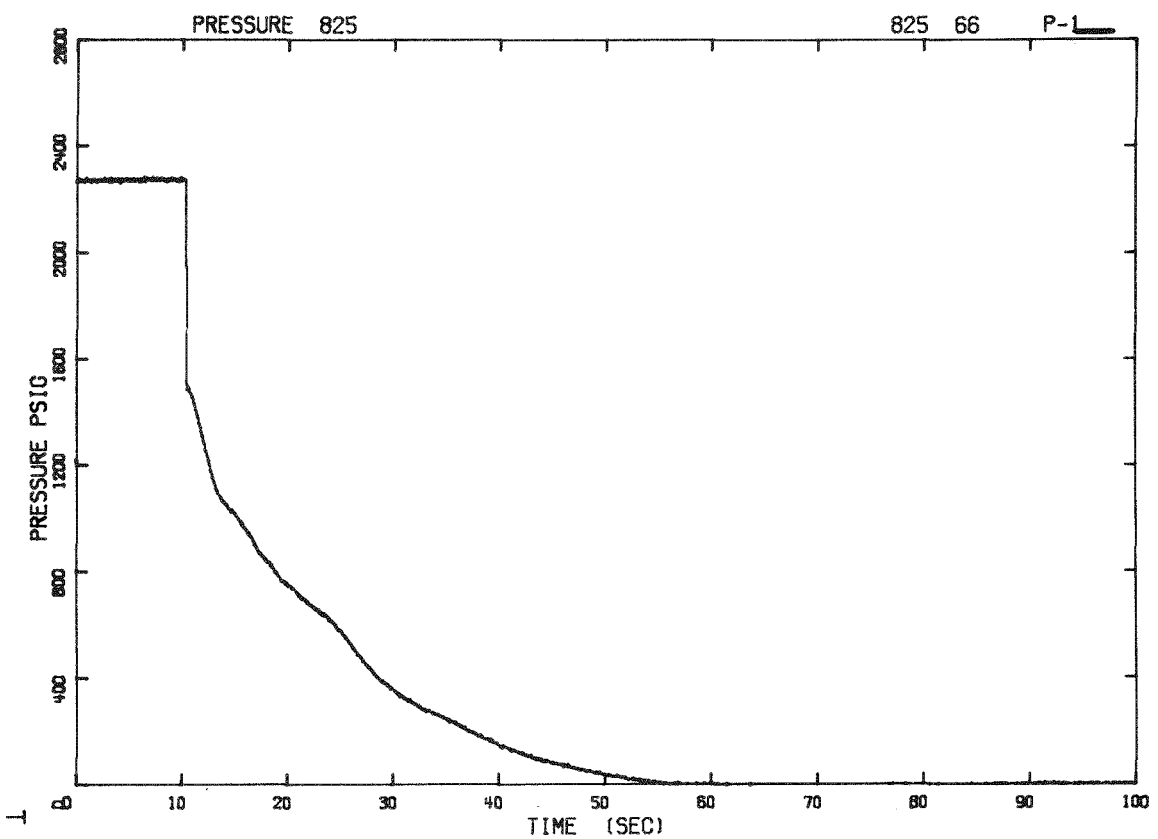

Fig. C-7 Pressure at vessel outlet - Test 825.

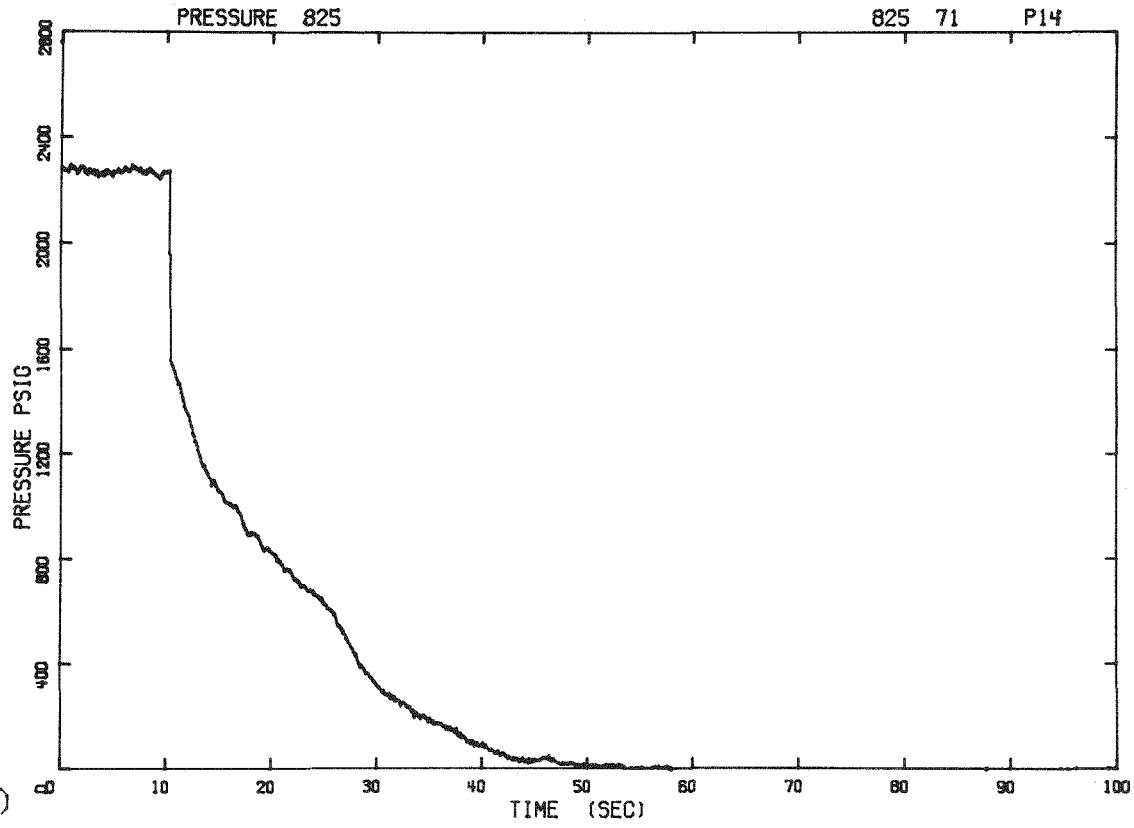

Fig. C-8 Pressure at vessel inlet - Test 825.

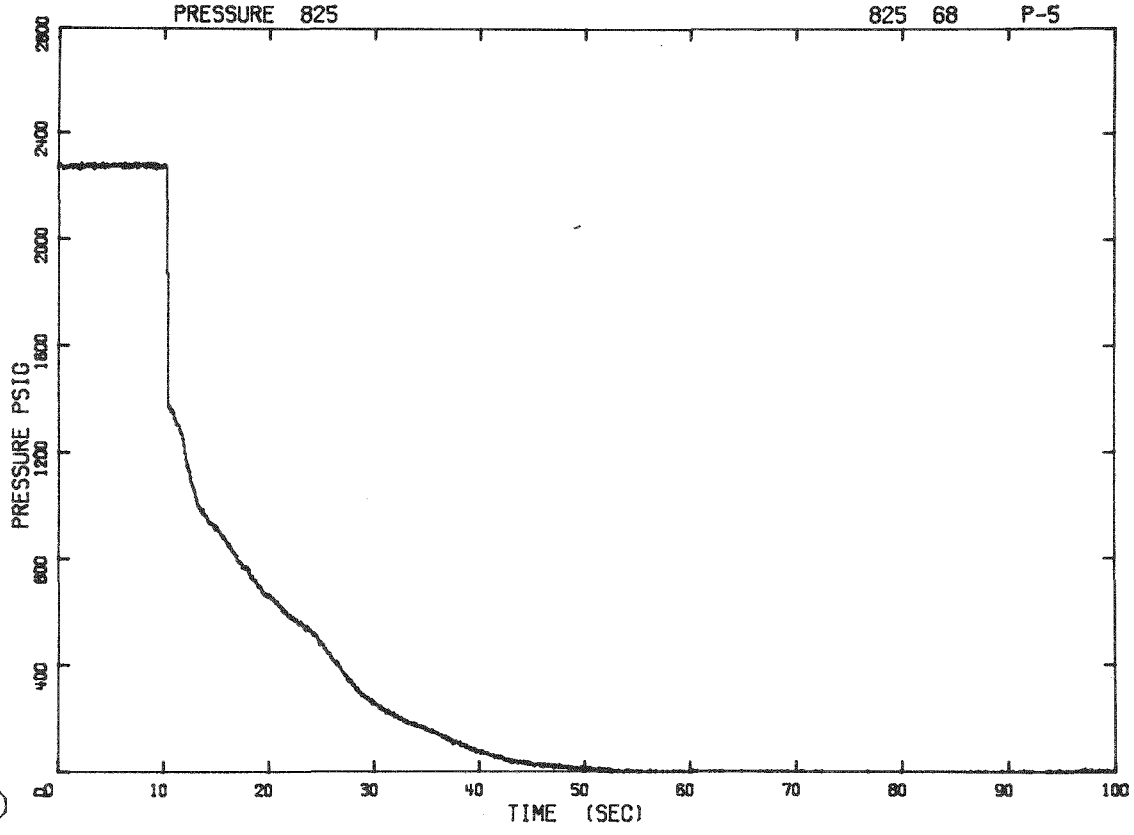

Fig. C-9 Pressure at steam generator inlet - Test 825.

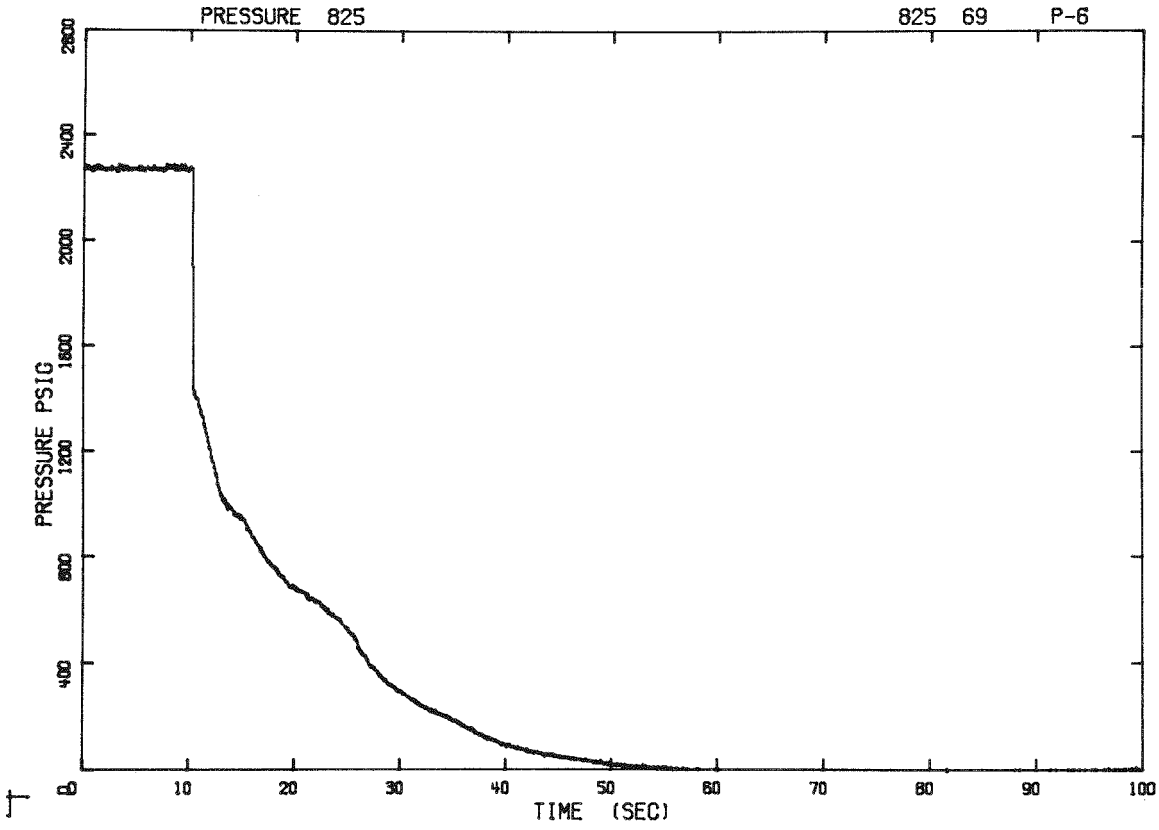

Fig. C-10 Pressure at steam generator outlet - Test 825.

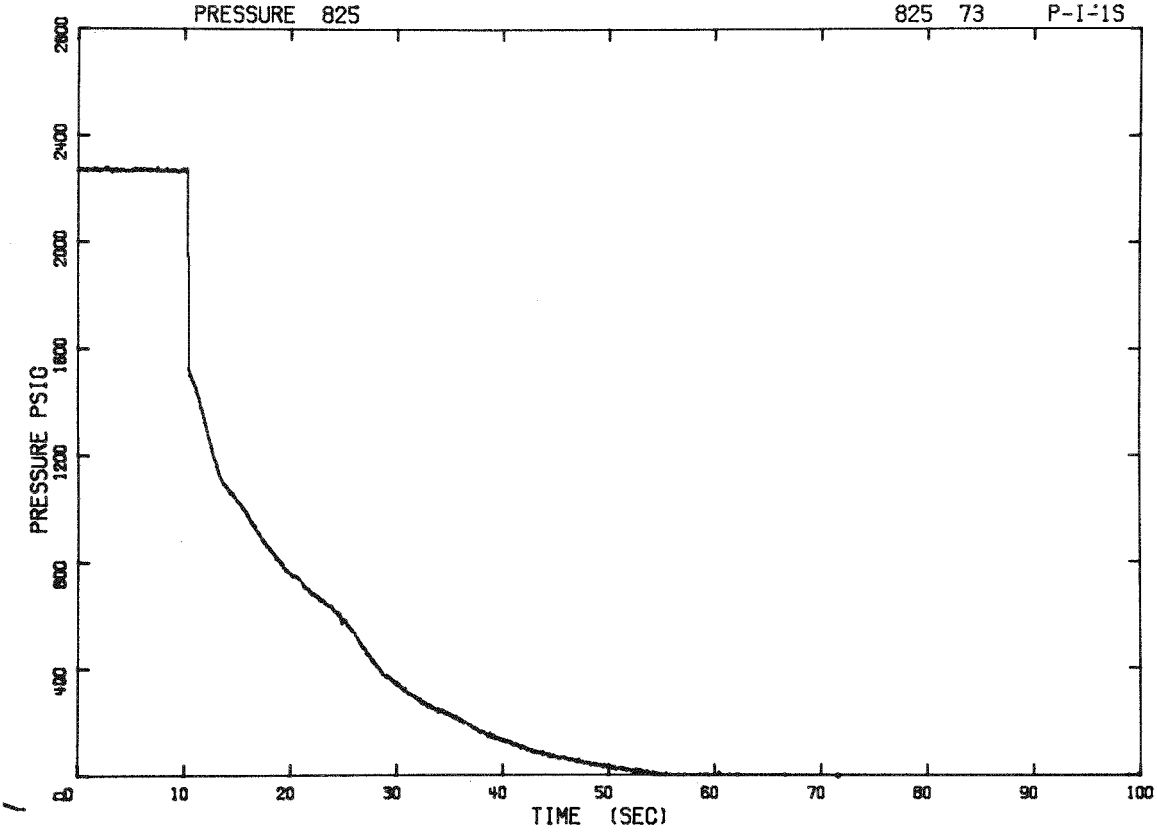

Fig. C-11 Pressure in vessel inlet plenum - Test 825.

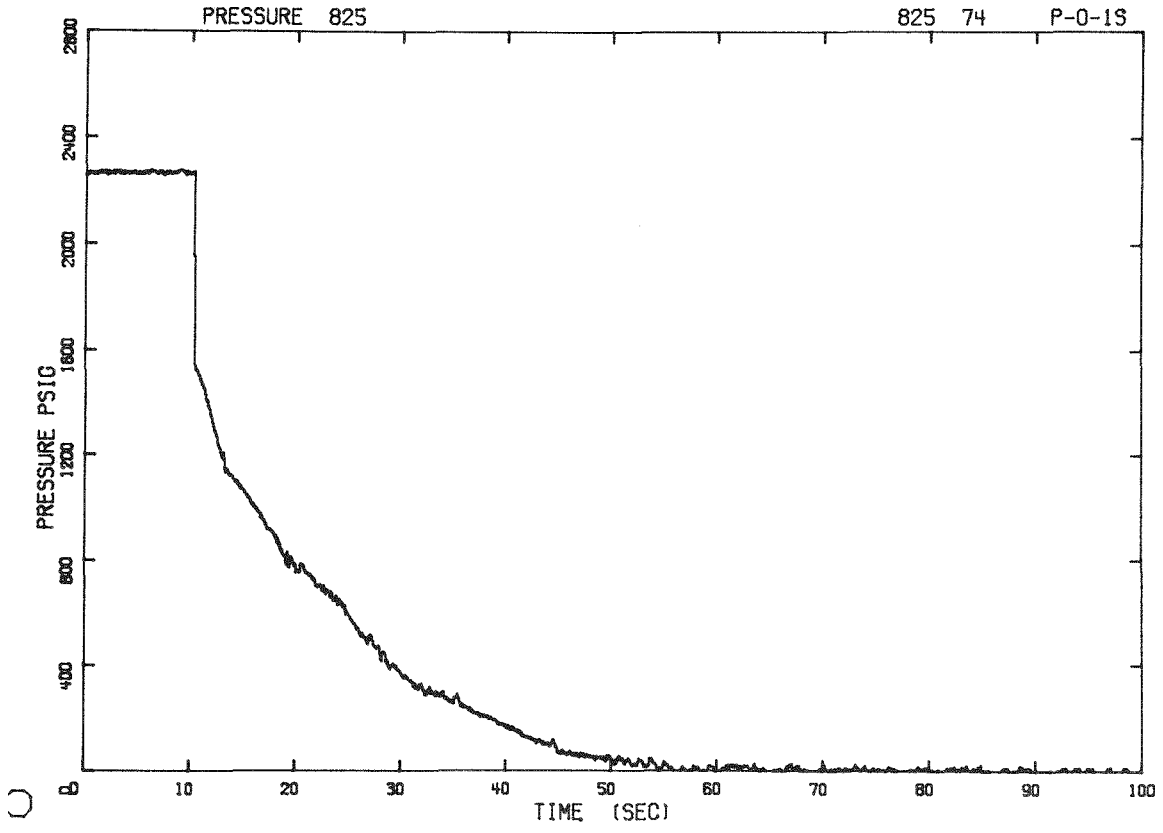

Fig. C-12 Pressure in vessel outlet plenum - Test 825.

II. MATERIAL TEMPERATURE BEHAVIOR

Figures C-13 through C-29 represent the material temperature behavior during decompression for both Tests 824 and 825. The specific identification and location of detectors, is given in Appendix B, Figure B-3. These selected temperature traces give typical rod behavior during the transient for different elevations and locations within the core structure. The onset of DNB and the response of the pins is particularly evident in Figures C-24, -26, and -28, which represent the temperature behavior at the rod top location.

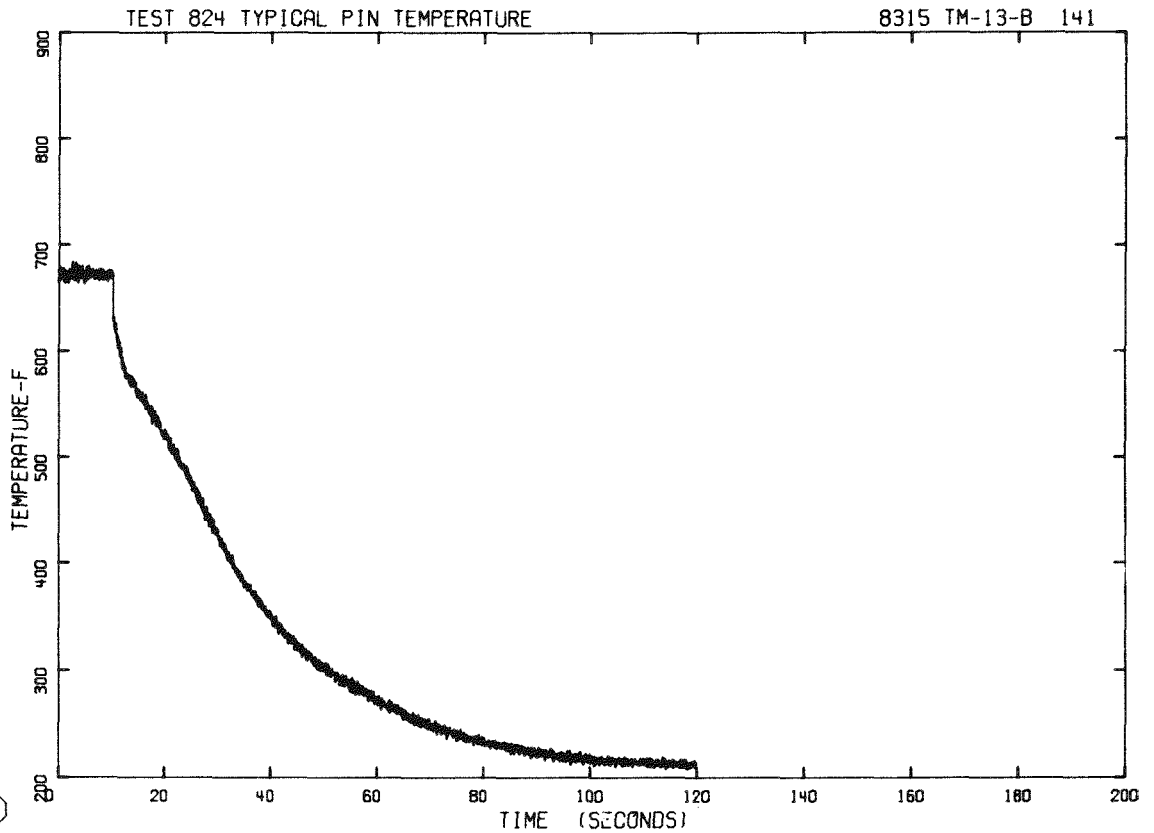

Fig. C-13 Pin temperature - Pin 13 bottom - Test 824.

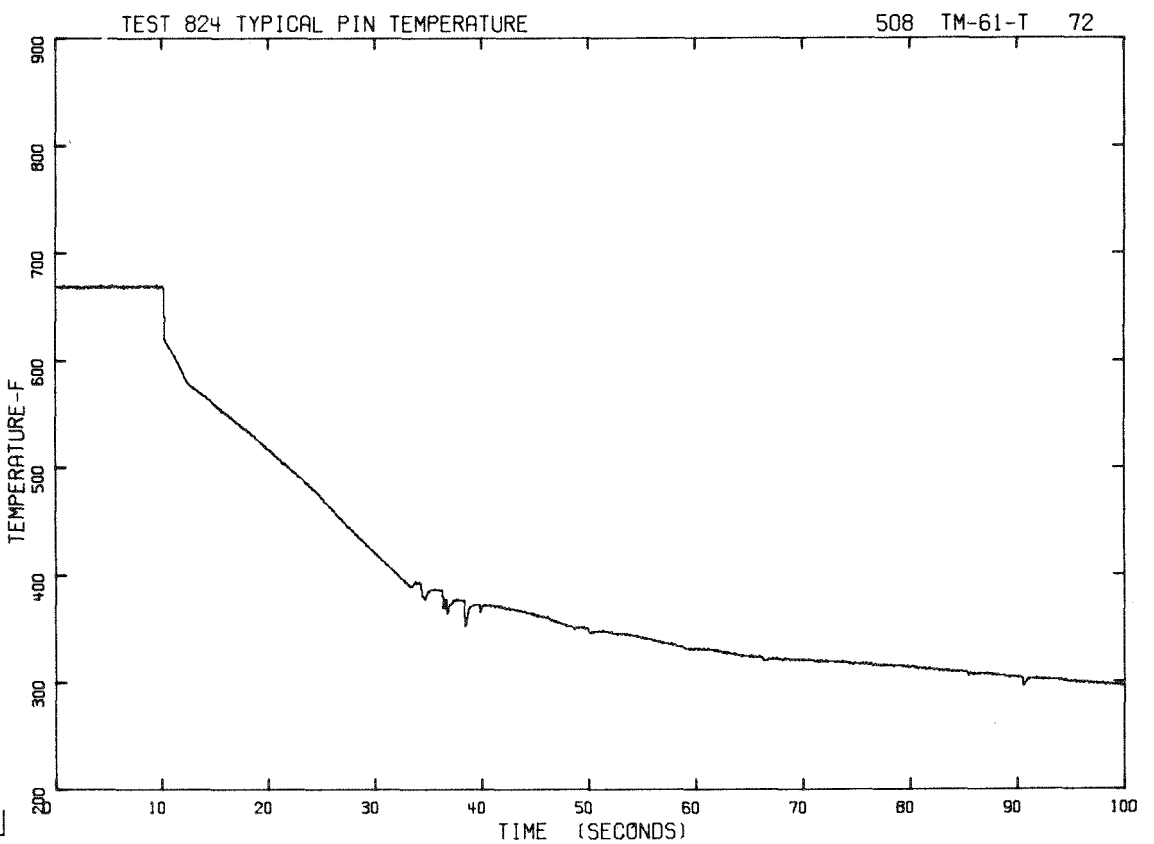

Fig. C-14 Pin temperature - Pin 61 top - Test 824.

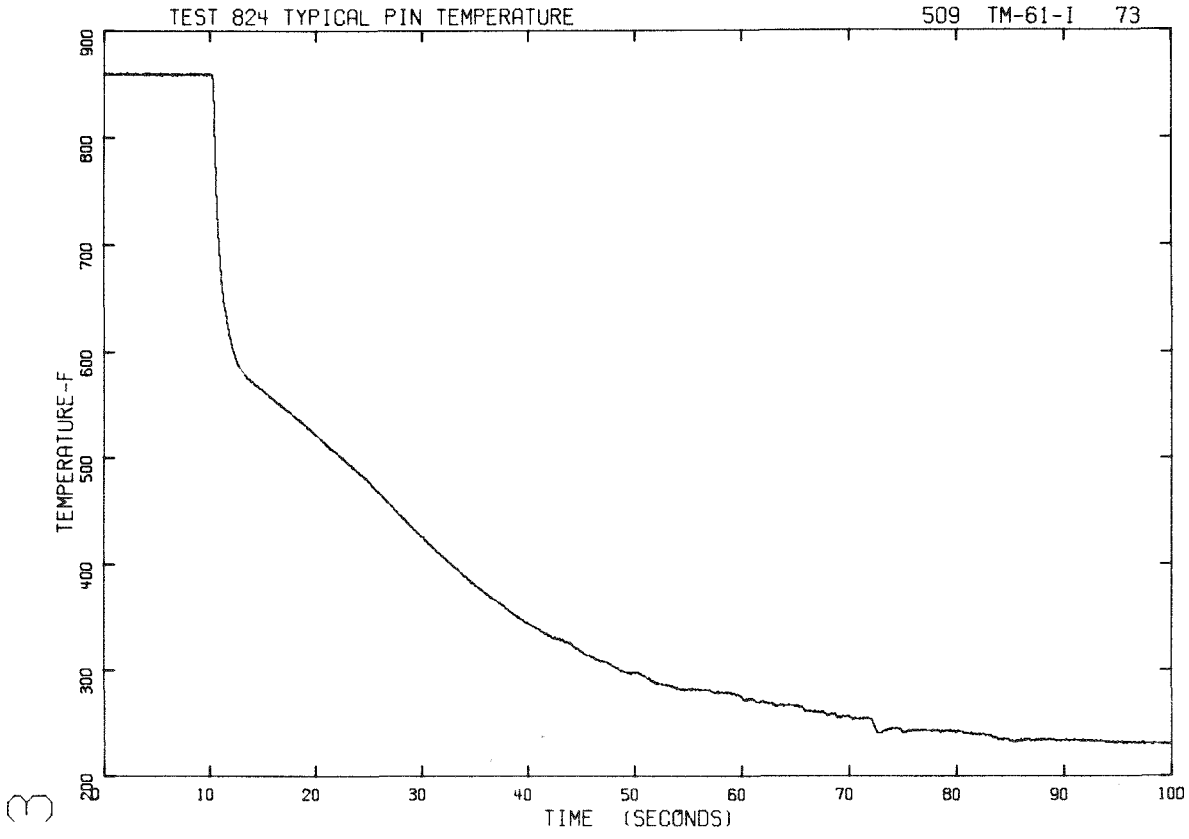

Fig. C-15 Pin temperature - Pin 61 insulation - Test 824.

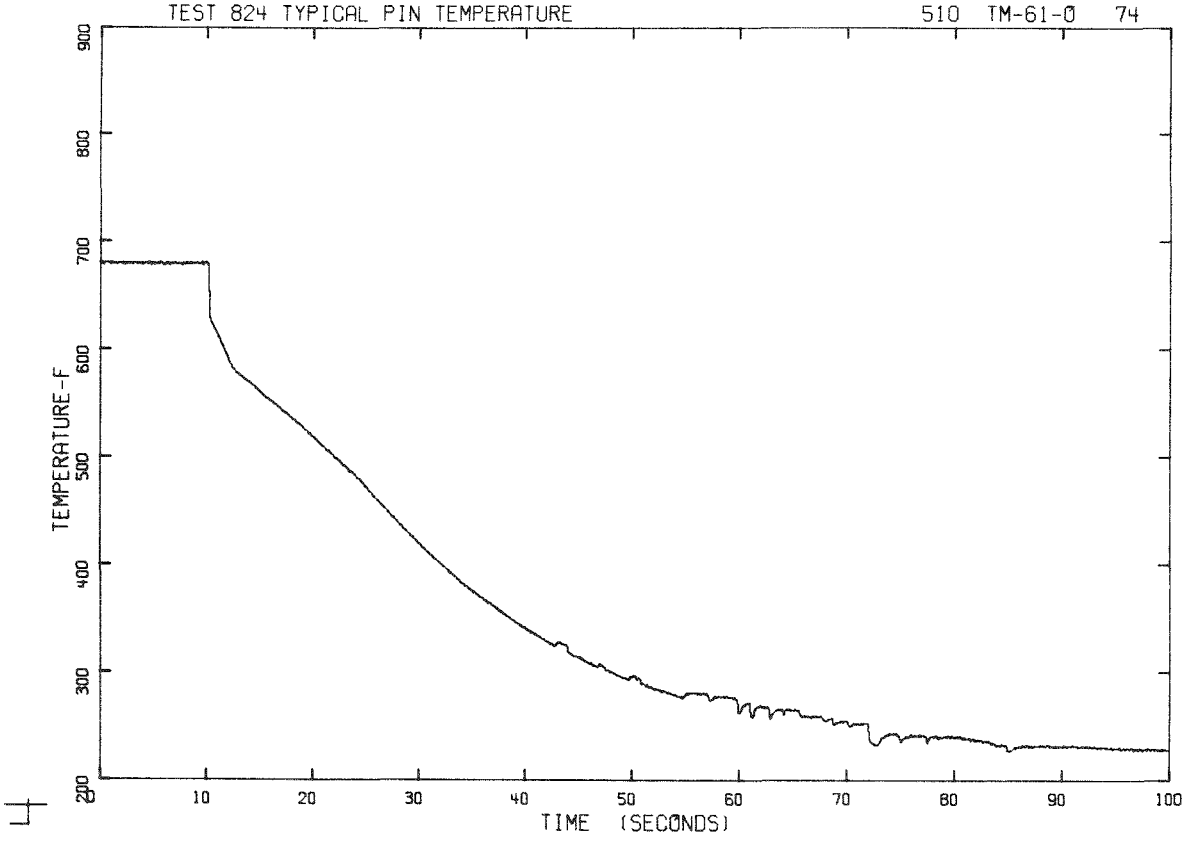

Fig. C-16 Pin temperature - Pin 61 middle - Test 824.

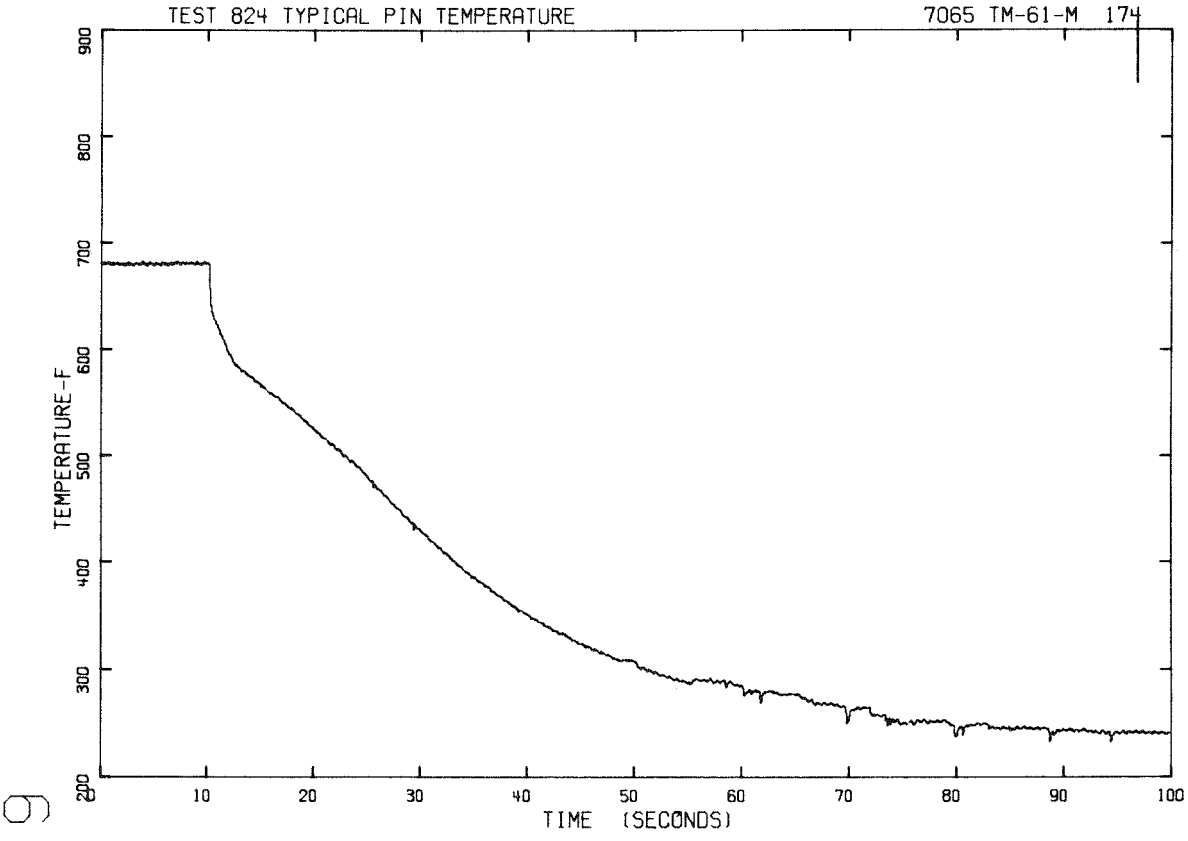

Fig. C-17 Pin temperature - Pin 61 middle - Test 824.

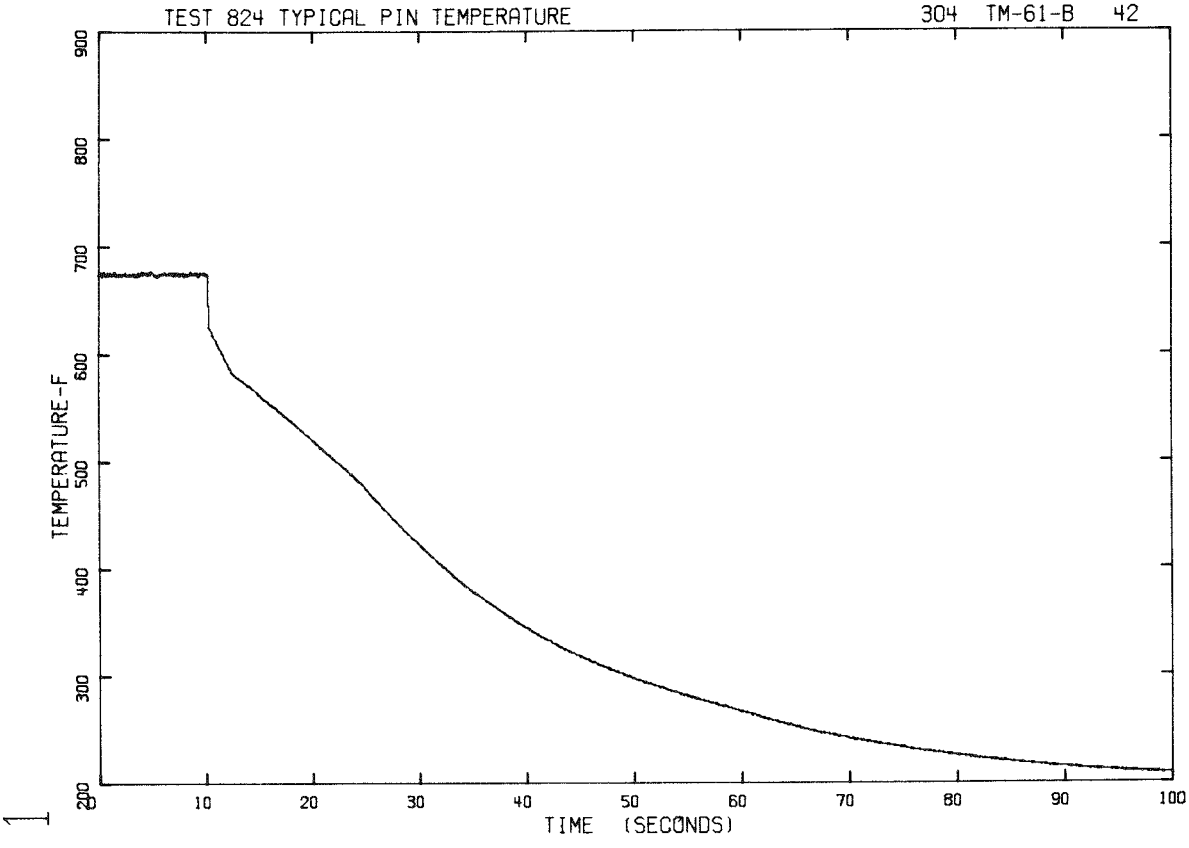

Fig. C-18 Pin temperature - Pin 61 bottom - Test 824.

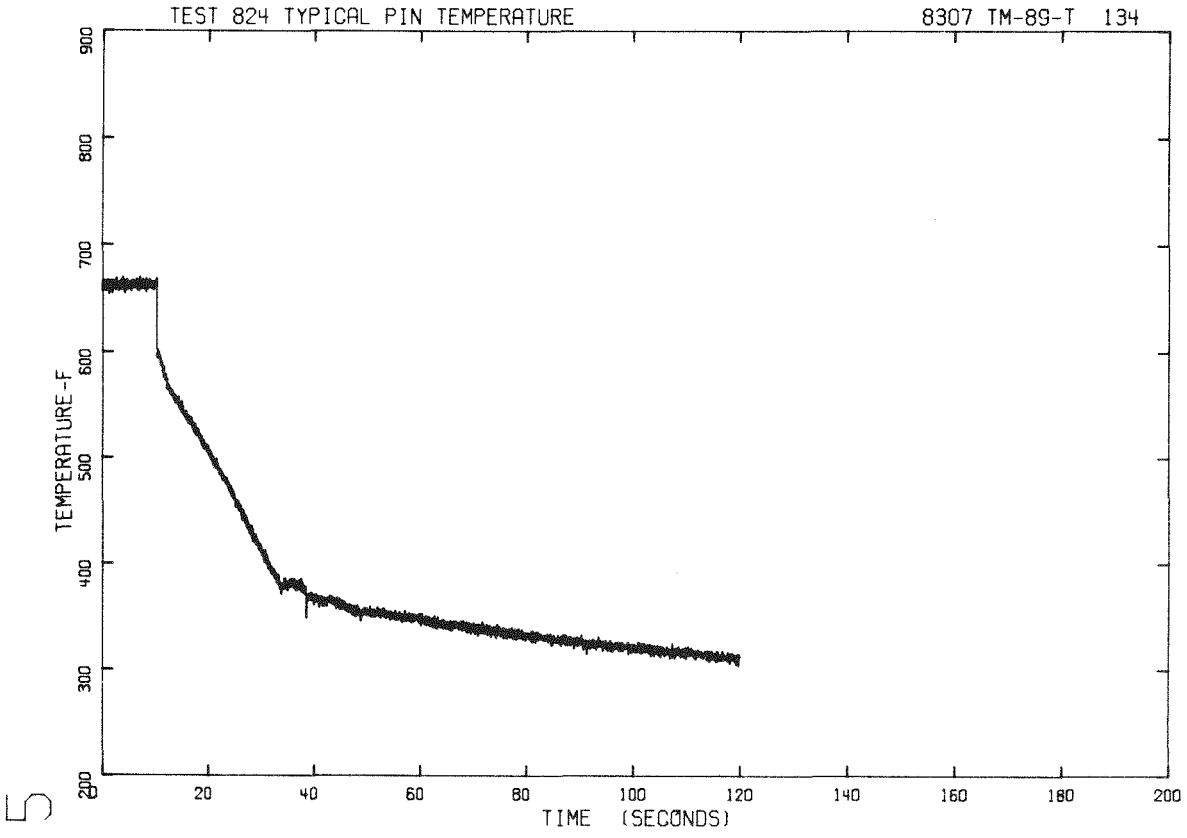

Fig. C-19 Pin temperature - Pin 89 top - Test 824.

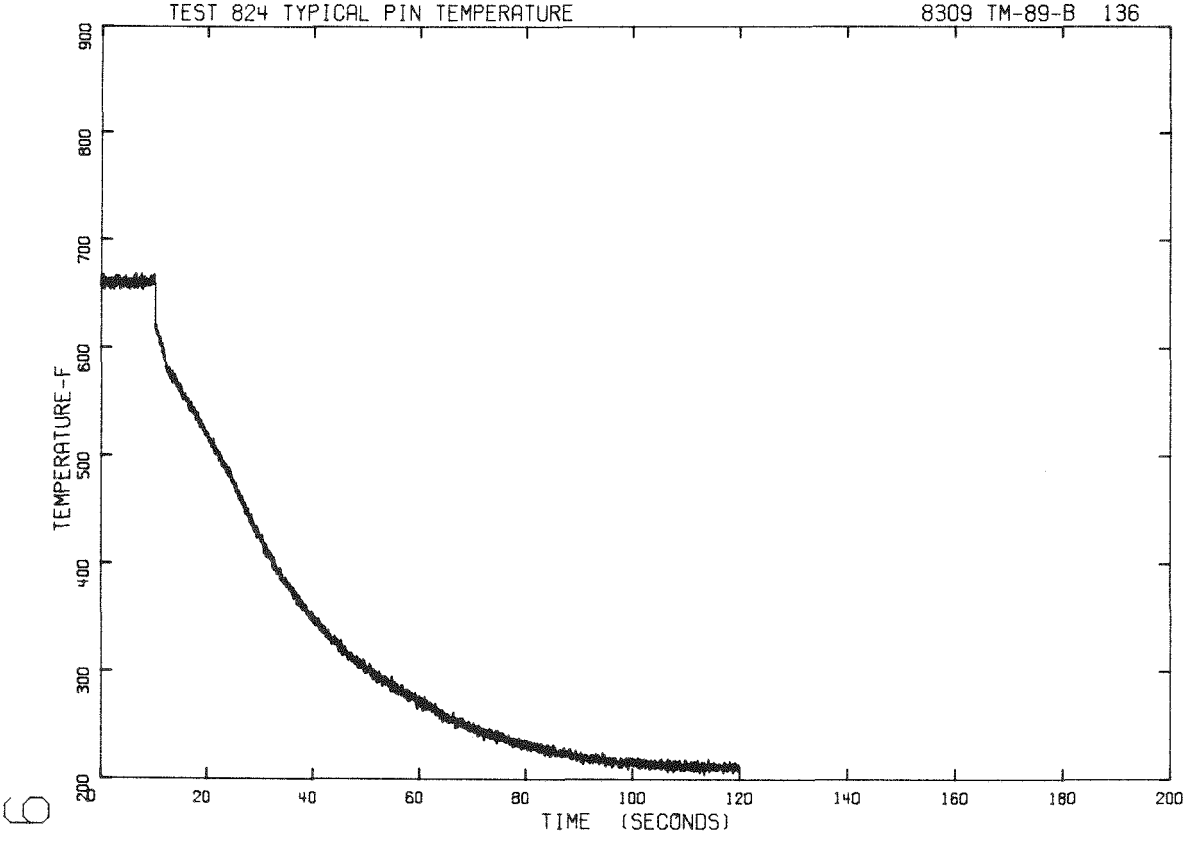

Fig. C-20 Pin temperature - Pin 89 bottom - Test 824.

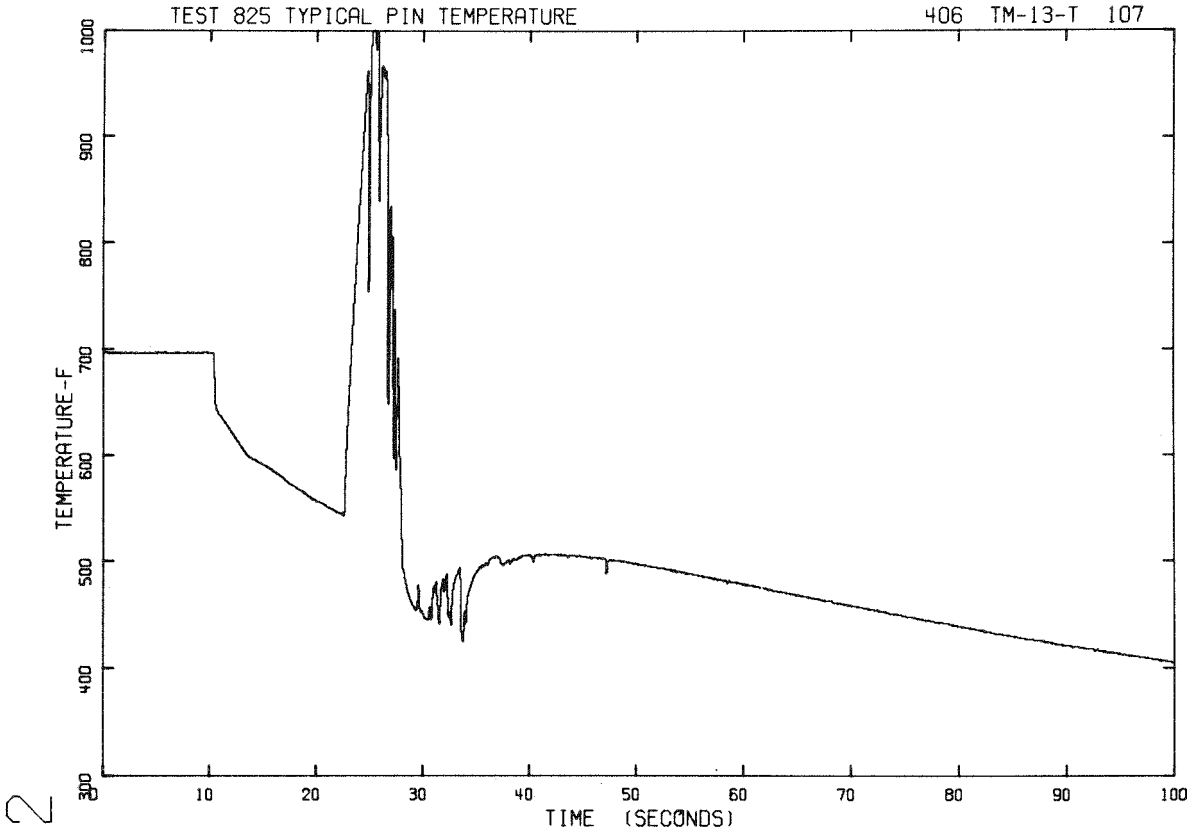

Fig. C-21 Pin temperature - Pin 13 top - Test 825.

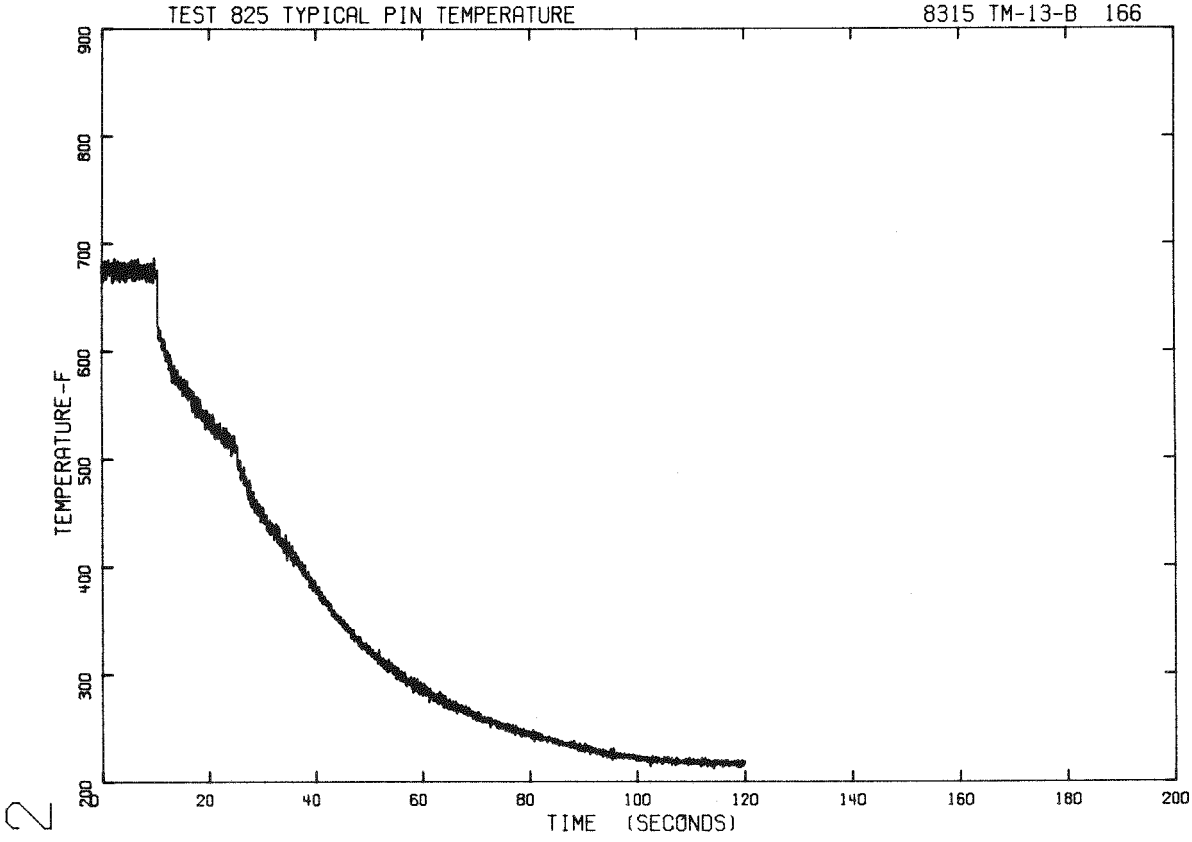

Fig. C-22 Pin temperature - Pin 13 bottom - Test 825.

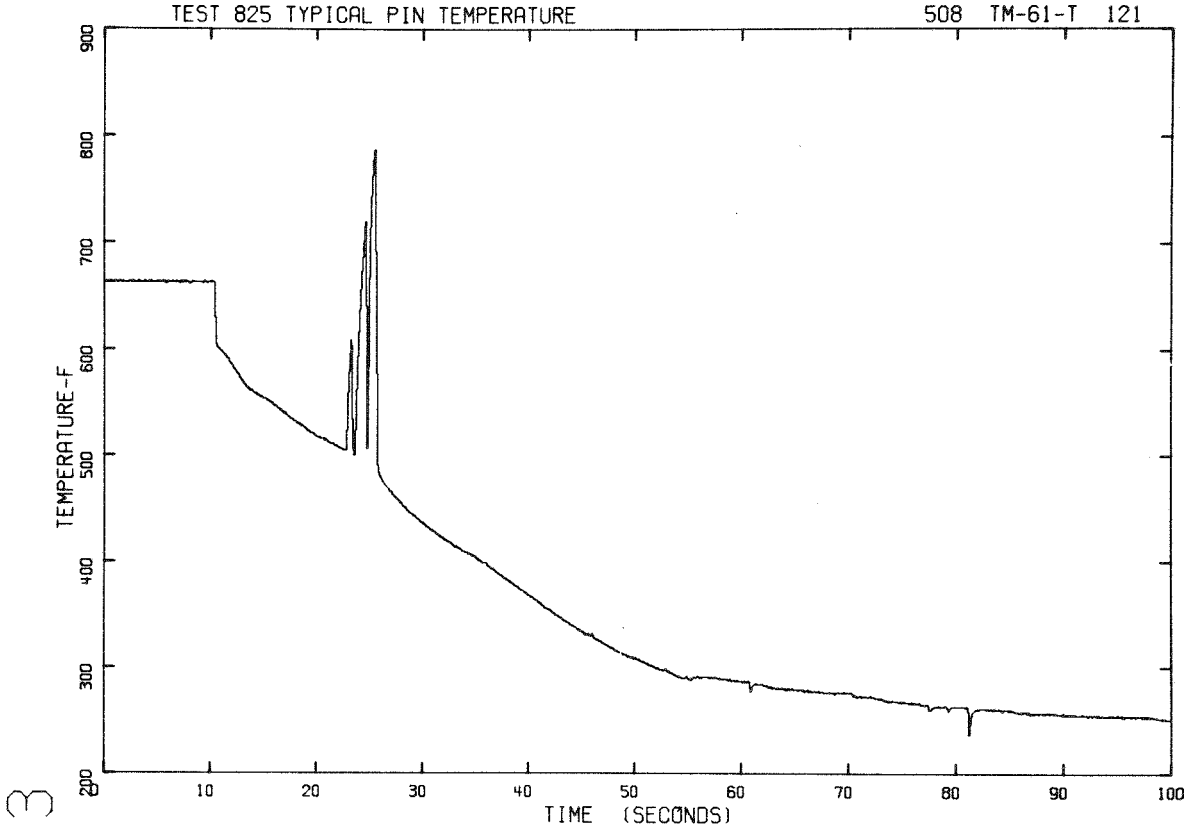

Fig. C-23 Pin temperature - Pin 61 top - Test 825.

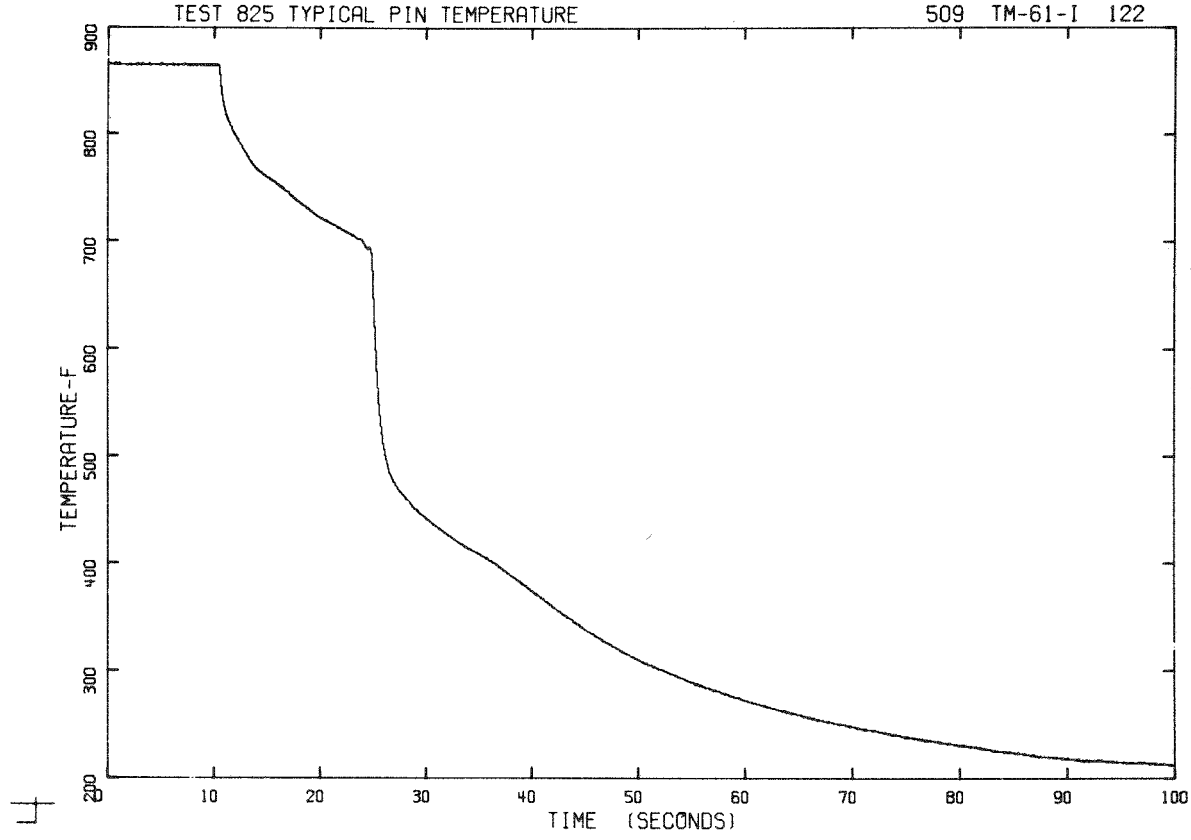

Fig. C-24 Pin temperature - Pin 61 insulation - Test 825.

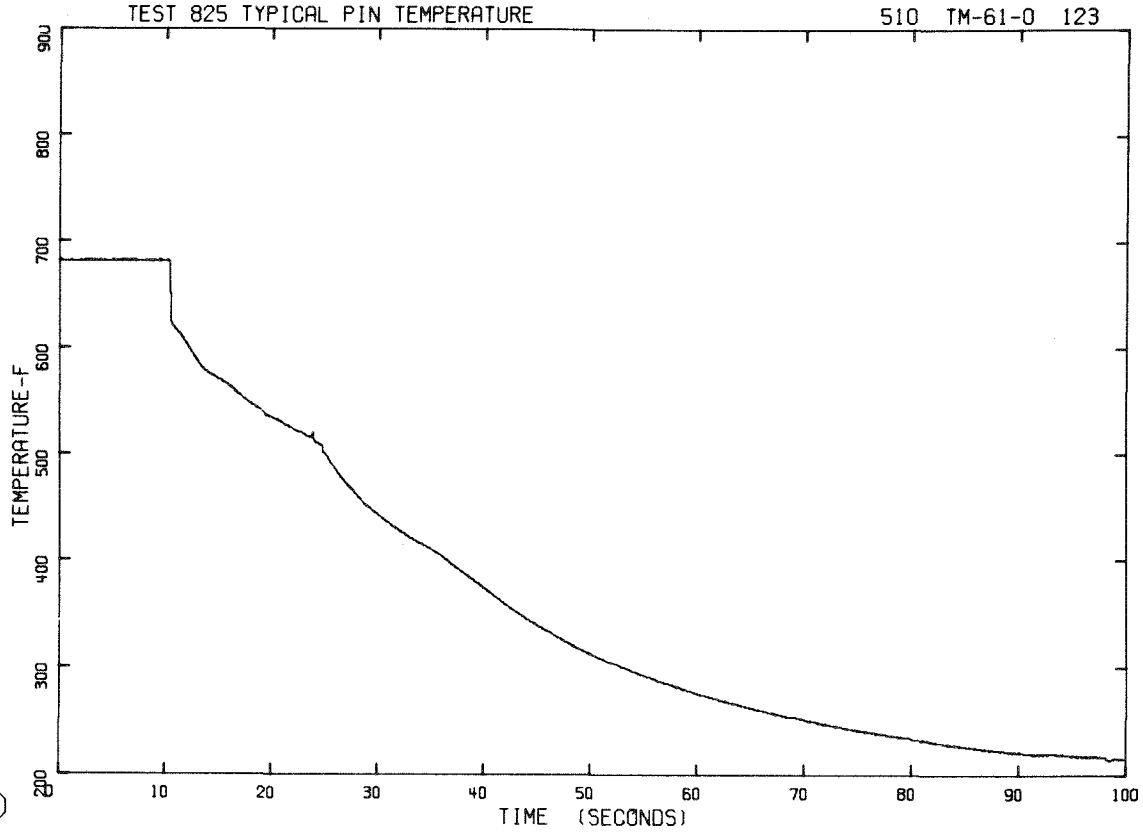

Fig. C-25 Pin temperature - Pin 61 middle - Test 825.

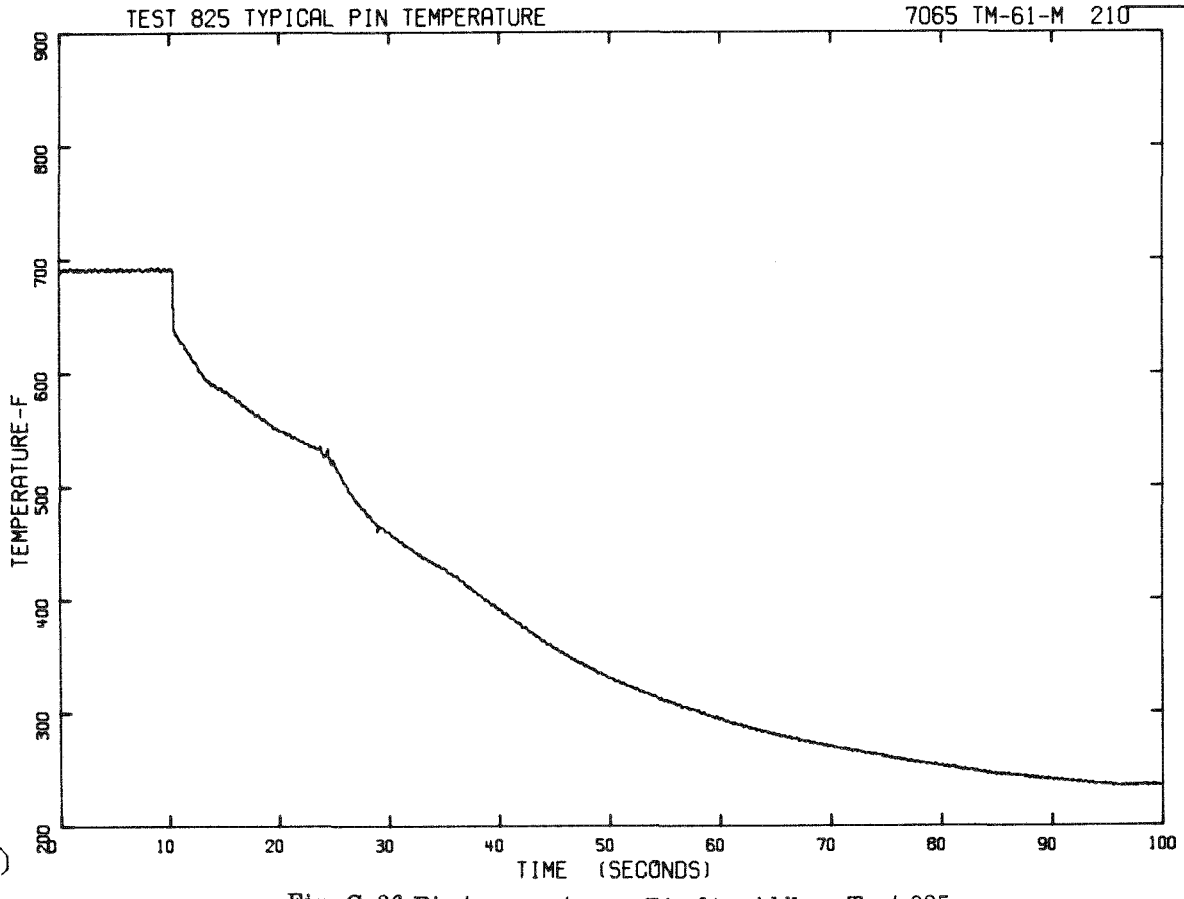

Fig. C-26 Pin temperature - Pin 61 middle - Test 825.

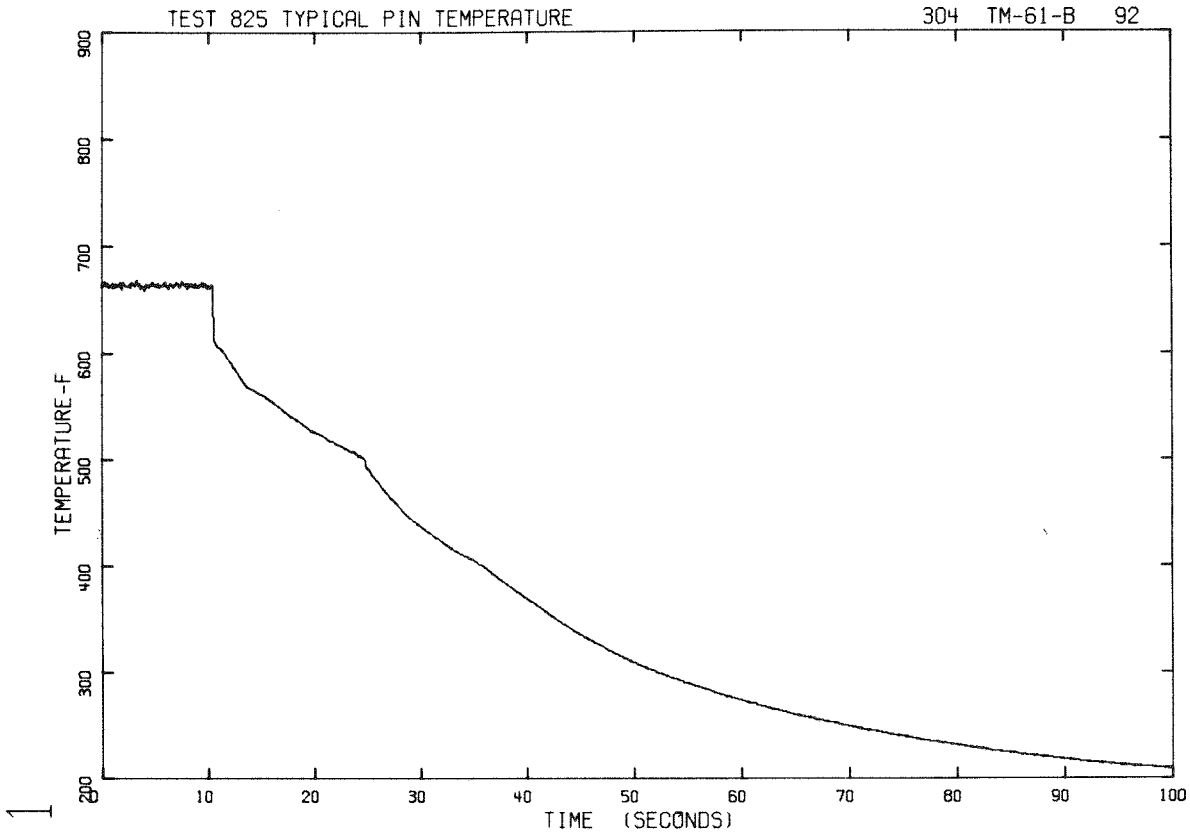

Fig. C-27 Pin temperature - Pin 61 bottom - Test 825.

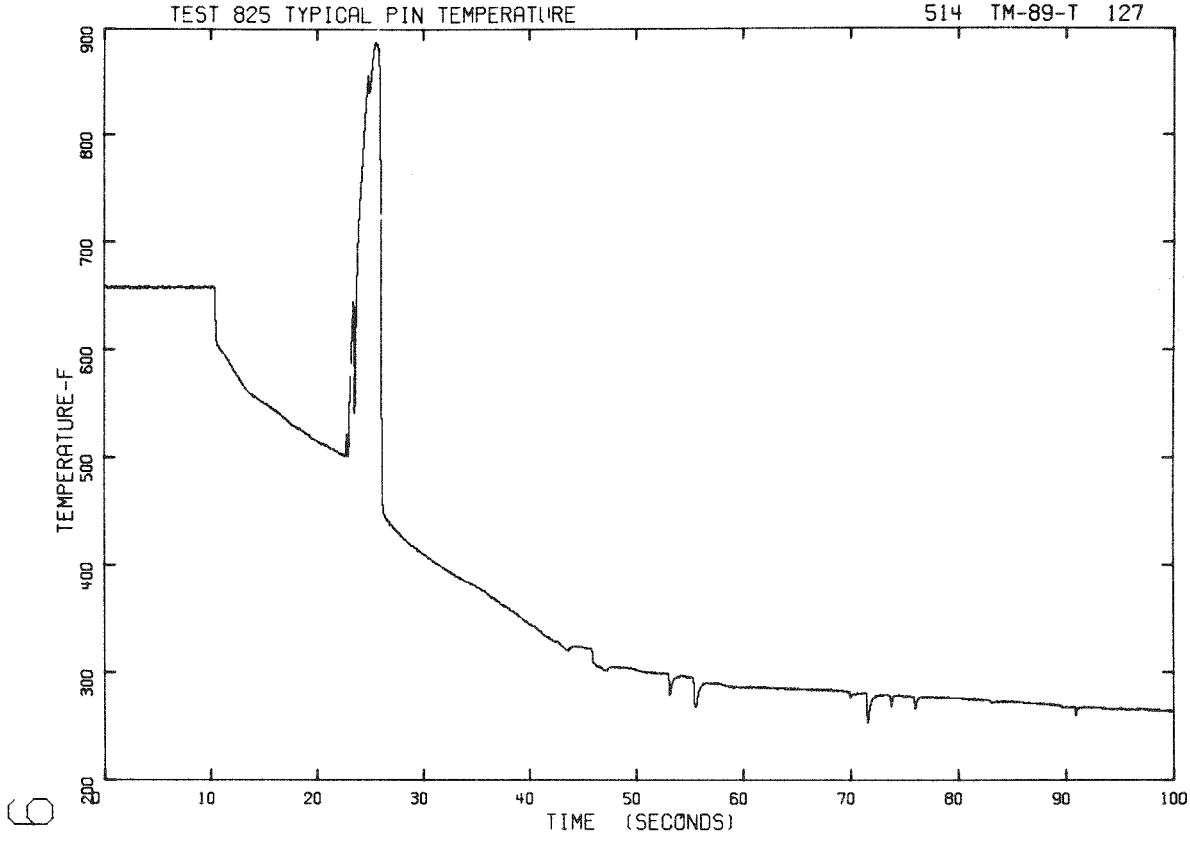

Fig. C-28 Pin temperature - Pin 89 top - Test 825.

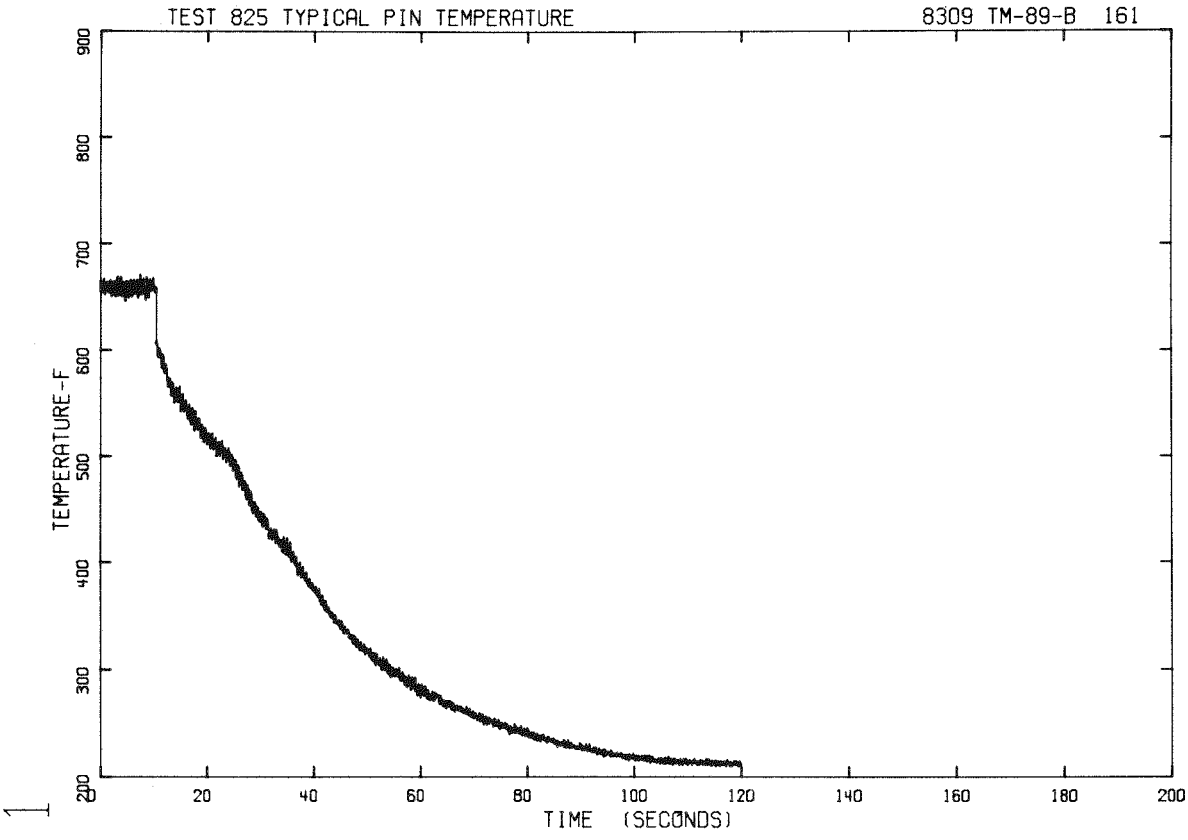

Fig. C-29 Pin temperature - Pin 89 bottom - Test 825.

III. FLUID TEMPERATURE BEHAVIOR

Figure C-30 shows the loop fluid temperature behavior at Station 5 (steam generator inlet) for Test 825 and illustrates the breakaway or erratic temperature behavior of the detector due to high quality - low velocity fluid near the detector.

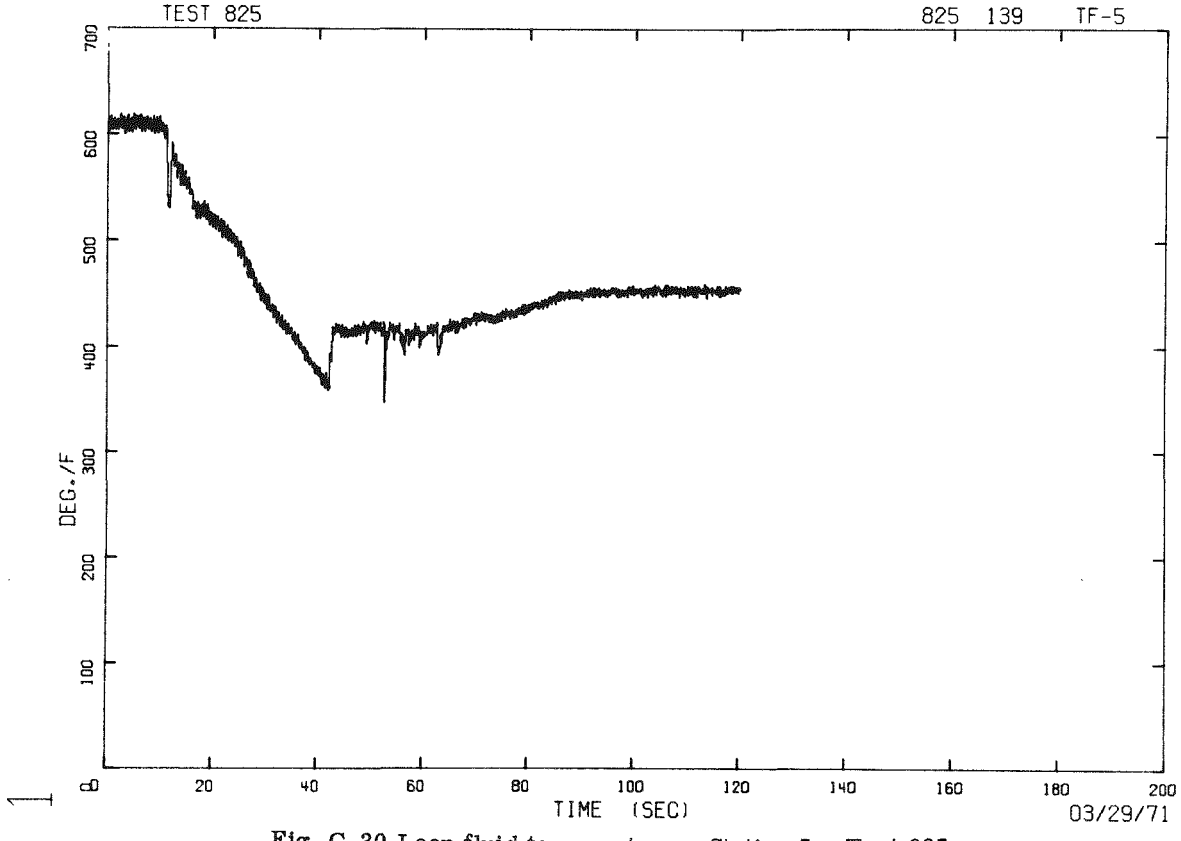

Fig. C-30 Loop fluid temperature - Station 5 - Test 825.

IV. MOMENTUM FLUX

Figure C-31 presents the momentum flux drag disc measurement at Station 1 (vessel outlet) for Test 824. The data in this figure require application of a linear correction with time to account for thermal drift as outlined in Appendix B, Section B-IV. The corrected output must then be converted to momentum flux by using the calibration curve for this particular detector and the measured density at Station 1.

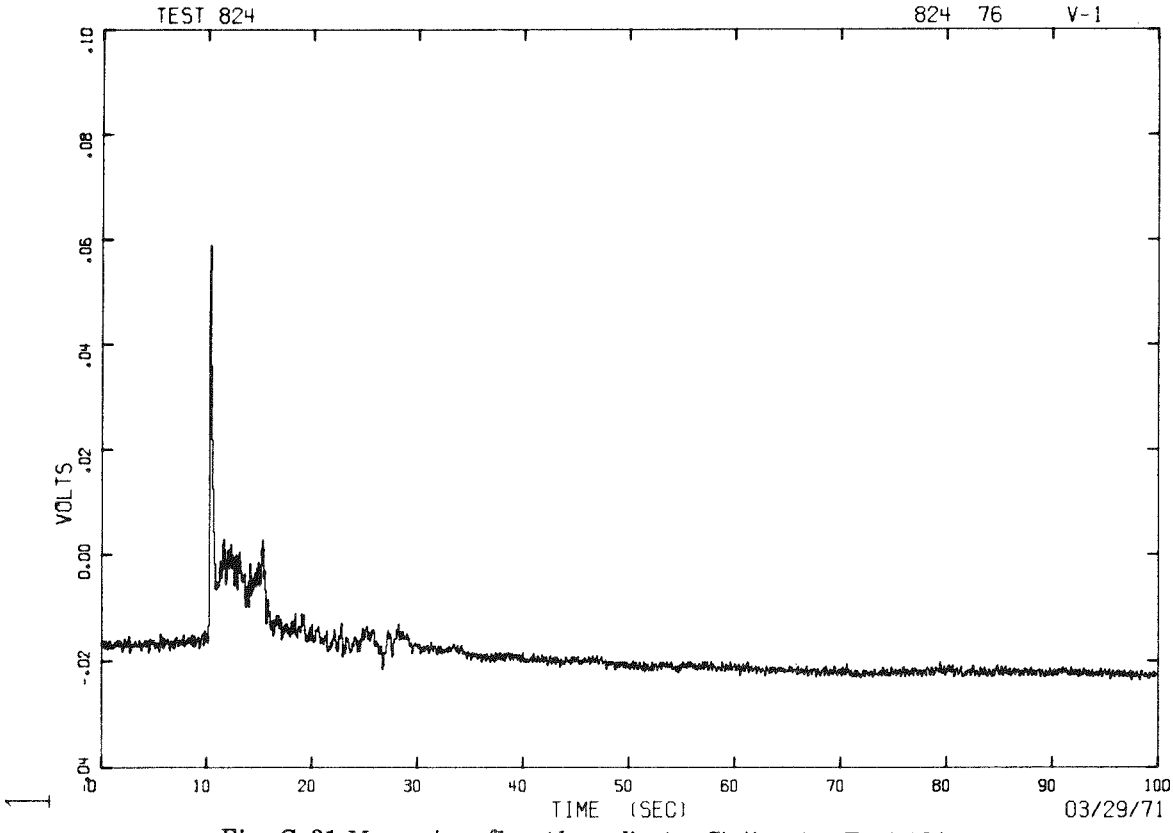

Fig. C-31 Momentum flux (drag disc) - Station 1 - Test 824.

V. THRUST

Figures C-32 and -33 represent typical thrust data from the load cell for Test 825. LC-4A is a horizontal load cell located at the top horizontal vessel support. A positive initial value of load at the cell reflects thermal expansion of system piping during the warmup process. Thrust load resulting from blowdown of the system is found by assigning a zero thrust at the time of rupture (that is, by determining the change from the initial value). Load cells experience long-term drift because of thermally-induced piping expansion and contraction and because of the thermal sensitivity of the instrument. However, of primary interest is thrust loading during subcooled blowdown and early saturated blowdown (periods of maximum load); negligible temperature change occurs during this time and no correction for thermal drift is applied to the data.

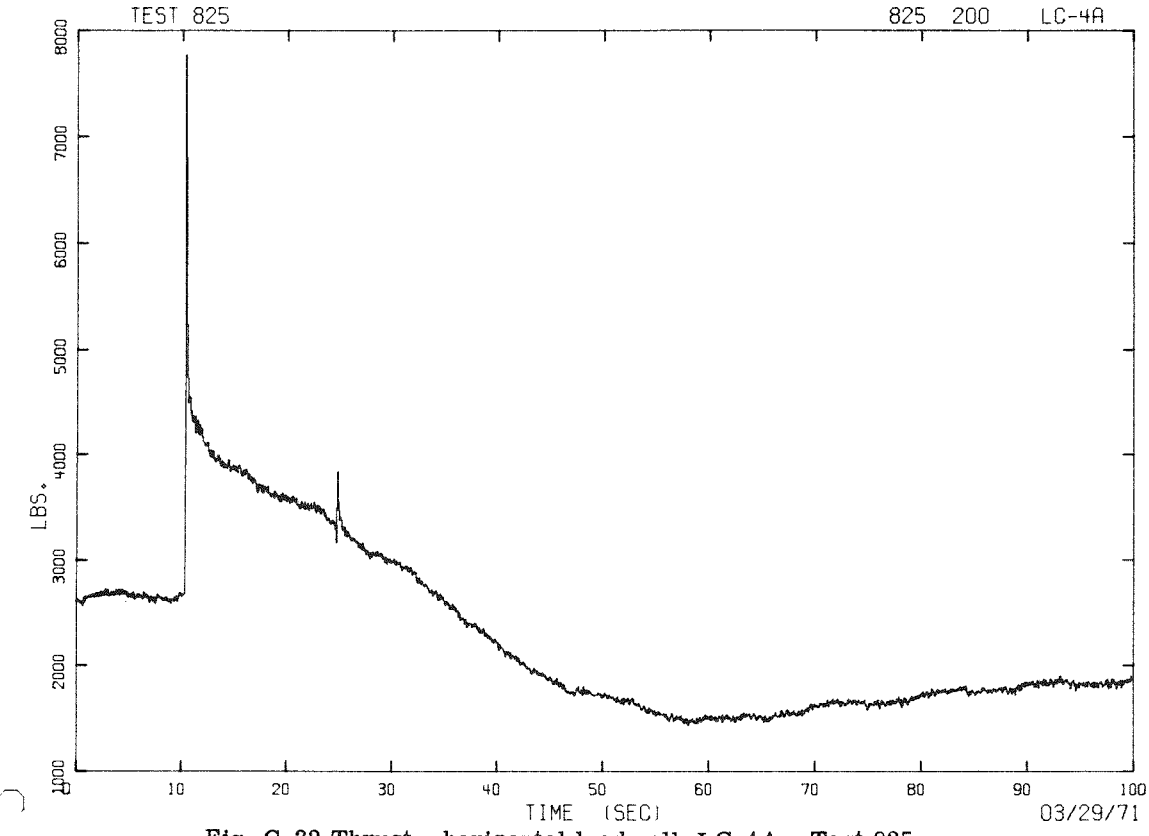

Fig. C-32 Thrust - horizontal load cell LC-4A - Test 825.

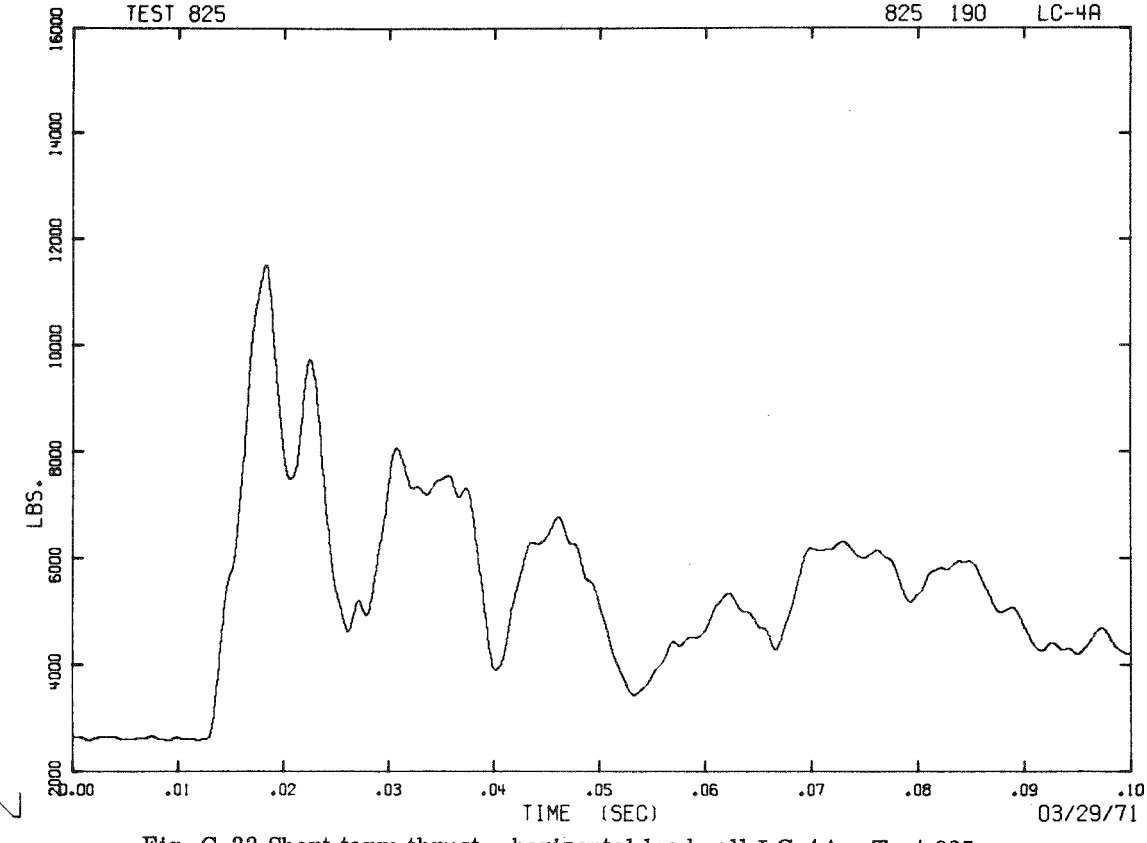

Fig. C-33 Short term thrust - horizontal load cell LC-4A - Test 825.

VI. LOOP PIPING STRAIN

Figure C-34 presents the circumferential loop piping strain at Station 1 (vessel outlet) for Test 824. This figure illustrates the subcooled decompression strain and the large thermally induced strain during saturated blowdown.

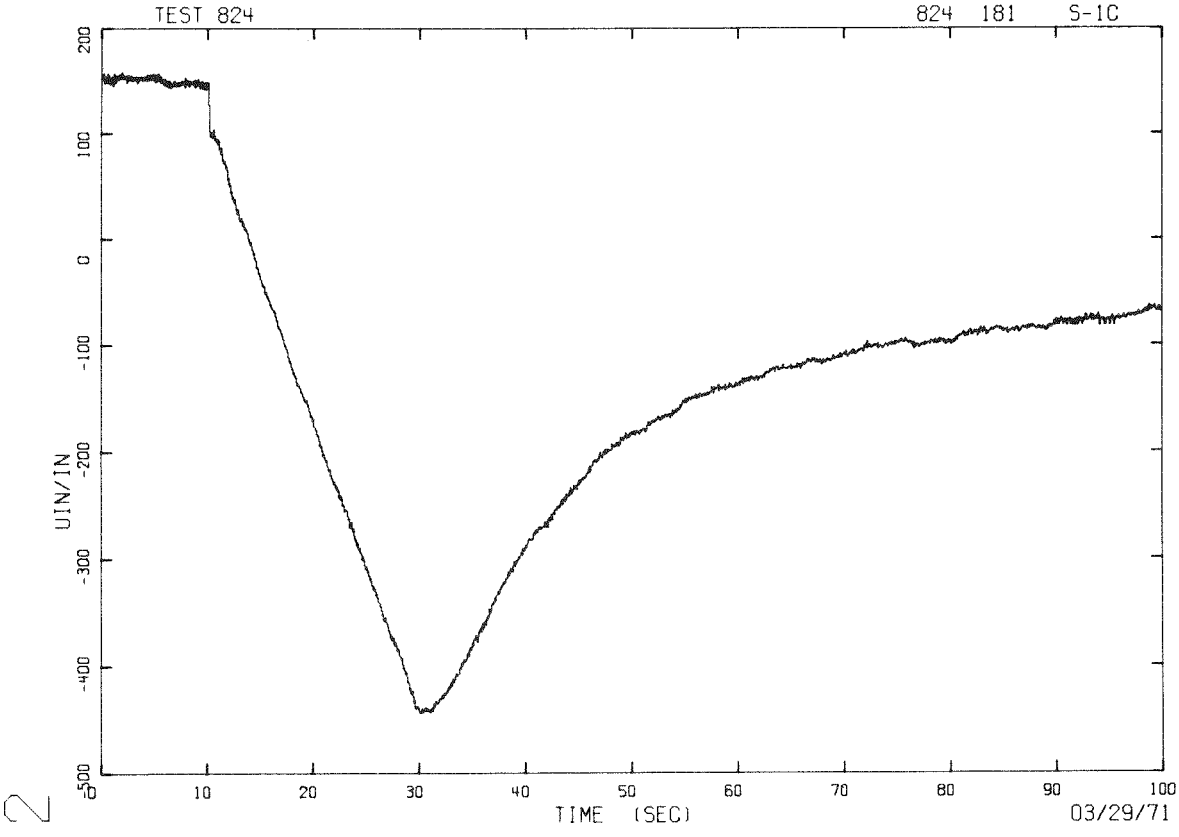

Fig. C-34 Loop strain - Station 1 - Test 824.